Research Report 2008
Project No: A-08/ 001

ATRANS
ASIAN TRANSPORTATION RESEARCH SOCIETY

Development Of A Falling weight deflectometer (FWD) for evaluating the pavement conditions

November 2009

Development Of A Falling weight deflectometer (FWD) for evaluating the pavement conditions

902/1 9th Floor, Glas Haus Building, Soi Sukhumvit 25 (Daeng Prasert),
Sukhumvit Road, Klongtoey-Nua, Wattana, Bangkok 10110, Thailand
Tel. (66) 02-661-6248 FAX (66) 02-661-6249
http://www.atransociety.com (font style –arial)

November, 2009
Printed in Thailand

ASIAN TRANSPORTATION RESEARCH SOCIETY

List of Members

• Project Leader •

Dr. Chakree Bamrungwong [1]

• Project Members •

Dr. Koonnamas Punthutaecha [1]
Dr. Kitti Manokhoon[1]
Dr. Warat Kongkitkul [2]
Dr. Sompote Youwai [2]
Dr. Pornkasem Jongpradist [2]

[1] Department of Rural Roads,
Bangkok, Thailand.

[2] Department of Civil Engineering,
Faculty of Engineering,
King Mongkut's University of Technology Thonburi,
Bangkok, Thailand.

ABSTRACT

A series of falling weight deflectometer (FWD) tests and plate load tests (PLT) were performed in a laboratory to evaluate the surface stiffness values of flexible pavement structures as single layer system (subgrade) and two-layer system (unpaved surface and paved surfaced), and to compare the results from these three types of test with the corresponding PLT results that were used as reference data. In this research, it was found that the stiffness values originally obtained from the FWD tests were higher than the values from the PLT. The differences in the results between FWD and PLT are, at least, attributed to: a) dynamic behavior; and b) viscous behavior of tested materials.

In single layer system on subgrade, it was attempted to adjust the FWD test results by taking the two above-mentioned factors into consideration which are: a) time-lag for dynamic behavior; and b) rate-sensitivity coefficient (β) for viscous behavior of tested materials. Then, it was found that the FWD test results became close to the ones by PLT. On the other hand, in two-layer system, there is no close-form solution to directly determine the rate-sensitivity coefficients (β) value for adjusting for loading rate effects at the stage in this research.

When following the AASHTO approximation method, for unbound surface (subgrade and unpaved surface conditions), it was found that the stiffness values by FWD test become close to the ones by PLT test. In contrast, it is clearly seen that for bound surface (paved surface), the degree of closeness of the approximated stiffness values to the ones by PLT test is less than the one of the unbound surface.

For all type of tests in this research, the stiffness values evaluated by undamped harmonic motion (UHM) by FWD tests are lower than the values from PLT tests. Then, after adjustment for the remain efficiency (E_f), FWD results are close to the results from PLT tests

Therefore, after having adjusted for these factors, FWD test can be applied to use in place of PLT to accurately obtain the stiffness value of pavement structure.

Dr. Chakree Bamrungwong
(Project leader)

TABLE OF CONTENTS

List of Tables

List of Figures

ATRANS
Research
Report
2008

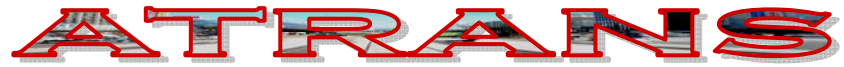

ASIAN TRANSPORTATION RESEARCH SOCIETY

CHAPTER I INTRODUCTION

1 INTRODUCTION

Nowadays, a number of methods to evaluate stiffness values of pavement structure in the field have been proposed. However, when stiffness evaluations were performed by these different methods on the same pavement structure, the results were largely different. Therefore, it is necessary to know the real stiffness values and the respective relevant methods to obtain them because they are very important to be used in designing of a new pavement structure and in maintenances.

Mairaing et al. (1982) described a method for compaction control during construction of pavement layers. That is, dry density evaluated by field density test was used as the parameter to control stiffness values. However, to evaluate stiffness values before and after construction in the field, static plate load tests (PLT) were usually performed to determine the modulus of subgrade reaction (*k* value). Although PLTs are standardized following many national and international standards (e.g., ASTM, AASHTO) but it is time-consumed and expensive.

Falling Weight Deflectometer (FWD) is a nondestructive testing (NDT) device which can evaluate stiffness values of pavement structure. FWD has many advantages over PLT, that is, it is convenient and economical. In general, however, using FWD to reliably evaluate pavement stiffness is still not very popular (Shahin, 1994) because most of FWD testing devices and analysis of test results have not been standardized (Bush III and Baladi, 1989).

In 1988, the first international symposium on nondestructive testing of pavements and backcalculation of moduli was held in Baltimore. Several methods to evaluate stiffness values were presented and the results showed that NDT methods including FWD provided stiffness values that are higher than the ones obtained by conventional methods and a wide range of stiffness values for the same tested materials was reported (Bush III and Baladi, 1989). In addition, from the stiffness values evaluated by other NDTs in many cases including in-situ and laboratory tests, it was found that they are higher than the values obtained by conventional methods (e.g., AASHTO, 1993; Ping et al., 2002; George, 2003; Loizos et al., 2003).

There are many different factors that affect the FWD test results such that the FWD-evaluated stiffness values are higher than the values obtained from conventional

methods. The purposes of this research are to describe the factors that influence the FWD-test results, affecting the evaluated stiffness values to be higher than ones obtained by conventional methods.

1.1 Research Objectives

This research has purposed the following objectives:

1 To investigate the rate-effect and dynamic-effect from FWD that affect the pavement stiffness values.

2 To develop an analysis framework taking into account the rate-effect and dynamic-effect for evaluating to the real pavement stiffness values.

3. To propose the simple method to reliably evaluate the stiffness values by FWD device.

1.2 Scope and Limitation of Research

This research focuses on interpreting the mechanisms of the aforementioned phenomena on the modulus of subgrade reaction (*k* value). The flexible pavement structures: 1) single layer as subgrade; and 2) two-layer pavement structure as unpaved surface and paved surface, were used to research and the corresponding PLT results are used as reference data. The deflection values of loading plate and load pressure in vertical direction were measured and synchronized for integrated analysis of the responses from dynamic impaction to develop a framework for evaluating stiffness values.

Only the single layer is was considered in the analysis framework taking into account the rate-effect and dynamic-effect for evaluating to the real pavement stiffness values.

In this research, all the tests were performed in a temperature-controlled laboratory at 25 $^{\circ}C$. A physical model of flexible pavement structure both single and two-layer systems were prepared in a cylindrical-shape concrete-container and the KMUTT sand was used for preparing the subgrade layer. The surface layers are the gravel layer and asphaltic concrete layer for modeling the unpaved surface and paved surface, respectively.

CHAPTER 2 LITERATURE REWIEW

2 LITERATURE REVIEW

2.1 Introduction

One of the most reliable methods available for determining the structural condition of an in-service pavement is the use of nondestructive testing (NDT). The NDT method has two major advantages over destructive testing as follow:

(1) the destructive testing, by definition, disturbs the underlying paving layers or requires removal of the pavement samples to a laboratory for testing, whereas NDT is truly an in-situ test that evaluates the pavement conditions without any material disturbance or modification.

(2) the advantage of NDT is that the tests are relatively quick and inexpensive, allowing more of them to be completed while causing less disruption to traffic than destructive testing.

In general, however, the amount of destructive testing needed to evaluate a pavement in conjunction with NDT is minimal (Shahin, 1994) because most of NDT testing is not standardized (Bush III and Baladi, 1989). In the future, more properties of materials can be extracted from NDT testing if the dynamic analysis was suggested (Lytton, 1989).

2.2 Flexible Pavement Structure

AASHTO (1993) defined the flexible pavement structure as (Fig. 2.1): the combination of subbase, base course, and surface course placed on a subgrade to support the traffic load and distribute it to the roadbed soil. The meaning of each word is:

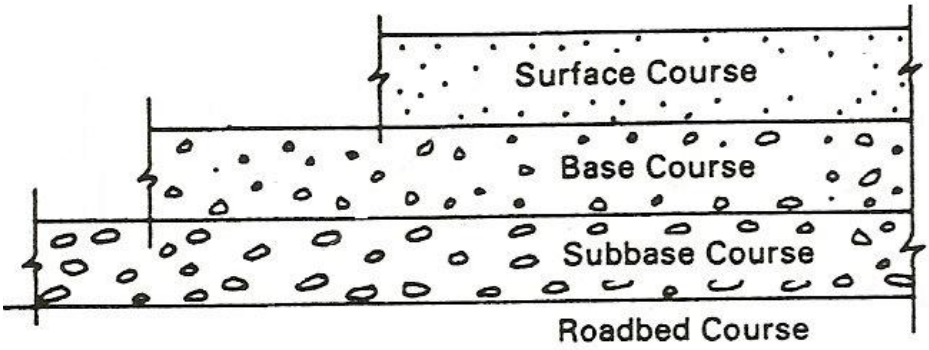

Figure 2.1 Flexible pavement structure (after AASHTO, 1993).

Surface Course: The surface course of a flexible structure consists of a mixture of mineral aggregates and bituminous materials placed as the upper course and usually constructed on the base course. In addition to its major function as a structural portion of the pavement, it must also be designed to resist the abrasive forces of traffic, to reduce the amount of surface water penetrating into the pavement, to provide a skid-resistance surface, and to provide a smooth and uniform riding surface.

Base Course: The base course is the portion of the pavement structure immediately beneath the surface course and it is constructed on the subbase course. Its major function in the pavement is structural support and usually consists of aggregates: e.g., crushed stone, crushed slag, crushed gravel and sand, or combinations of these materials. Specifications for base course are generally considerably more stringent than the one for subbase materials in requirements for strength, plasticity, and gradation.

Subbase Course: The subbase course is the portion of the flexible pavement structure between the roadbed soil and the base course. It usually consists of a compacted layer of granular material, either treated or untreated. In addition to its position in the pavement, it is usually distinguished from the base course material by less stringent specification requirements for strength, plasticity, and gradation. The subbase material should be of significantly better quality than the roadbed soil.

Subgrade: The subgrade is the lowermost material placed in the flexible pavement structure or placed on unmoved soil from cuts in the normal grading of the roadbed. It is the foundation for the flexible pavement structure. Sometimes, we called the subgrade as Foundation Soil or Roadbed Soil (The Asphalt Institute, 1968).

2.3 Nondestructive Testing (NDT)

Lytton (1989) summarized and presented the uses of nondestructive testing (NDT) to determine the properties of pavement layers, which are required for the accurate evaluation, design and management. These properties include:

1. layer thickness,

2. binder content in asphalt bound layers,

3. the elastic stiffness of each layer (meaning either the elastic modulus or the stress-strain relationship of stress-dependent materials),

4. fatigue properties for both load and thermal fatigue processes,

5. permanent deformation properties of each layer,

6. residual stress in-situ, and

7. other properties.

Accurate measurements of these properties are necessary for making realistic predictions of the remaining pavement life, designing overlays and recycling layers. Most of these properties are practically measured at present; however, there is no reason why methods to measure them nondestructively can be found very limitedly.

The most common property determined by NDT is the elastic stiffness of each layer. The chosen method (i.e., linear elastic modulus or the characteristics of nonlinear stress-strain relation) should be compatible with the method that used to be used in preparing design calculations (e.g., multilayered elastic or finite element method). In addition, for consistency, the same method should be employed to predict the remaining life, to monitor changes of layer properties with time and to be used in specification testing. Faikratok and Sonthong (1998) explained on the NDT equipments used in making the measurements, including:

1. static or slowly moving loads: e.g., Benkelman Beam and LaCroix Deflectographe and Plate Load Test, etc.

2. steady-state vibration: e.g., Dynaflect, Road Rater, WES 16 kip Vibrator, Crops of Engineer 71-kN Vibrotor and Federal highway Administration's Cox van, etc.

3. impulse loads which can be separated into two methods as:

"near field" impulse loads method: e.g., Dynatest Weight Deflectometer, Kuab Falling Weight Deflectometer and Phoenix Falling Weight Deflectometer, etc.

"far field" impulse loads method or wave propagation methods (e.g., Shell-Vibrator).

In this research, the NDT equipments type static load (Plate Load Test; PLT) and the *"near field"* impulse load (Falling Weight Deflectometer; FWD) are used to evaluate the stiffness values in laboratory. The results from two methods are compared where defined

the Plate Load Test is the referent equipment and the *"far field"* impulse loads methods is omitted.

Output responses are measured on the surface measurements or with depth below the surface measurements with all of the same sensors, but the loading conditions below the surface measurements may include moving traffic. The measurements are made with:

(i) geophone that sense the velocity of motion,

(ii) accelerometers, and

(iii) linear variable differential transformers (LVDT) that measure displacement.

Lytton (1989) defined the terms "near field" and "far field" by refering to the behavior of the surface of the pavement where the measurements are made (Fig. 2.2). The "near field" is located within the deflection basin around the load that is applied. Surface deflections are made up of two components: a) the vertical deflections due to the load, and b) the propagation of wave laterally across the surface. The "far field" is located outside of the deflection basin, where the surface motions is principally due to wave propagation. The distinction between "near field" and "far field" surface motion is determined primarily by the size of the deflected basin under a design wheel load, because the behavior of the materials beneath the load is different from that in the far field. The upper pavement layers in the near field are in tension due to the imposed curvature of the surface, and all layers are in and elevated level of stress.

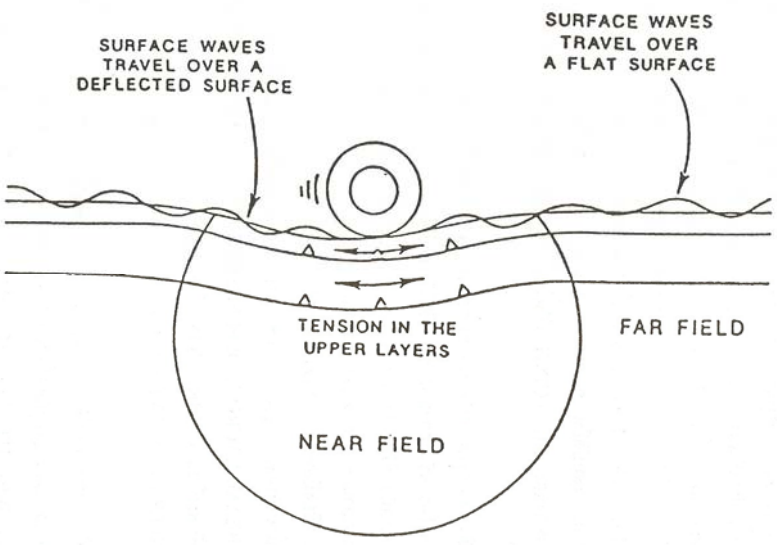

Figure 2.2 Schematic illustration of near field and far field characteristics (after Lytton,

1989).

2.4 Types of NDT Equipment

Shahin (1994) presents that there are three different types of commercially available deflection testing devices. The devices are grouped based on loading modes as: impulse loads, steady-state vibration, and static. The impulse nondestructive testing devices are the most recently developed and they are better in simulating the load from a moving tire. Discussion of all the three device types as follows:

2.4.1 Static or Slowly Moving Loads

Static deflection equipment applies either a static or a slow-moving load to the pavement surface and measures the resulting def1ections.

Benkelman Beam: The Benkelman Beam is a simple hand-operated deflection device (Fig. 2.3). It consists of a support beam and a probe arm. The probe arm is 3.05 m (10 ft) long and is pivoted at a point 2.44 m (8 ft) from the probe which rests upon the pavement surface. It is used by placing the tip of the probe between the dual tires of a loaded truck, typically an 80 kN (18,000 lb) axle load. As the loaded vehicle moves away from the beam, the rebound or upward movement of the pavement is recorded. Some problems encountered with this device include:

(1) the need to ensure that the front supports are not in the deflection basin; and

(2) the difficulty or inability to determine the shape and size of the deflection basin.

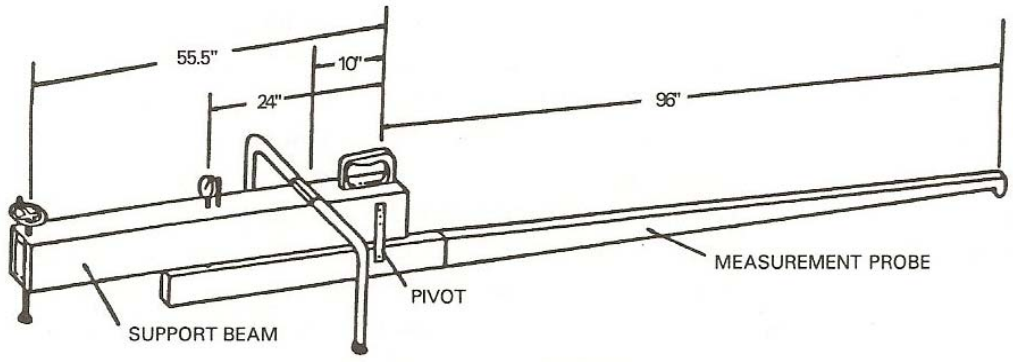

Figure 2.3 Schematic illustration of the Benkelman Beam (after Shahin, 1994).

La Croix Deflectograph: The La Croix Deflectograph consists of two beam-type devices mounted to a truck by means of a common frame (Fig. 2.4). The beams are used

to measure the def1ections caused by the rear axle of the vehicle. During testing, the frame is lowered to the pavement surface in front of the oncoming dual rear wheels. The beam will rotate from the deflection caused by the approaching wheels, and this rotation is measured by inductive displacement transducers and is converted into deflections. The measurements continue until the wheels pass over the point where the beams contact the pavement. This method allows the deflection basin to be analyzed, as long as the legs on the frame are unaffected by the deflection basin. The load can be varied between 53.5 kN and 116 kN (12,000 lb and 26,000 lb) on the rear axle.

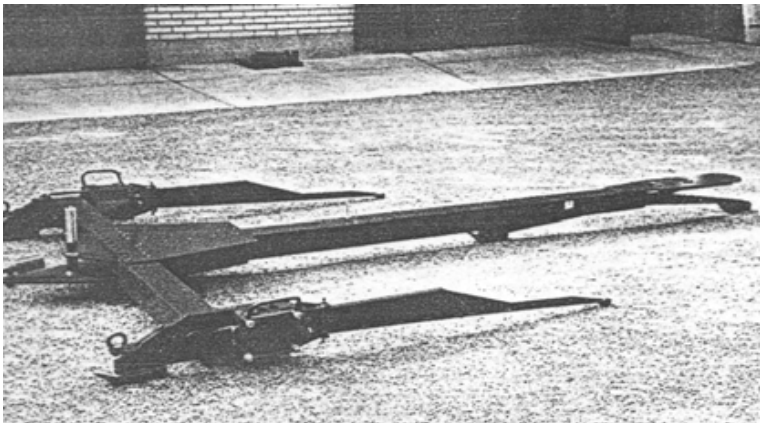

Figure 2.4 Illustration of the dual beams used in the La Croix Deflectograph (after Umass, n.d.).

Plate Load Test: Plate Load Test is the popular method is used evaluated the stiffness of the soil layer (Fig. 2.5). The two standard methods are approved by ASTM including: repetitive static plate load tests and nonrepetitive static plate load tests (ASTM, 2004). The results from two methods are similar in term of load and deflection relationship and the modulus of subgrade reaction (k values) is calculated. The disadvantages of this method are that used more time and more cost to evaluate the soil stiffness in the each locations.

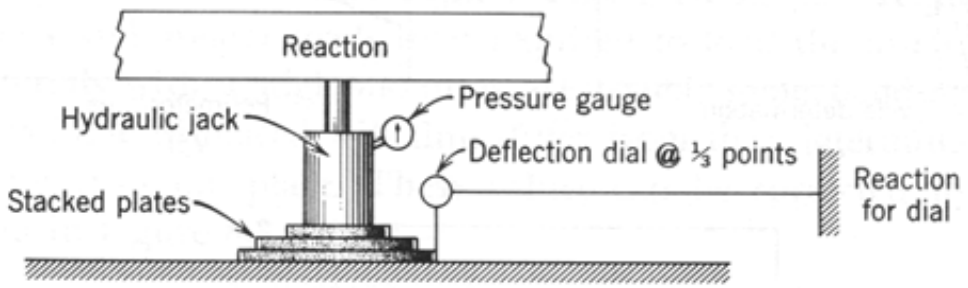

Figure 2.5 Schematic illustration of field Plate Load Test (after Huang, 2003)

2.4.2 Steady-State Vibration

All steady-state dynamic deflection devices use a similar mode of operation. A relatively large static preload is applied to the pavement, and a sinusoidal vibration is created by the dynamic force generator. The magnitude of the peak-to-peak dynamic force must be less than the static force (Fig. 2.6), so the vibratory device always applies a compressive force of varying magnitude on the pavement. The deflections are measured by accelerometers or velocity sensors. These sensors are placed directly under the center of the load and at specified distances from the center, usually at 0.3 m (1 ft) intervals.

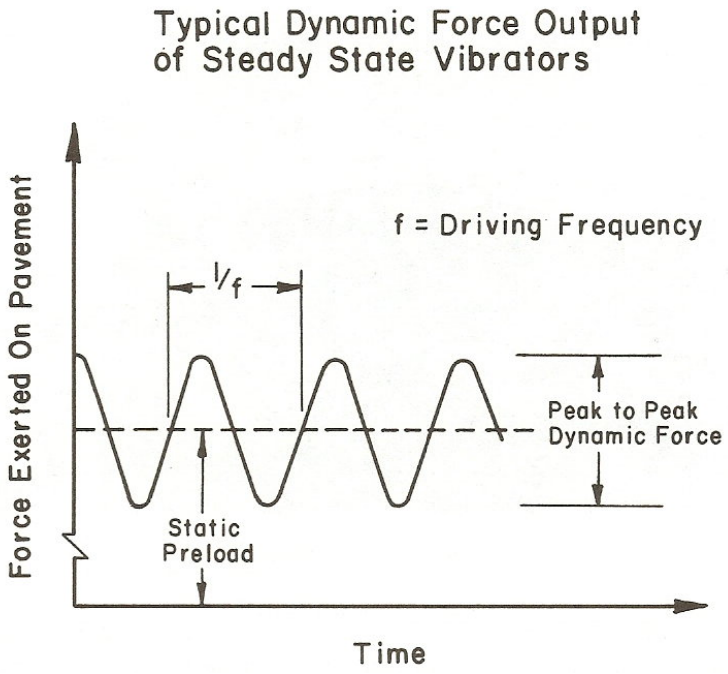

Figure 2.6 Typical dynamic force output of steady-state vibrators (after Shahin, 1994).

The advantage of this type of equipment over the static equipment is that a reference point is not required. An inertial reference is used so that the change in deflection can be compared to the magnitude of the dynamic force. On the other hand, disadvantages of this method are that the actual loads applied to pavements are not in the forms of steady-state vibration and that the use of relatively large static load could have some effects on the behaviors of stress-sensitive materials (e.g., Shahin, 1994; Huang, 2003). The following steady-state vibration deflection equipments will be discussed:

Dynaflect: The Dynaflect was one of the first commercially available steady-state dynamic deflection devices (Fig. 2.7). It is trailer mounted and can be towed by a standard vehicle. A static weight of 8.9 kN to 9.3 kN (2,000 lb to 2,100 lb) is applied to the pavement through a pair of rigid wheels. A dynamic force generator is used to produce a 4.45 kN (1,000 lb) peak-to-peak dynamic loads at a frequency of 8 Hz. The dynamic force is superimposed on the static force, and the deflections due to the dynamic force are measured by five velocity transducers (i.e., geophones).

The normal sequence of operations is to locate the device to the test location and hydraulically lower the loading wheels and transducers to the pavement surface. A test is then performed and the data are recorded. If the next test site nearby, the device can be transported on the loading wheels at speed up to 9.6 km/h (6 mph.) After the last test is completed, the loading wheels and transducers are hydraulically lifted and locked in a secure position. The fixed magnitude and frequency of the loading are the major limitations of the device.

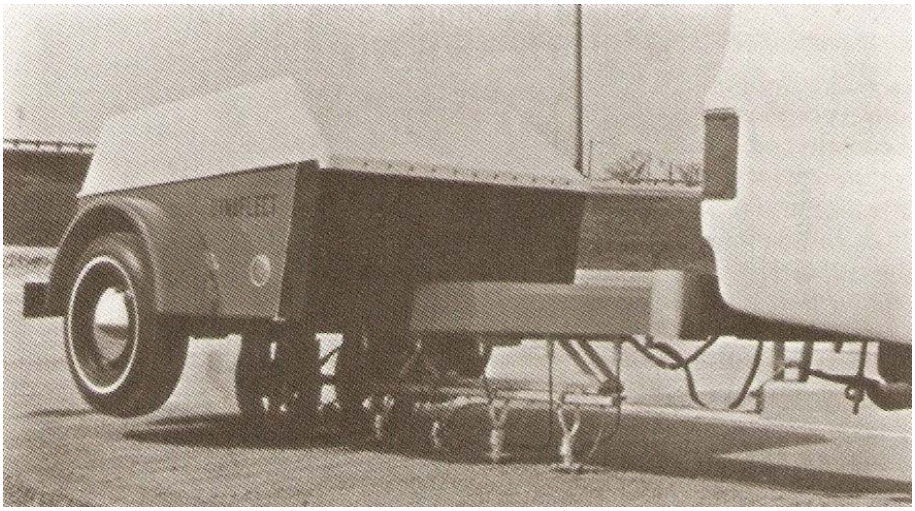

Figure 2.7 Illustration of the Dynaflect (after Shahin, 1994).

Road Rater: The Road Raters are available in several models (Fig. 2.8). The models vary primarily in the magnitude of the loads, with the static loads ranging from 10.7 kN to 25.8 kN (2,400 lb to 5,800 lb) and the peak-to-peak dynamic loads ranging from 2.2 kN to 35.6 kN (500 lb to 8000 lb). The loading frequency can be varied continuously from 5 Hz to 70 Hz (in 0.1-cycle/sec increments). Four velocity transducers are used to measure the deflection basin. The major limitations of this equipment include the small levels of load for the lighter models and the need for a heavy static load for the heavier model.

Figure 2.8 Illustration of the Road Rater Model 2008 (after Shahin, 1994).

***WES 16-kip Vibrator*: The WES 16-kip Vibrator (Fig. 2.9) is contained in a 10.97 m (36 ft) semitrailer and was produced by the U.S. Waterways Experiment Station (WES). It uses a 16,000 lb static preload and a dynamic force generator that will produce peak-to-peak loading of around 30,000 lb. The loading frequency can be varied from 5 Hz to 100 Hz. The dynamic load is measured by a set of three load cells mounted on the 0.46 m (18 in.)-loading plate. Velocity transducers are used to measure the deflection under the load plate and at preselected distances from it. The entire operation is automated. This device was designed and built specifically for airfield evaluation. WES believes that a heavy load is needed to accurately model pavement response to loading by heavy aircraft (Green and Hal1, 1975).**

Figure 2.9 Illustration of the WES 16-kip Vibrator (after Shahin, 1994).

2.4.3 "Near Field" Impulse Load

The devices used in impulse load method are ones that deliver a transient force impulse to the pavement surface and called "the falling weight deflectometer (FWD)". The force is generated by a mass (falling weight) with a guide system. The mass is raised to one or more predetermined heights and then dropped. The resulting force pulse transmitted to the pavement approximates the shape of a half-sine wave. The impulse loads devices have relatively low static preloads. The preload will vary from a few hundred to few thousand pounds based on the device. Thus, the negative effects of a high preload are avoided (e.g., Shahin, 1994; Huang, 2003). Three different impulse loading devices will be discussed including:

Dynatest Weight Deflectometer: The Dynatest Weight Deflectometer, such as Model 8003 Falling Weight Deflectometer (Fig. 2.10), is a trailer-mounted system and can be towed by a standard-sized automobile. By varying drop height and weight size, force magnitudes can be changed from 6.7 kN to 107 kN (1500 lb to 24,000 lb). This force is transmitted to the pavement through a loading plate, having 11.8 in. (300 mm) in diameter, to provide a load pulse plate and a strain-type transducer measures the magnitude of the load in the form of a half sine wave with a duration from 25 to 30 ms. The magnitude of load is measured by a load cell. The deflections are measured using velocity transducers (normally seven transducers) which are mounted on a bar and automatically lowered to the pavement surface with the loading plate. One transducer is placed at the center of the loading plate. A computer located in the tow vehicle controls the entire operation and records the data from the sensors.

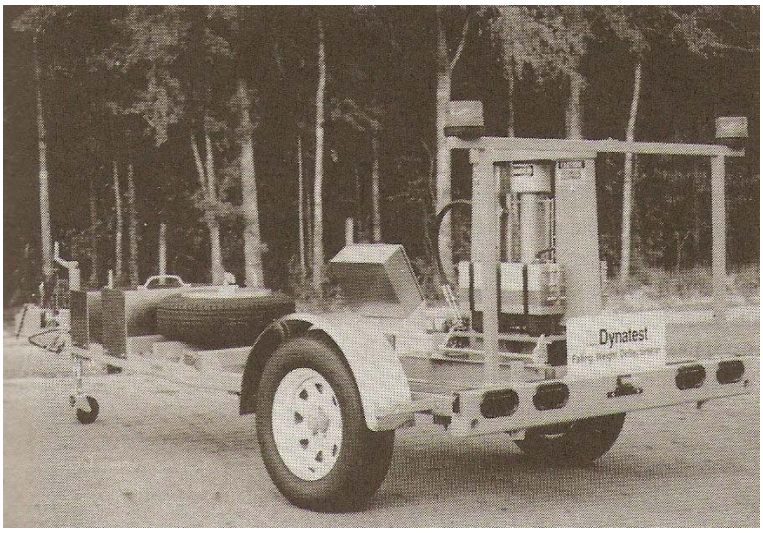

Figure 2.10 Illustration of the Dynatest Model 8003 (after Shahin, 1994).

Figure 2.11 Illustration of the KUAB Falling Weight Deflectometer (after Shahin, 1994).

***KUAB Falling Weight Deflectometer*: The KUAB Falling Weight Deflectometer (Fig. 2.11) created the impulse force by dropping a set of two weights (Fig. 2.12) from different drop heights and weights, an impulse force ranging from 13.4 kN to 294.4 kN (3,000 lb to 66,000 lb) can be generated. The load is transferred through a segmented loading plate (Fig. 2.13), having 300 mm (11.8 in.) in diameter. Each loading plate is divided into four quarter-circle segments that are mounted with in a common hydraulic pressure chamber. Each segment of the load plate is free to conform to the shape of the pavement surface being tested. A two-mass falling weight system is used to create smoother rise of the force pulse on pavements with both stiff and soft subgrade support. Deflections are measured by five transducers.**

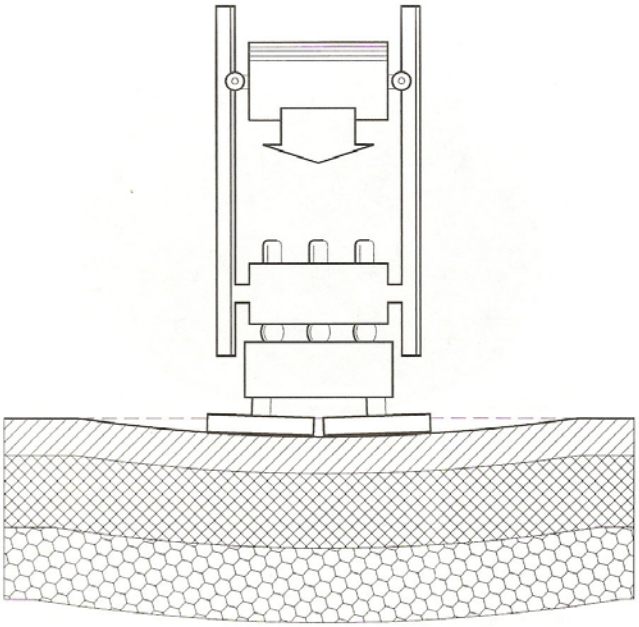

Figure 2.12 Schematic diagram showing two-mass system of the KUAB Falling

Weight Deflectometer (after Shahin, 1994).

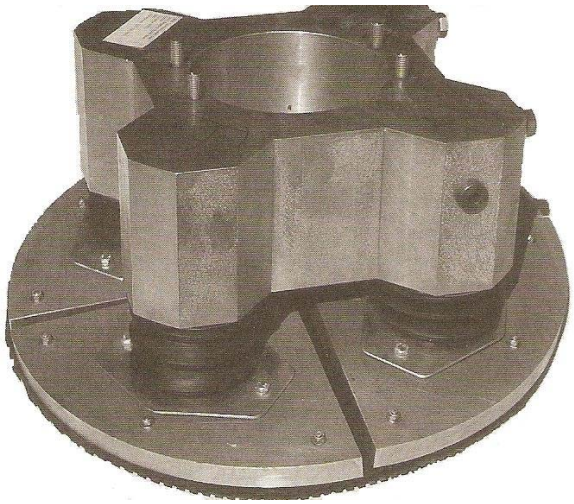

Figure 2.13 Illustration of the segmented loading plate (after Shahin, 1994).

Phoenix Falling Weight Deflectometer: The Phoenix Falling Weight Deflectometer is an earlier version of deflectrometers (Fig. 2.14). A single weight is dropped from different heights to develop impact loads from 10 kN to 50 kN (2,248 lb to 11,240 lb). The load is transferred to the pavement through a plate, having 300 mm (11.8 in.) in diameter. Deflections are measured by three transducers, one at the center of the loading plate and the others at 300 mm and 750 mm (11.8 in. and 19.5 in.) radially from the center.

Figure 2.14 Illustration of the Phoenix Falling Weight Deflectometer Model Prima 100

(after Grontmij and Carl Bro, 2007).

2.5 Factors affecting Deflection Values

Huang (2003) summarized the major factors that affect deflections, which must be carefully considered when conducting nondestructive tests including:

2.5.1 Loading Conditions

Load Magnitude: The magnitude of loads have a great affection of pavement deflections. Load levels ranging from as little as 4.46 kN to over 223 kN (1000 lb to over 50,000 lb) are available. Some NDT devices offer the potential to vary the applied loads and found that light loads do not sufficiently stress the underlying layers of heavy traffic highway and airport pavements (e.g., Hall, 1975; Bush III et. al., 1985; Ullidtz and Stubstad, 1985; Huang, 2003; FAA, 2004). The load-deflection relationship of pavements is often nonlinear, and test results obtained by using small loads which have to be extrapolated over one or two orders of magnitude can result in serious errors. To accurately characterize pavement response under design loads, the load level of the NDT device should be selected as closely as possible to those design load values (FAA, 2004). Figure 2.15 shows an example of the nonlinear relationship between load and deflection. This means that characterizing pavement response to a heavy load through the use of a small load could be very misleading (Shahin, 1994). Under a light load, the force may not seat the pavement and may not excite the full strength of the supporting subgrade (Bush III et al., 1985).

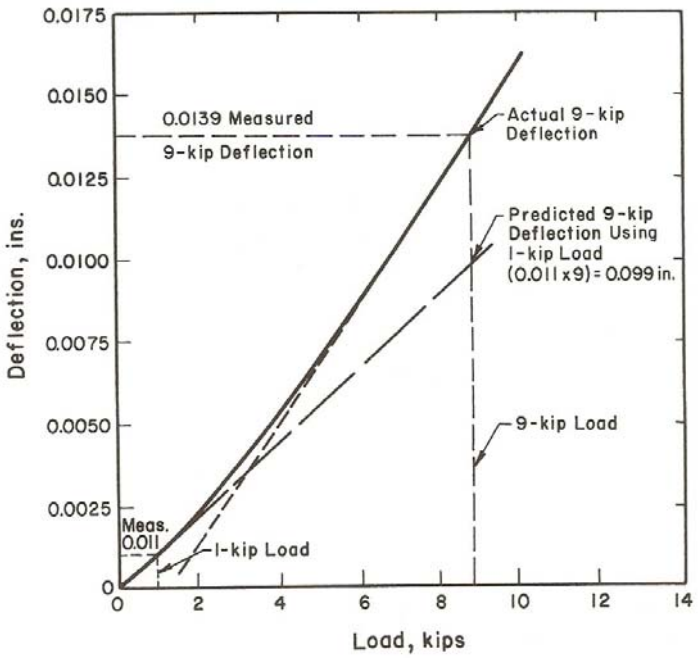

Figure 2.15 Illustration of nonlinear relationship between load and deflection (after Shahin, 1994).

Loading Mode: Even if the magnitude of the load is held constant, the pavement response can vary greatly depending on the mode of the loading. Normally, the load pulse is not symmetric (Fig. 2.16), therefore using the total length of load pulse duration to describe loading time could be misleading. It is strongly recommended that the time from zero to peak load or 'rise time' should be used for instead, unless the pulse happens to be symmetric.

With the Falling Weight Deflectometer device, the peak deflection is measured in each sensor position when it occurs, and a deflection bowl is constructed using peak deflections even though they did not occur at the same time. Figure 2.17 shows time history of the load pulse and the deflections measured from plate center to 1.8 m radially away. In spite of this, the data are often analyzed as if there was a stationary bowl, using the maximum values as if they existed at the same time. An attempt to minimize this error was developed by the KUAB Falling Weight Deflectometer. This was achieved by increasing the rise-time so that it would be closer to that of a moving vehicle. By using a sufficiently long rise-time, the time-lag between sensor peak deflections is minimized. Figure 2.18 demonstrates the def1ections from plate center to 120 cm radially vary for two different rise times. For the longer rise time, the peak def1ections at 0 and 60 cm away occur almost at the same instant. The effect of the load pulse shape and rise time cannot be overlooked because it can affect the peak values of center def1ection by as much as 10 % to 20 % (Royal Institute of Technology, 1980)

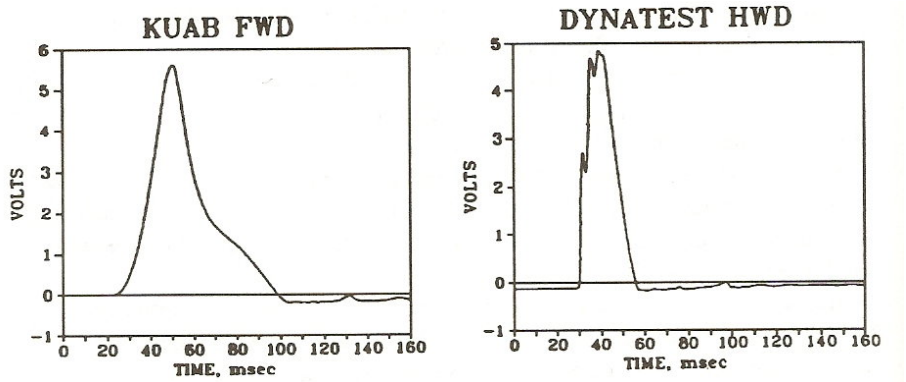

Figure 2.16 Illustration of typical load pulse plots (after Shahin, 1994).

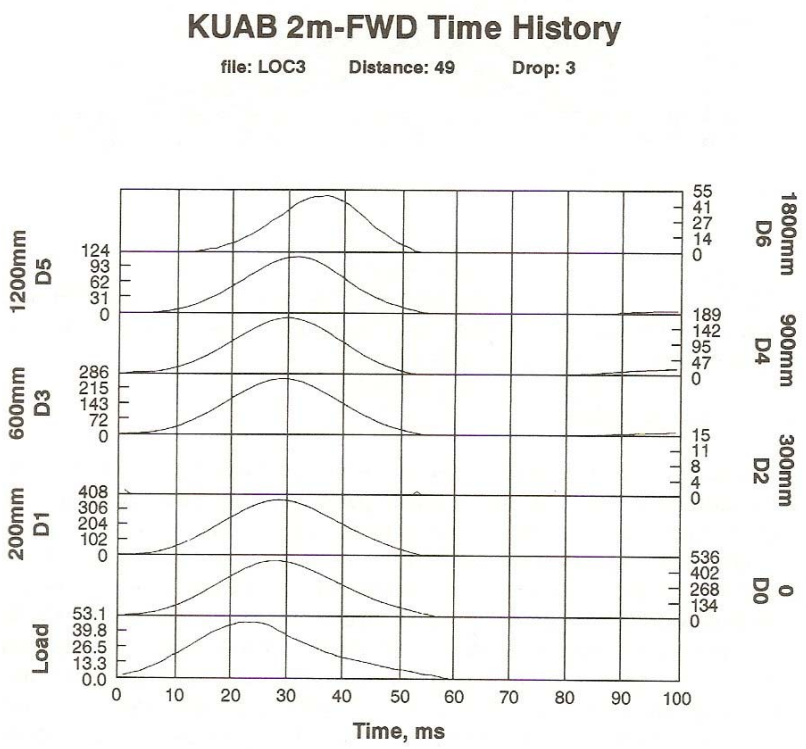

Figure 2.17 Time history for the Falling Weight Deflectometer load pulse and deflections 0-1,800 mm from the load center (after Shahin, 1994).

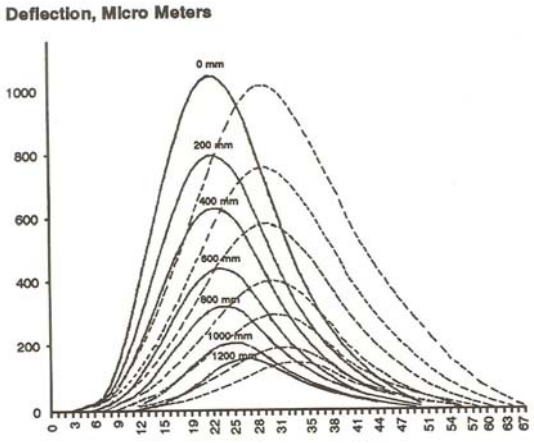

Figure 2.18 Time histories for deflection from 0 to 1,200 mm from the load center for different rise times (after Shahin, 1994).

***Load Distribution*: Touma et al. (1990) conducted a field test in which a pressure-sensitive film was placed under two Falling Weight Deflectometer devices, one with a segmented load plate and the other with a solid load plate. The segmented plate was above described in the section of the KUAB Falling Weight Deflectometer. The measured pressure distributions under the segmented and solid plates are shown in Fig. 2.19 for the three different pavements. Mechanistic analysis using the field data showed that, if**

full contact is assumed when in reality it did not occur, significant errors reaching 100 % may result in the back-calculated layer moduli. Because it is difficult and impractical to measure the load distribution associated with each field test, it is important to utilize a loading plate of such design to ensure full contact with the pavement for all conditions.

2.5.2 Climate Conditions

Pavement Temperature: Shahin (1994) explained that the pavement temperature is a factor that must be closely monitored during test. When testing asphalt pavements, the deflection changes as pavement temperature varies because the stiffness of the asphalt layer is a function of its temperature. At higher temperatures, the asphalt stiffness is reduced, thus increasing deflections. An example of the relation between asphaltic concrete stiffness and temperature is shown in Fig. 2.20. Figure 2.21 shows an example of the impact of the asphaltic concrete stiffness on surface deflection as measured at 0, 305, 660 and 915 mm (0, 12, 26, and 36 in.) from the center of the loading plate. The highest impact of the asphaltic concrete stiffness is at "D_0" and there is very small impact on "D_{36}". This is to be expected, as the sensor located at 915 mm (36 in.) away from the center where the load will induces deflections mostly occurred in the subgrade.

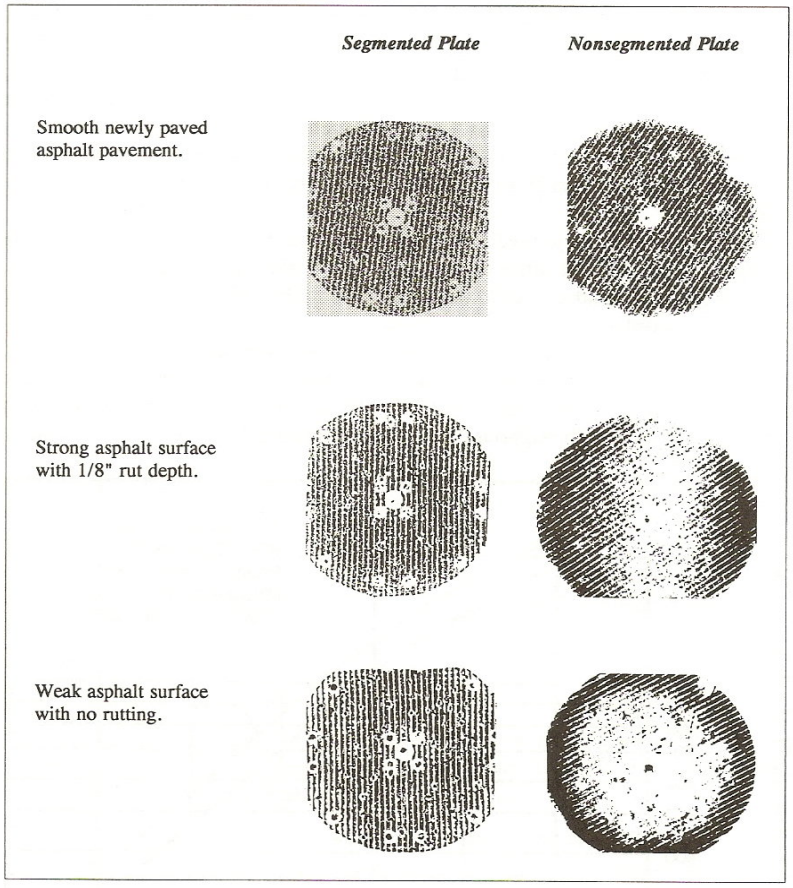

Figure 2.19 Actual pressure distribution under rigid and segmented plate (after Touma et al., 1990).

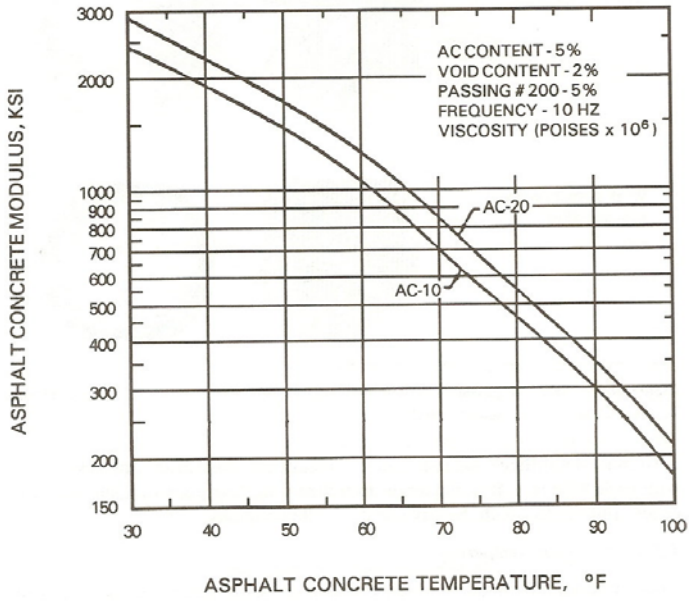

Figure 2.20 Typical asphaltic concrete modulus-temperature relationship (after Thompson, 1984; Shahin, 1994).

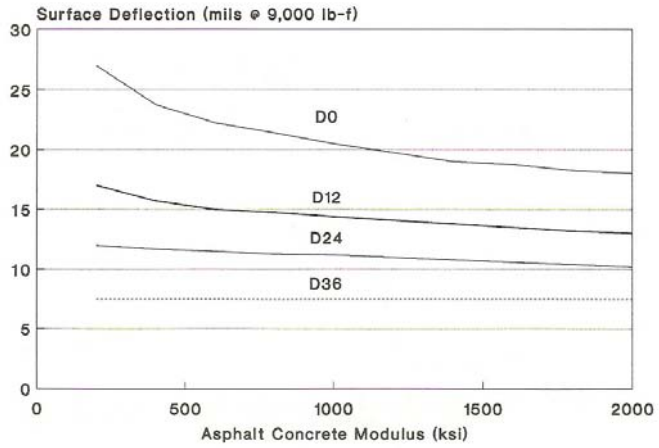

Figure 2.21 Relationship between surface deflection and asphaltic concrete modulus (after Shahin, 1994).

***Testing Season*: FHWA (1984) summarized that the seasonal testing is an important factor for analyzing deflections. There are basically four distinct seasonal periods in cold climatic areas (Fig. 2.22) as follows:**

(1) The period of deep frost when the pavement is very strong,

(2) The period during which the frost is beginning to disappear from the pavement subgrade system and the deflection increases greatly due to saturated pavement layers system,

(3) The period during which the excess pore water from the melting frost leaves the pavement or subgrade and the soil begins to recover, and the deflection decreases rapidly, and

1 The period during which the def1ection levels off slowly as water content slowly decreases.

2.5.3 Pavement Conditions

Pavement Structure: The deflection of a pavement in response to an applied load represents an overall system response. It is important to remember that the complete pavement system consists of all constructed layers (i.e., subbase, base, surfacing) plus the subgrade itself. The deflected surface profile is commonly referred to as the deflection “basin” or "bowl." The shape of the basin, including maximum deflection under the load and tapering def1ection away from the load, is an important parameter in the analysis of pavement systems. In general, a weaker system will deflect more than a stronger system under the same load; however, the exact shape of the basin is related to the strengths of the individual component layers. The deflection basin “area” is a calculated value based on surface deflections (Shahin, 1994).

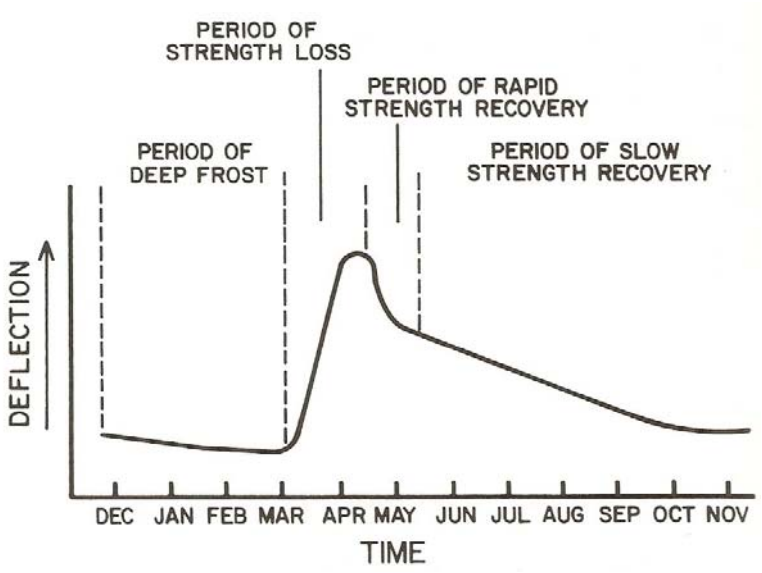

Figure 2.22 Seasonal effects on pavement deflection (after The Asphalt Insitute, 1981 Shahin, 1994).

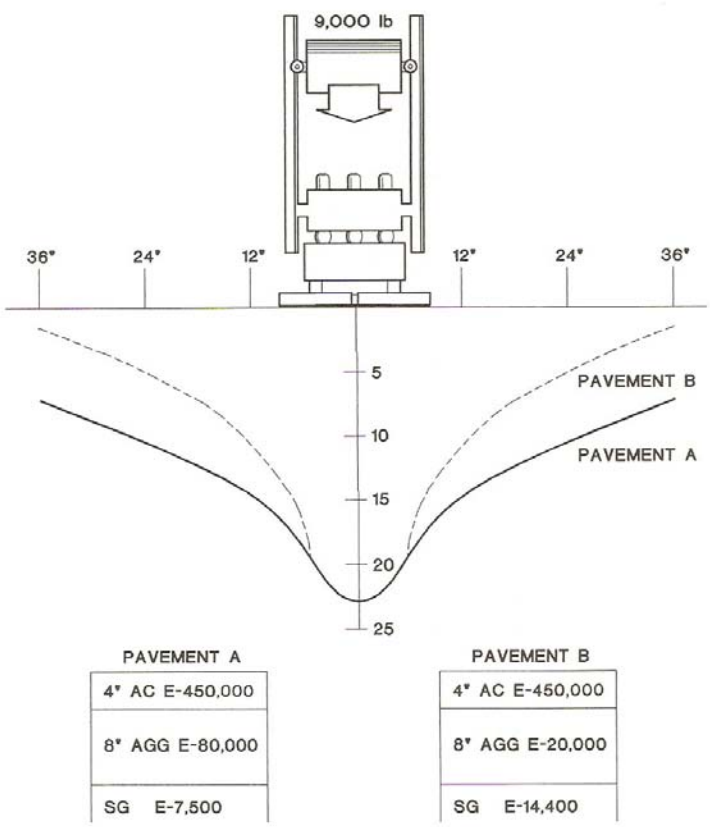

Figure 2.23 Comparison of deflection basin of two pavements (after Shahin, 1994).

Figure 2.23 presents two deflection basins obtained from computer simulation of two pavement systems of equal thickness but different component strengths. Although the maximum deflection is the same in both cases, the shapes of the basins are different. For Case A ("Strong"), the basin area equals 551.94 mm (21.73 in.) For Case B ("Weak"), the basin area is 430.78 mm (16.96 in.) The Area is computed by Eq. 2.1 as illustrated in Fig. 2.24 for deflections measured at 0, 305, 610, and 915 mm (0, 12, 24, and 36 in.) from the center of the plate.

$$\text{Area} = 6\left[1 + 2\left(\frac{D_{12}}{D_0}\right) + 2\left(\frac{D_{24}}{D_0}\right) + \frac{D_{36}}{D_0}\right] \quad \textbf{(2.1)}$$

where:

Area **= the deflection basin area in inches; and**

D_i **= the surface deflection at radial distance *i* in inches.**

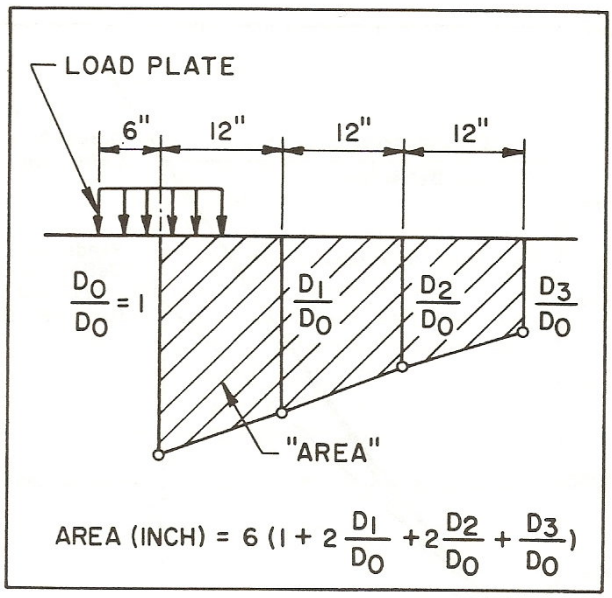

Figure 2.24 Calculation of basin area (after Hoffman and Thompson, 1981; Shahin, 1994).

2.6 Flexible Pavement Material Behavior

2.6.1 Unbound Material Behavior

Unbound materials exhibit a stress-dependent response. Usually, the more stress is applied, the stiffer the material in the layer will respond (Almassy, 2002). Material behaviors are irrecoverable deformation after each load application. After the first few load applications, the resilient (recoverable) deformation increases more than the irrecoverable deformation. If the load is small when compared to the strength of the material and is repeated for a large number of cycles, the deformation under each load application is nearly completely recoverable and proportional to the load level and can be considered as elastic one (Haung, 2003). This behavior of unbound materials is characterized by resilient modulus. For repeated load triaxial tests with constant confining stress, the resilient modulus is defined as the ratio of the peak axial repeated deviator stress to the peak recoverable axial strain of the specimen as written in Eq. 2.2 (Lekarp et al., 2000). The response of deformation of granular material layers under traffic loading is characterized by a resilient deformation and a permanent deformation, which is illustrated in Fig. 2.25 (Kancherla, 2004).

NAASRA (1987) introduced that the Poisson's ratio of unbound materials is equal to 0.35. However, generally, the Poisson's ratio range between 0.30 to 0.35, depending on the different soil types.

$$M_R = \frac{(\sigma_1 - \sigma_3)}{\varepsilon_1} \quad (2.2)$$

where:

M_R = the resilient modulus,

σ_1 = the major principal or axial stress,

σ_3 = the minor principal or confining stress, and

ε_1 = the major principal or axial resilient strain.

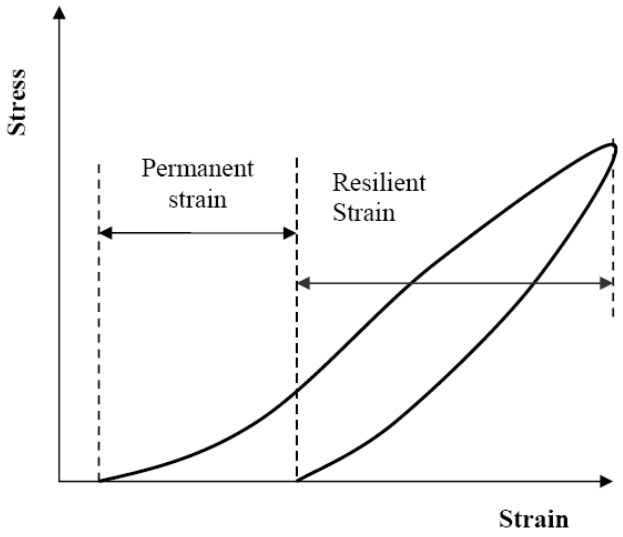

Figure 2.25 Strains in unbound materials during one load cycle (after Kancherlka, 2004).

2.6.2 Asphaltic Concrete Behavior

Van Der Poel (1954) described that the behaviors of asphaltic cement and asphaltic concrete are viscoelastic and their stiffness (S_b) values depend on temperature and loading time. The relationships between stiffness of asphaltic cement under different temperatures and loading time as shown in Fig. 2.26. It has found that the behavior of asphaltic cement at short period was elastic and at long time period was viscous. The calculation of stiffness is as follows:

$$S_b = \frac{3\eta}{t} \quad (2.3)$$

where:

S_b = the stiffness of asphaltic cement,

η = the dynamic viscosity, and

t = the loading time.

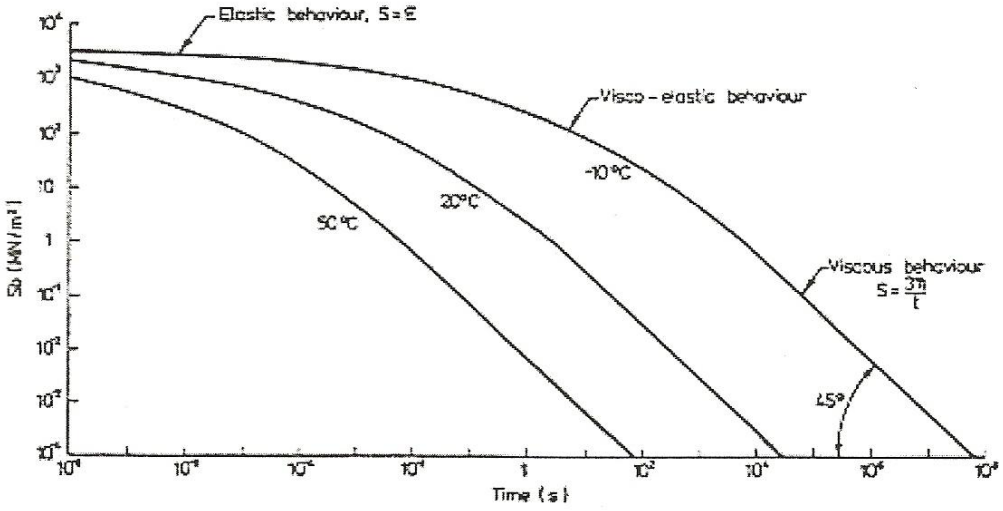

Figure 2.26 Relationships between stiffness of asphaltic cement at different temperatures and loading time (after Van Der Poel, 1954).

Barkdale and Hicks (1972) reported results from repeated triaxial loading tests on the samples of asphaltic concrete. It was found that binder content of asphaltic cement, air void, and particle size of aggregate had less effect on stiffness value.

Sousa and Monismith (1987) studied the dynamic modulus of asphaltic concrete by varying different temperatures and loading frequencies when subjected to sinusoidal loading (Fig. 2.27). The stiffness of asphaltic concrete tended to decrease an increase in the temperature. On the other hand, stiffness of asphaltic concrete tended to increase which an increase in loading frequency.

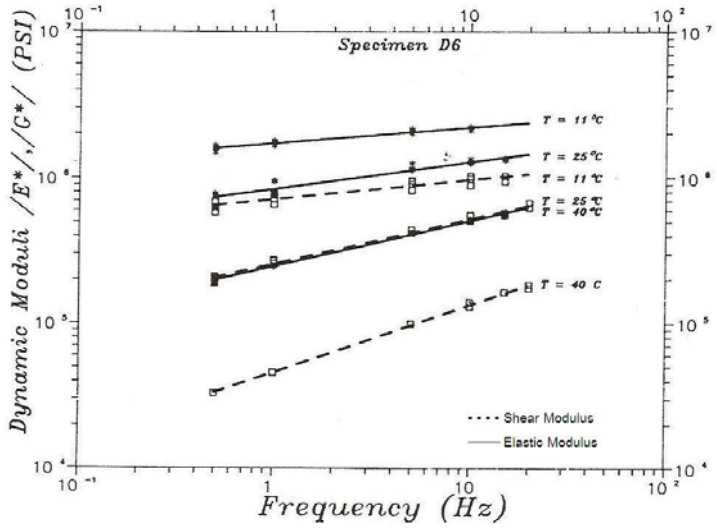

Figure 2.27 Relationships between dynamic moduli of asphaltic cement at different temperatures and frequency (after Sousa and Monismith, 1987).

Ruenkrairergsa and Phromsorn (2001) studied properties of asphaltic concrete pavements in Thailand and proposed that the Poisson's ratio (ν) was equal to 0.35, when the temperature ranges between 15 °C to 25 °C and equal to 0.40 when the temperature ranges between 35 °C to 40 °C, successively. The average stiffness modulus of asphaltic concrete ranges between 2,468 MPa to 13,181 MPa.

2.7 Light Falling Weight Devices (LFWD)

2.7.1 Characterization of LFWD

The Light Falling Weight Device (LFWD) is a small-scale of the general FWD (Fig. 2.28). During a field test with the LFWD, an impact load is applied to the subsoil via a rigid circular steel plate (loading plate). The device consists of a falling weight and a guide rod. The falling weight is dropped down along the guide rod and hits a shock absorber. In general, the falling height is approximately 0.7 m. The rod rests on a sphere at the middle of the load plate (without connection), and thus only compressive force can be transferred onto the loading plate. A sensor installed in the center of the loading plate records the acceleration, which subsequently renders the (maximum) plate displacement (Adam and Adam, 2003).

In a simplified procedure, the average maximum plate displacement of three consecutive tests leads to an approximation of the dynamic deformation modulus of the tested soil layer. Thereby, the maximum soil-contact stress is hypothetically assumed to be a constant (i.e., assumed to be independent of the soil type). Eventually, the dynamic deformation modulus can be related to the compaction degree of the tested soil layer.

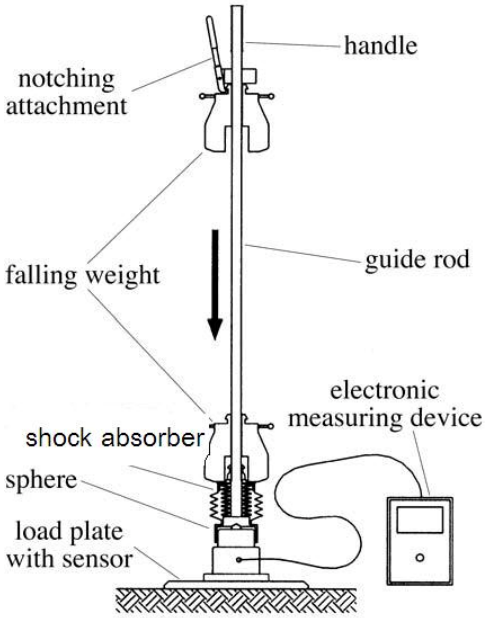

Figure 2.28 Schematic illustration of the Light Falling Weight Devices (LFWD) (after Adam and Adam, 2003).

2.7.2 Dynamic Simulation

In general, the dynamic analysis is based on modeling of the impact of a rigid weight on a simple soil mass-spring-dashpot model. For soils that are nearly incompressible (e.g., saturated), as is the case of pavements, soil mass can be ignored without compromising the model's accuracy (e.g., Lysmer, 1965; Verbic and Veletsos, 1972). Thus, the model simplifies essentially to a rigid mass impinging to a spring-dashpot system (Fig. 2.29). A discussion on the subject by Thilakasiri et al. (1996) and Roesset et al. (1996) provided some additional interesting clues about the suitability of the model, mainly in experimental endeuce support of its validity.

The equation that describes the motion of a rigid mass (M) impinging vertically on a spring-dashpot system, and remaining in contact with it thereafter, is the well-known linear equation for a single degree of freedom system as written in Eq. 2.4:

$$M\ddot{u} + C\dot{u} + Ku = Mg \qquad \textbf{(2.4)}$$

where:

M **= the summation of the mass between the mass of the plate of the FWD (M_p) and the mass of the falling weight (M_w)**

C **= characteristic parameters of the spring,**

K = characteristic parameters of the dashpot,

g = the gravitational acceleration,

u = the deformation,

$\dot{u}, \ddot{u}$ = the first and second derivatives of u over time.

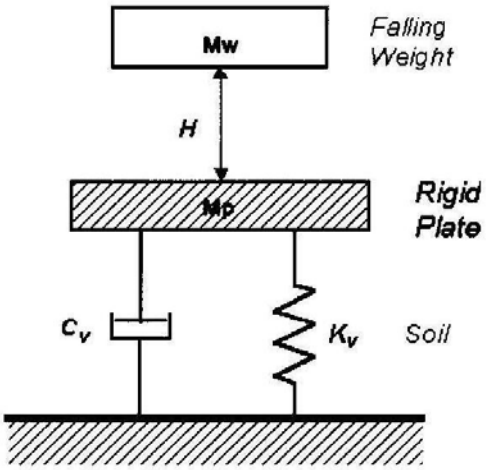

Figure 2.29 The rigid mass impinging to rigid plate on spring-dashpot system in parallel (after Loizos et al., 2003).

For impulse-load NDT equipment, the force-pulse duration is the length of time between an initial rise in the dynamic load until it dissipates to near zero. FAA (2004) recognized a pulse duration in the range of 20 ms to 60 ms as being typical for most impulse-load devices. Likewise, rise time is the time between an initial rise in the dynamic load and its peak before it begins to dissipate. Typical rise times for impulse load devices are in the range of 10 ms to 30 ms. The typical dynamic load pulse of the LFWD is shown and described in Fig. 2.30.

2.8 Comparison of Stiffness Evaluation between FWD and Conventional Methods

When comparing results evaluated from FWD methods with the results from traditional methods, it was found that, fore almost every case, the stiffness values from FWD methods were higher than ones from traditional methods. George (2003) reported measured elastic stiffness moduli of foundation materials by using various methods: i.e., Loadman, German Dynamic Plate Bearing Test (GDP), and TRL Foundation Tester (TFT). It was found that the results from field tests suggested the following stiffness relationship: TFT = 0.9 FWD and GDP = 0.6 FWD, with a significant degree of scattering.

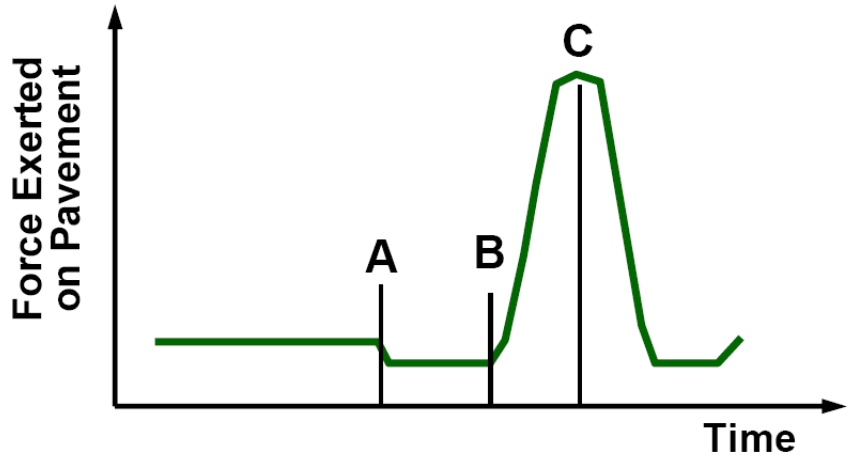

Figure 2.30 Typical load pulse of the Light Falling Weight Devices (LFWD): A) time at which load is released; B) time at which load makes first contact with load plate; and C) peak load reached (after FAA, 2004).

Loizos et al. (2003) compared the mean values of the subgrade modulus for all tested sections obtained by different methods of analysis as presented in Fig. 2.31. It is observed that the dynamic analysis of FWD provides higher estimates when compared to the static analysis, with the ratio of the two ranging between 0.82 to 0.88.

Ping et al. (2002) compared the values of resilient modulus (M_r) from laboratory with the resilient modulus from FWD-backcalculated. The comparison is shown in Fig. 2.32. There was a reasonable correlation relationship existed between the FWD- backcalculated moduli and the laboratory resilient moduli based on in-situ conditions with identical states of stress. The regressive equation is $M_{r(FWD)} = 1.6539 M_{r(LAB)}$ with $R^2 = 0.3$.

From the foregoing comparison, the FWD-backcalculated moduli were about 1.65 times higher than the laboratory resilient moduli. The ratio is in general agreement with the suggestion by the AASHTO design guide that the FWD-backcalculated moduli are approximately two to three times higher than the laboratory determined moduli (AASHTO, 1993)

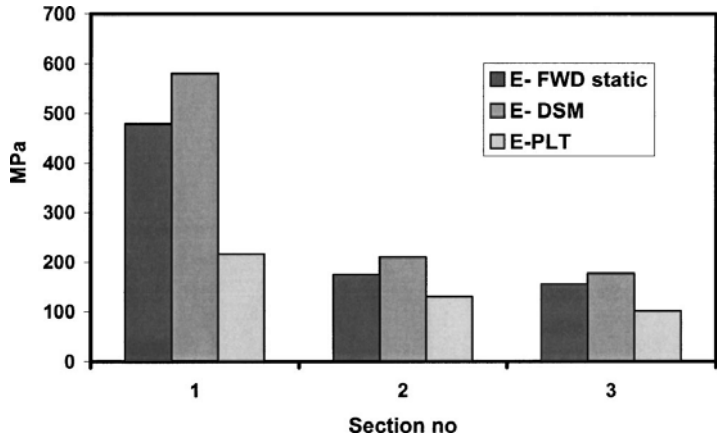

Figure 2.31 Mean modulus values obtained by different methods of analysis (after Loizos et al., 2003).

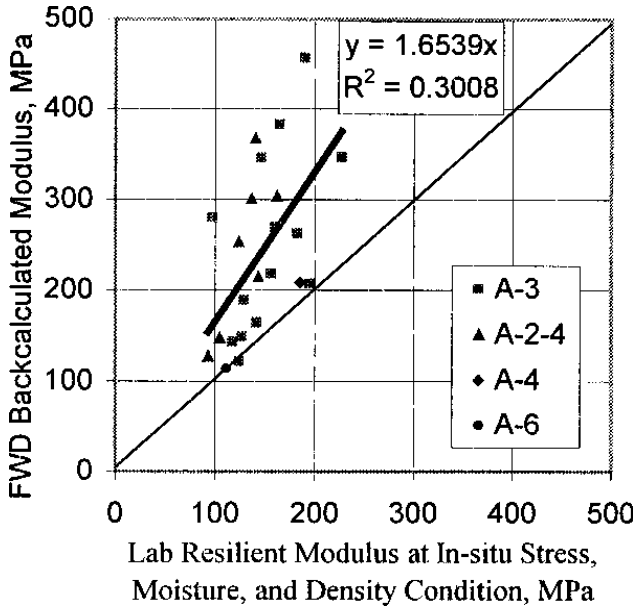

Figure 2.32 The modulus of resilient (M_R) at in situ condition versus FWD backcalculated (after Ping et al., 2002).

2.9 Effect of Different Stiffness Values between FWD and Conventional Methods

2.9.1 Dynamic Effects

The relationship between load and deformation under the impact load that the maximum force and the maximum deflection exhibit at the different times and the different time was called "time-lag". The time-lag is the effect of the damping properties of the material and the wave propagation (Brigham, 1974).

For purely elastic materials, stress and strain are in the same phase, such that the response of one caused by the other is immediate. On the other hand, for purely viscous materials, strain lags stress by a 90- degree phase lag (Wikipedia, n.d.).

Generally, geomaterials are viscoelastic materials whose that behaviors are somewhere in between these two types of the above-mentioned material, exhibiting some lag in strain. Burmister (1943; 1945; 1947) proposed an equation for calculating the stiffness values of material based on elastic theory as follow:

$$E = \frac{\pi \sigma_0 r}{2\Delta}\left(1-\nu^2\right) \tag{2.5}$$

where:

E = the modulus of elasticity of the material,

σ_0 = the peak pressure applied to the circular plate,

r = the radius of the circular plate,

Δ = the peak deflection of the plate associated with the pressure, and

ν = the Poisson's ratio.

2.9.2 Loading Rate Effects

Loading rate effect is herein defined as a time-dependent stress-strain response of a given type of geomaterial due to the viscous property, typically noted by creep deformation, stress-relaxation and strain rate effects on stress-strain behavior during monotonic loading (ML). The viscous property is a function of instantaneous irreversible (or visco-plastic) strain rate ($\dot{\varepsilon}^{ir}$ or $\dot{\varepsilon}^{vp}$) and other relevant parameters, not by time (Di Benedetto et al., 2002, 2005; Tatsuoka et al., 2002, 2003a, 2008; Tatsuoka, 2004, 2007).

2.9.2.1 Non-linear three-component model

Non-linear three-component model has a basic structure as shown in Fig. 2.33a. Figure 2.33b shows the stress decomposition in the case of triaxial compression (TC) and plane strain compression (PSC) tests. According to this model, irrespective of viscosity type, with or without cohesion and whether ageing is active or not, the stress (i.e., the effective stress), σ_{ij}, represented by point *B* in Fig. 2.33b, is obtained by adding the viscous stress component, σ_{ij}^{v}, represented by the vector $\overrightarrow{FB}$, to the inviscid (or rate-independent) stress component, σ_{ij}^{f}, at the same irreversible strain, ε_{ij}^{ir}, represented by stress point *F*. The strain rate, $\dot{\varepsilon}_{ij}$, is obtained by adding the irreversible (or inelastic or visco-plastic)

strain rate, $\dot{\varepsilon}_{ij}^{ir}$, to the elastic strain rate, $\dot{\varepsilon}_{ij}^{e}$. *E* and *P* bodies connected in series represent classical elasto-plastic models. The most challenging part is adequate modelling of *V* body, as it interacts in a very complicated way with *P* body while it is very difficult to experimentally evaluate its properties (Di Benedetto et al., 2002; Tatsuoka et al., 2002).

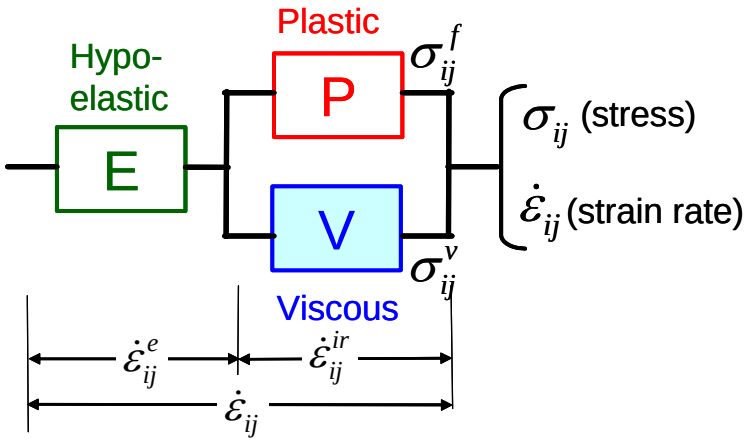

a)

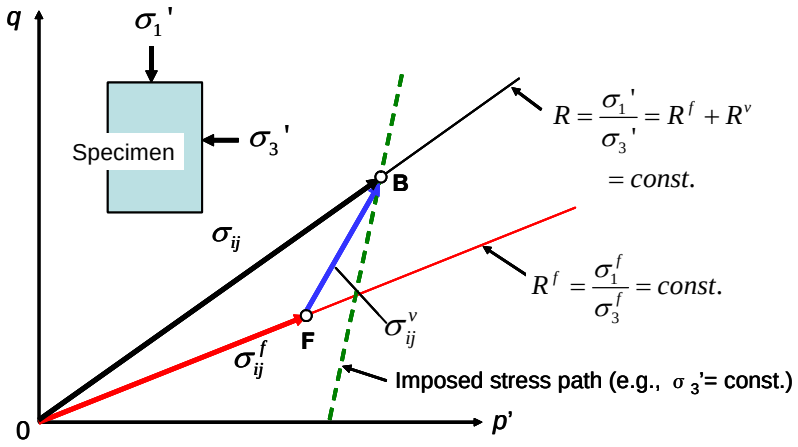

b)

Figure 2.33 a) Non-linear three-component model (Di Benedetto et al., 2002; Tatsuoka et al., 2002); and b) stress parameters on $q = (\sigma_1' - \sigma_3') - p' = (\sigma_1' + 2\sigma_3')/3$ plane in TC and PSC tests.

A given strain increment, $d\varepsilon$, consists of an elastic (i.e., rate-independent and reversible) component, $d\varepsilon^{e}$, and a rate-dependent and irreversible (i.e., inelastic or visco-plastic) component, $d\varepsilon^{ir}$, as:

$$d\varepsilon = d\varepsilon^{e} + d\varepsilon^{ir} \tag{2.6}$$

$d\varepsilon^{e}$ takes place only in component E, and is obtained by a hypo-elastic model, which has a set of elastic moduli that are all a function of instantaneous stress state (and also strain history when relevant).

A given effective stress, σ, consists of an inviscid (i.e., rate-independent) component, σ^{f}, and a viscous (i.e., rate-dependent) component, σ^{v}, as:

$$\sigma = \sigma^{f} + \sigma^{v} \tag{2.7}$$

σ^{f} is a unique function of irreversible strain, ε^{ir}, in the monotonic loading (ML) case along a fixed stress path in which the irreversible strain rate, $\dot{\varepsilon}^{ir} = d\varepsilon^{ir} / dt$, is always positive irrespective of the sign of stress rate, $\dot{\sigma}$. The $\sigma^{f} - \varepsilon^{ir}$ relation becomes hysteretic under cyclic loading conditions. The related flow rule is modeled in terms of σ^{f} similarly as the conventional elasto-plastic theories. So, any elasto-plastic model can be extended to a non-linear three-component model by adding the σ^{v} component appropriately.

The viscous stress increment, $d\sigma^{v}$, develops by either $d\varepsilon^{ir}$ or its rate, or both. Then, "the increment $d\sigma^{v}$ when $\varepsilon^{ir} = \tau$" is given as:

$$\left[d\sigma^{v} \right]_{(\tau)} = \left[d\left\{ \sigma^{f}\left(\varepsilon^{ir}\right) \cdot g_{v}\left(\dot{\varepsilon}^{ir}\right) \right\} \right]_{(\tau)} \tag{2.8}$$

It is assumed that Eq. 2.8 can be applied to all the types of viscosity described in this research. $g_{v}\left(\dot{\varepsilon}^{ir}\right)$ is the viscosity function, which is always zero or positive, given as follows for any strain $(d\varepsilon^{ir})$ or stress $\left(\sigma^{f}\right)$ path (with or without cyclic loading; i.e., irrespective of the sign of $\dot{\varepsilon}^{ir}$):

$$g_{v}(\dot{\varepsilon}^{ir}) = \alpha \cdot [1 - \exp\{1 - (\frac{|\dot{\varepsilon}^{ir}|}{\dot{\varepsilon}_{r}^{ir}} + 1)^{m}\}] \quad (\geq 0) \tag{2.9}$$

where:

$|\dot{\varepsilon}^{ir}|$ = the absolute value of $d\varepsilon^{ir}$, and

α, $\dot{\varepsilon}^{ir}$ and m = the positive material constants (dimensionless).

These constants α, $\dot{\varepsilon}^{ir}$ and m for a given type of geomaterial are determined based on the rate-sensitivity coefficient, β (Di Benedetto et al., 2002; Tatsuoka et al., 2002, 2006; Tatsuoka, 2004).

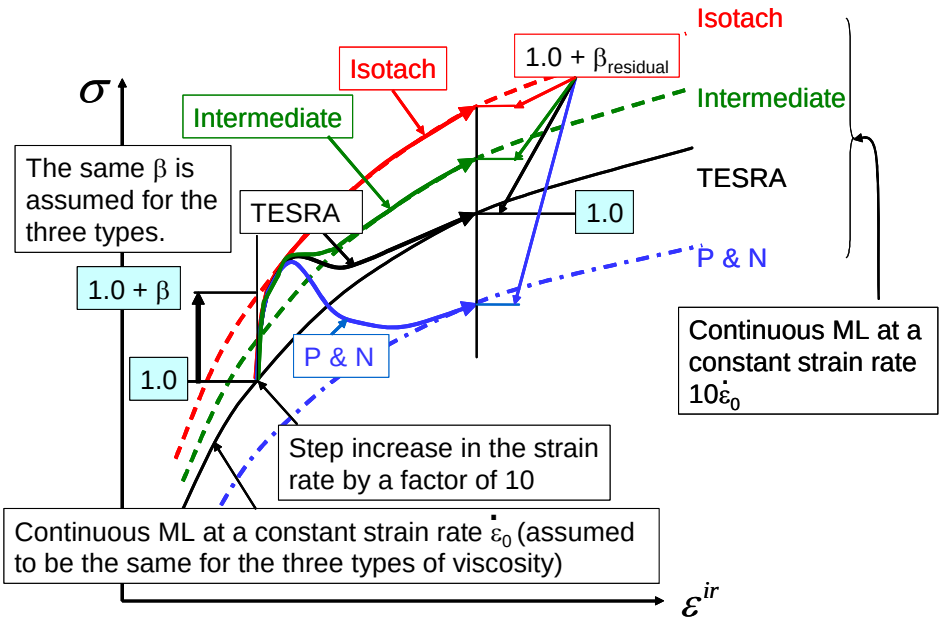

Figure 2.34 Different viscosity types of geomaterial and definition of the rate sensitivity coefficient (in the case of strain rate change by a factor of 10) (after Di Benedetto et al., 2004: Tatsuoka, 2004; Enomoto et al., 2006; Tatsuoka, 2006).

2.9.2.2 Viscosity Function

In Fig. 2.34, it is assumed that the $\sigma - \varepsilon^{ir}$ relation before a step change in the strain rate by a factor of 10 is the same for different viscosity types. The changing rate of stress upon a step change in the irreversible strain rate is defined as the rate-sensitivity coefficient, β, as follows (Di Benedetto et al., 2004; Tatsuoka, 2004; Tatsuoka et al., 2006):

$$\beta = \frac{\Delta\sigma / \sigma}{\log\left\{\left(\dot{\varepsilon}^{ir}\right)_{after} / \left(\dot{\varepsilon}^{ir}\right)_{before}\right\}} \qquad (2.10)$$

where $\Delta\sigma$ is the stress jump upon a step change in the strain rate (more rigorously, upon a step change in $\dot{\varepsilon}^{ir}$ at a fixed value of ε^{ir}), which is equal to a jump in

σ^v and $\Delta\sigma^v$, σ is the total stress when the strain rate is stepwise changed, which is equal to the instantaneous value of $\sigma^f + \sigma^v$ and $(\dot{\varepsilon}^{ir})_{after}$ and $\left(\dot{\varepsilon}^{ir}\right)_{before}$ are the irreversible strain rates after and before a step change, $(\dot{\varepsilon}^{ir})_{after} / (\dot{\varepsilon}^{ir})_{before} = 10$ where in the illustration in Fig. 2.34. For simplicity, the same value of β is assumed for the different viscosity types. The actual β value is a function of soil type (Enomoto et al., 2006; Tatsuoka, 2006).

For Unbound Materials: Di Benedetto et al. (2002) and Tatsuoka et al. (2002) defined the viscosity function for unbound geomaterial (i.e., clay, sand and gravel) using the effective principal stress ratio, $R = \sigma_1'/\sigma_3'$, as the stress parameter (i.e., R for σ and $R^f = \sigma_1^f{}'/\sigma_3^f{}'$ for σ') of the three-component model (Fig. 2.33a) and expressed Eq. 2.8 as summarised below.

$$R^v\left(\gamma^{ir}, \dot{\gamma}^{ir}\right) = R^f\left(\gamma^{ir}\right) \cdot g_v\left(\dot{\gamma}^{ir}\right) \tag{2.11a}$$

where γ is the shear strain $\left(= \varepsilon_1 - \varepsilon_3\right)$. The incremental form is:

$$d\{R^v\left(\gamma^{ir}, \dot{\gamma}^{ir}\right)\} = d\{R^f\left(\gamma^{ir}\right) \cdot g_v\left(\dot{\gamma}^{ir}\right)\} \tag{2.11b}$$

Referring to Fig. 2.35, the viscous stress ratio, R^v, is obtained as:

$$R^v = R - R^f \tag{2.12}$$

where R is the measured values of σ_1'/σ_3', which is equal to $(\sigma_1^f + \sigma_1^v)/(\sigma_3^f + \sigma_3^v)$. The current stress state (σ_1', σ_3') (before a step change in the strain rate) is represented by point ***B*** in Fig. 2.35. R^f is the inviscid principal stress ratio, equal to σ_1^f / σ_3^f. The current inviscid stress state (σ_1^f, σ_3^f) is represented by point ***F***. Note that R^v is not equal to σ_1^v / σ_3^v, but equal to $(\sigma_1^f + \sigma_1^v)/(\sigma_3^f + \sigma_3^v) - (\sigma_1^f / \sigma_3^f)$. For example, in TC at a constant σ_3', R^v is equal to σ_1^v / σ_3^f if $\sigma_3^v = 0$. Kiyota and Tatsuoka (2006) showed that Eq. 2.11b together with Eq. 2.12 are relevant also to describe the viscous property of sand in the triaxial extension tests at a fixed confining pressure, σ_1'.

The viscosity function, $g_v\left(\dot{\gamma}^{ir}\right)$, of Eq. 2.11, which is relevant to the TC, TE and PSC test conditions, is obtained from Eq. 2.9 as:

$$g_v(\dot{\gamma}^{ir}) = \alpha \cdot [1 - \exp\{1 - (\frac{|\dot{\gamma}^{ir}|}{\dot{\gamma}_r^{ir}} + 1)^m\}] \quad (\geq 0) \tag{2.13}$$

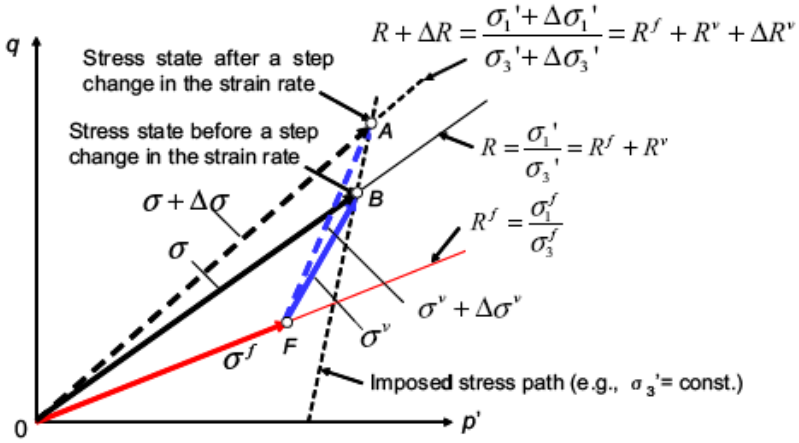

Figure 2.35 Viscosity function defined in terms of effective principal stress ratio, R (after Di Benedetto et al., 2002; Tatsuoka et al., 2002).

The parameters of Eq. 2.13 are determined from experimental data as follows. Points *B* and *A* in Fig. 2.35 represent the stress states, respectively, before and after a step change in the irreversible shear strain rate, $\dot{\gamma}^{ir}$. The associated jump in R, ΔR, is due solely to a change in $\dot{\gamma}^{ir}$ made at a fixed irreversible shear strain keeping R^f constant. Figure 2.36 shows a typical test result showing the definition of ΔR. Figure 2.37 shows typical data showing the relationships between the ratio of ΔR to the instantaneous value of R when the strain rate is stepwise changed and the logarithm of the ratio of the axial strain rates after and before a step change, which is essentially the same as the ratio of the irreversible shear strain rates, $(\dot{\gamma}^{ir})_{after} / (\dot{\gamma}^{ir})_{before}$. The results from the simulation by the three-component model (Fig. 2.33a) of these data are also presented in this figure. It may be seen from this figure that the following linear relation, which is independent of R, fits the data:

$$\frac{\Delta R}{R} = \beta \cdot \log_{10}\left(\frac{\dot{\gamma}_{after}^{ir}}{\dot{\gamma}_{before}^{ir}}\right) = b \cdot \ln\left(\frac{\dot{\gamma}_{after}^{ir}}{\dot{\gamma}_{before}^{ir}}\right) \tag{2.14}$$

where β is the rate-sensitivity coefficient; and $b = \beta / \ln 10$. The value of β of sand is rather insensitive to changes in the void ratio, the effective confining pressure and the wet condition (Nawir et al., 2003; Tatsuoka et al., 2006). Eq. 2.14 can be rewritten to the incremental form:

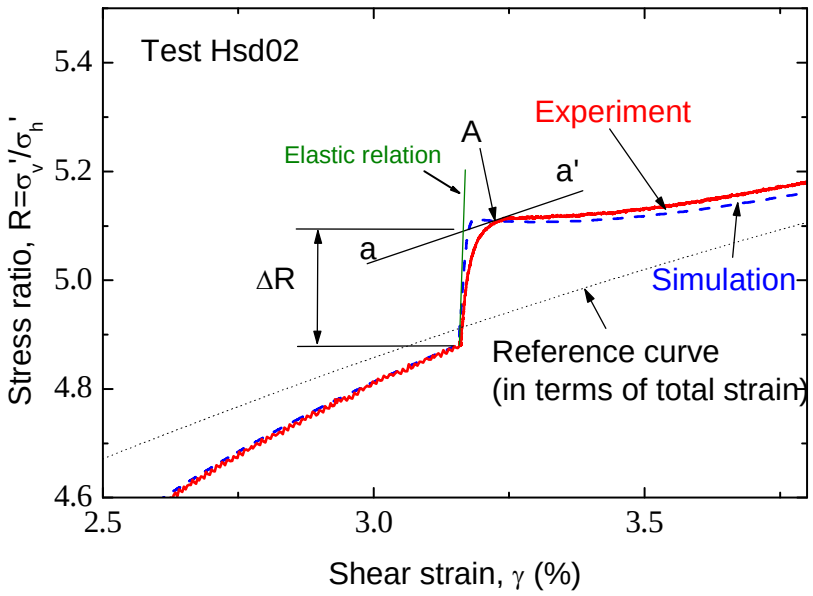

Figure 2.36 Definition of stress ratio jump ΔR by a step change in the irreversible shear strain rate in a drained PSC test on Hostun sand (after Di Benedetto et al., 2002).

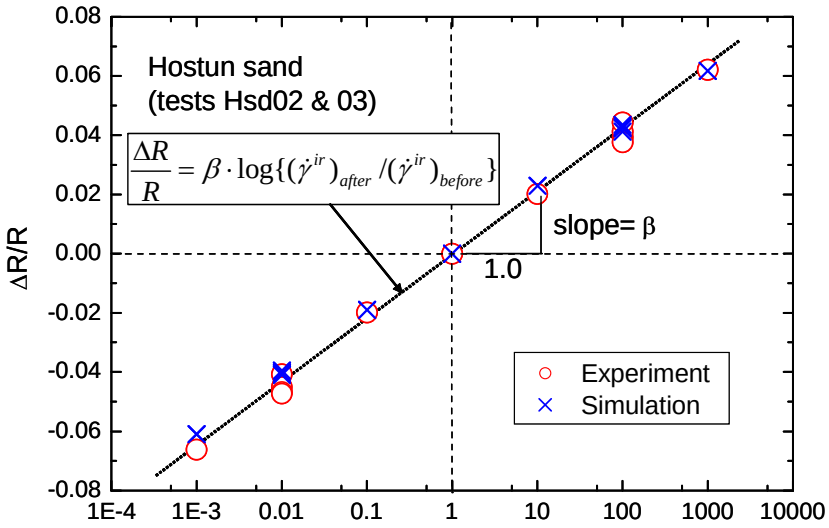

Ratio of strain rates after and before a step change

Figure 2.37 Definition of rate-sensitivity coefficient β in drained PSC tests on Hostun sand (Di Benedetto et al., 2002).

$$\frac{dR}{R} = b \cdot d\left(\dot{\gamma}^{ir}\right) \tag{2.15}$$

dR in Eq. 2.15 is defined for a fixed value of $\dot{\gamma}^{ir}$ and so for a fixed value of R^f (i.e., the value when the stress jump starts). Therefore, we obtain $dR = dR^v = d\{R^f \cdot g_v(\dot{\gamma}^{ir})\} = R^f \cdot d\{g_v(\dot{\gamma}^{ir})\}$ referring to Eq. 2.11b. Then, referring to Eqs. 2.11a and 2.12, we obtain:

$$\frac{R^f \cdot d\left\{g_v\left(\dot{\gamma}^{ir}\right)\right\}}{R^f + R^v} = \frac{R^f \cdot d\left\{g_v\left(\dot{\gamma}^{ir}\right)\right\}}{R^f \cdot \left\{1 + g_v\left(\dot{\gamma}^{ir}\right)\right\}} = \frac{d\left\{g_v\left(\dot{\gamma}^{ir}\right)\right\}}{1 + g_v\left(\dot{\gamma}^{ir}\right)} = b \cdot d\left(\ln \dot{\gamma}^{ir}\right) \tag{2.16}$$

This equation is assumed to be valid to any imposed stress path satisfying the loading conditions, $\dot{\gamma}^{ir} > 0$, changing σ_1' or σ_3' or both. To obtain the viscosity function, $g_v(\dot{\gamma}^{ir})$, we do not need to obtain the location of point *F* (i.e., we do not need to obtain the values of σ_1^f and σ_3^f as well as σ_1^v and σ_3^v) and actually we cannot obtain these values only from such experimental data as shown in Figs. 2.36 and 2.37. Then, we obtain:

$$d\left\{\ln\left(1 + g_v(\dot{\gamma}^{ir})\right)\right\} = b \cdot d\left(\ln \dot{\gamma}^{ir}\right) \tag{2.17a}$$

By integrating Eq. 2.17a with respect to $\dot{\gamma}^{ir}$, we obtain:

$$1 + g_v\left(\dot{\gamma}^{ir}\right) = c_v\left(\dot{\gamma}^{ir}\right)^b \tag{2.17b}$$

where c_v is a constant. As shown in Fig. 2.38, the viscosity function (Eq. 2.13) should be defined so that the linear part for a range of $\dot{\gamma}^{ir}$ for which Eq. 2.17b was derived has a slope equal to $b = \beta / \ln 10$. That is, Eq. 2.17b is valid only for a range of $\dot{\gamma}^{ir}$ larger than a certain lower limit while smaller than a certain upper limit. A relevant value should be assumed for parameter α, which represents the upper bound of $g_v(\dot{\gamma}^{ir})$ when $\dot{\gamma}^{ir}$ becomes infinitive. A parameter m is then obtained by trial and error.

For Bound Materials: The stress parameter R, which is used in the formulation of the viscous property for bound geomaterials should be replaced with a more relevant stress parameter. Kongsukprasert et al. (2004) shows the results from drained TC tests at

constant σ_3' on bound materials; compacted cement-mixed well-graded gravel, that the following relation is relevant in place of Eq. 2.14:

$$\frac{(\Delta q / p_a)_{d\varepsilon_a^{ir}=0}}{(q+q_c)/p_a} = \beta \cdot \log\left[(\dot{\varepsilon}_a)_{after} / (\dot{\varepsilon}_a)_{before}\right] \approx \beta \cdot \log\left[(\dot{\gamma}^{ir})_{after} / (\dot{\gamma}^{ir})_{before}\right] \quad (2.18)$$

where:

Δq = the jump of the deviator stress, q, upon a step change in the strain rate,

q_c = a constant, independent of *q* at which Δ*q* is obtained, and

p_a = 98 kPa.

As σ_3' is kept constant, the left-side term of Eq. 2.18 becomes:

$$\frac{\Delta\sigma_1'}{(\sigma_1'+c)} = \frac{\Delta(\sigma_1'+c)}{(\sigma_1'+c)} = \frac{\Delta(\sigma_1'+c)/(\sigma_3'+c)}{(\sigma_1'+c)/(\sigma_3'+c)} \quad (2.19)$$

Eq. 2.19 indicates that, for bound geomaterials, it is relevant to redefine R as $(\sigma_1'+c)/(\sigma_3'+c)$, where c is a constant equal to $q_c - \sigma_3'$, in Eqs. 2.11 and 2.12.

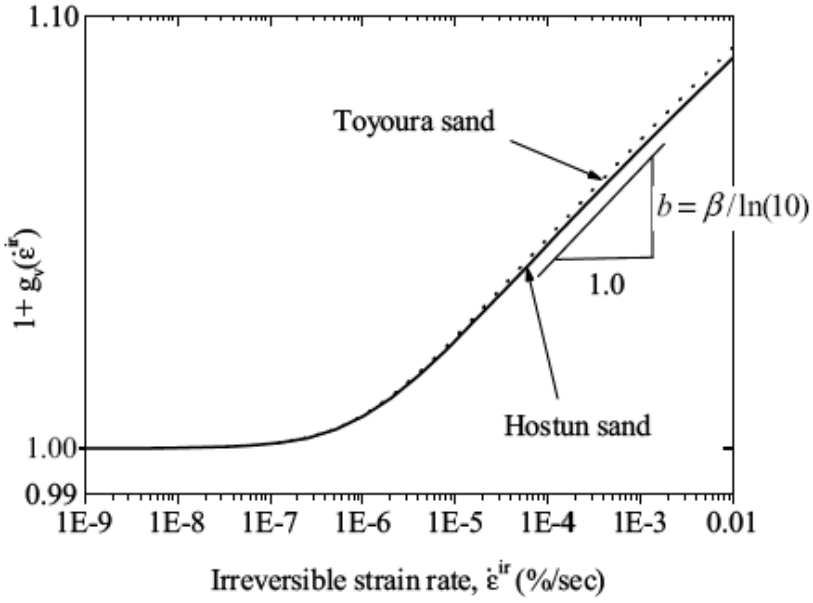

Figure 2.38 Viscosity functions of Toyoura and Hostun sands determined based on the values of β measured by drained PSC tests (Di Benedetto et al., 2002).

2.10 Free Vibration of a Spring-Mass System

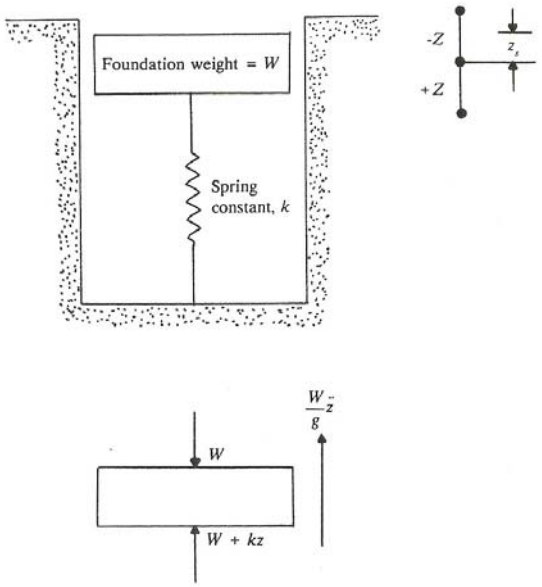

Figure 2.39 Free Vibration of a Spring-Mass System of rigid foundation (after Das, 1992)

Figure 2.39 shows a foundation resting on a spring. Let the spring represent the elastic properties of the soil. The load W represents the weight of the foundation plus that which comes from the machinery supported by the foundation. The time histories of displacements, z, can be calculated as (Das, 1992):

$$z = z_0 \cdot \cos\left(\sqrt{\frac{k}{m}} \cdot t\right) + \frac{v_0}{\sqrt{k/m}} \cdot \sin\left(\sqrt{\frac{k}{m}} \cdot t\right) \tag{2.20}$$

Now let

$$z_0 = Z\cos\alpha \tag{2.21}$$

and

$$\frac{v_0}{\sqrt{k/m}} = Z\sin\alpha \tag{2.22}$$

Substitution of Eqs. 2.21 and 2.22 into Eq. 2.20 yields:

$$z = Z\cos(\omega_n \cdot t - \alpha) \tag{2.23}$$

where

$$\alpha = \tan^{-1}\left(\frac{v_0}{z_0 \cdot \sqrt{k/m}}\right) \quad (2.24)$$

and

$$Z = \sqrt{z_0^2 + \left(\frac{v_0}{\sqrt{k/m}}\right)^2} = \sqrt{z_0^2 + \left(\frac{m}{k}\right) \cdot v_0^2} \quad (2.25)$$

where:

v_0 = the rate of displacement, z,

k = the spring constant,

m = the mass of foundation,

t = the elapsed time,

z = the displacement,

z_0 = the initial displacement due to selfweight of foundation,

Z = the maximum displacement,

α = the initial time of maximum displacement, and

ω_n = the natural angular velocity.

CHAPTER 3 METHODOLOGY

3 METHODOLOGY

3.1 Introduction

The method to evaluate the stiffness values of pavement structure by the FWD device is not standardized. On the other hand, the PLT method can be referred by various standard test agencies such as the American Society for Testing and Materials (ASTM), the American Association of State Highway and Transportation Officials (AASHTO), and Florida Department of Transportation (FDOT), etc.

In this research, the pavement structures were modeled from full scale to laboratory scale. That is, the subgrade layer in the field was modified and replaced by sand, and the unpaved surface pavement were modeled by gravel layer on the top of the subgrade layer. In addition, for paved surface, asphaltic concrete surface placed on the top of the subgrade layer was also modified and scaled down. All pavement surfaces were tested by FWD device and PLT method and were performed in a temperature-controlled laboratory (25°C). The studies in this research can be divided into two main parts as follows:

(1) Model test to understand the dynamic-effect and rate-effect that affect on the differences between FWD and PLT results.

(2) Integrated analysis of the response from dynamic load to develop a framework for evaluating of stiffness values of pavement surface.

Theoretical backgrounds of items (1) and (2) were described in Chapter 2. In this chapter, methodology will be shown to explain the differences between FWD and PLT results. Then, the method to evaluate the stiffness values of pavement structure by FWD device that are similar to the values obtained based on PLT results are presented.

3.2 Research Assumption

To develop a framework for evaluating of stiffness values in two-layer system, several assumptions are required to simplify the analysis. Due to that the model test are scaled down in laboratory in this research, some conditions and devices are not the same as in the field. Assumptions employed in this research can be listed as:

(1) For the boundary conditions of model test, it is very difficult to define a boundary within which the mobilized stresses ($\Delta\sigma_z$ and $\Delta\sigma_x$ or $\Delta\sigma_y$) in vertical and horizontal directions are equal to zero. Consequently, the mobilized stress at the boundary of model that is less than 5% of pressure on circular plate located at the center is treated acceptable.

(2) The steel loading plate acting on a surface layer is assumed as rigid plate and the contact plate pressure is uniform.

(3) The damping behavior of pavement materials in this research is assumed to be negligible.

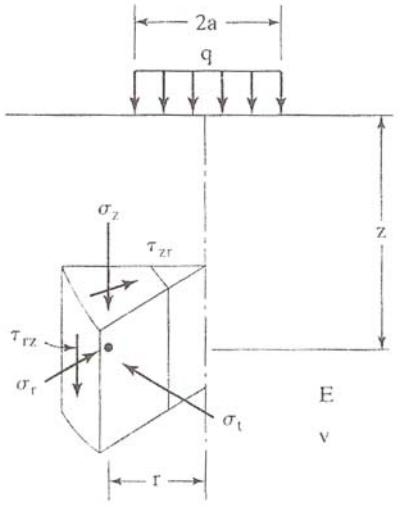

Figure 3.1 Schematic illustration of the stress raise under the uniformly circular plate (after Haung, 2003).

3.3 Boundary Conditions

Boussinesq (1885) proposed an equation to calculate the mobilized stress in soil mass due to loading for elastic homogeneous material, and the semi-infinite boundary. For uniform circular loading, the mobilized vertical stress can be calculated by Eq. 3.1 and Fig 3.1. Dimensions of container and loading plate are shown in Sections 3.5.1 and 3.5.3, respectively.

$$\Delta\sigma_z = \frac{3q}{2\pi z^2}\int_0^a\int_0^{2\pi}\left[\frac{1}{1+(\frac{r-a}{z})^2}\right]^{5/2} a\partial\theta\partial a = q(I_B) \qquad (3.1)$$

where:

$\Delta\sigma_z$ = the mobilized stress (kPa),

q = the load pressure on circular plate (kPa),

z = the depth below circular plate (m),

a = the circular plate radius (m),

r = the distance from center of circular plate in horizontal direction (m),

∂a = the first derivatives of R,

$\partial\theta$ = the first derivatives of perimeter, and

I_B = Boussinesq's Influence Factor.

3.4 Materials Preparation and Testing

3.4.1 KMUTT sand (for subgrade)

Subgrade layer in this research was modified and replaced by King Mongkut's University of Technology Thonburi Sand (KMUTT sand) as shown in Fig. 3.2. It is originally sedimented river bed sand from Ratchaburi province, Thailand. KMUTT sand was firstly prepared by sieving the original sand to pass through sieve No.40 (0.425 mm) and to retain on sieve No.100 (0.150 mm). Subsequently, it was washed by tap water to remove dust as well as undesired materials and then dried by an oven at temperature of 140°C for 24 hours to make it dried and eliminate any organic matter.

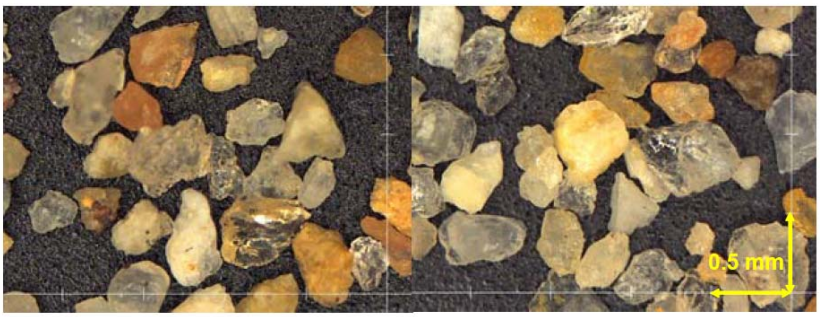

Figure 3.2 Particle photo of KMUTT sand.

3.4.2 Gravel (for unpaved surface)

Gravel layer (Fig. 3.3) was modified by coarse aggregates for modeling the gravel road (unpaved road surfaced). It was prepared by sieving the coarse aggregates to pass through sieve opening 3/8 in. (9.50 mm) and to retain on sieve No.4 (4.75 mm). Subsequently, it was cleaned by tap water and then dried by an oven at temperature of 140°C for 24 hours to make it dried and eliminate any organic matter, similar to KMUTT sand.

Figure 3.3 Particle photo of gravel.

Table 3.1 Gradation of aggregates for various type of asphaltic concrete layer.

DRR –Thailand Standard test No. 209-2545						DOT- USA State mix No.4	
Calling name	mm in.	9.5 (3/8)	12.5 (1/2)	19.0 (3/4)	25.0 (3/4)	Specification band	JMF
Type of layer		Wearing course	Wearing course	Binder course	Base course		
Thickness (mm)		25-35	40-70	40-80	70-100		
Sieving size							
mm	in.	Percent passing (by weight)					
37.5	1 1/2				100		
25.0	1			100	90-100		
19.0	3/4		100	90-100	-	100	100
12.5	1/2	100	80-100	-	56-80	85-100	93
9.5	3/8	90-100	-	56-80	-	72-88	85
4.75	No. 4	55-85	44-74	35-65	29-59	48-66	55
2.36	No. 8	32-67	28-85	23-49	19-45	30-47	37
1.18	No. 16	-	-	-	-	21-37	25
0.600	No. 30	-	-	-	-	15-27	17
0.300	No. 50	7-23	5-21	5-19	5-17	9-21	13
0.150	No. 100	-	-	-	-	6-16	10
0.075	No. 200	2-10	2-10	2-8	1-7	4-10	8
Asphaltic cement content (% by weight of aggregates)		4.0-8.0	3.0-7.0	3.0-6.5	3.0-6.0		

3.4.3 Asphaltic Concrete (for paved surface)

3.4.3.1 Aggregates

Generally, aggregates for asphaltic concrete including course aggregates, fine aggregates and mineral filler. In this research, aggregate for preparing asphaltic concrete including two parts of course aggregates and fine aggregates. For the good quality of specimens, the aggregates in use must be cleaned and classified as well-graded.

The particle distribution and size of aggregate used in this research were selected based on standard test number DRR 209-2545 of the Department of Rural Roads (DRR)-Thailand and Job Mix Formula (JMF) for a state mix No.4 of the Department of Transportation (DOT)-USA as shown in Table 3.1. For laboratory scale, asphaltic concrete layer thickness 50 mm. This thickness was reduce scaled-down this one from the original one. The original aggregate was for wearing course layer of which the size name was called "the 12.5 mm (1/2 in.)" and has maximum particle size of 19 mm (3/4 in.). Averagely, the particle size was scaled-down by a factor of 1.5 as:

$$B = 10^{\log(\frac{A}{x})} \qquad (3.2)$$

where:

B = the particle size after scaled-down (mm),

A = the particle size before scaled-down (mm), and

x = the scaled-down factor (equal to 1.5 in this research).

After scaled-down, the maximum particle size in this research is 12.5 mm and the percent finer of each particle sizes were shown in Table 4.5 in Section 4.2.3.1.

3.4.3.2 Asphaltic cement

Asphaltic cement used in this research is 60/70 grade following specification for hot-mixed asphaltic concrete by standard test number DRR 230-2545.

3.4.3.3 Mixing

Both the asphaltic cement of 60/70 grade and aggregates were heated in an oven for about two hours at temperature of $140 \pm 5\,^{o}C$ before bringing them for mixing (within one minute). Then, they were mixed on tray heated by a store as shown in Fig. 3.4, The amount of asphaltic cement used was at optimum asphaltic content of 5 % (by weight of aggregate) based on the Marshal's test results (Thaisri, 2007).

Figure 3.4 Mixing aggregates and asphaltic cement on a tray heated on a store.

3.4.3.4 Compaction

The specimen was compacted by hammer into two equivalent layers in cylindrical mold (inner diameter equal to 950 mm and 50 mm thickness) as shown in Fig. 3.5, with a controlled thickness of a compacted layer equal to 25 mm and a controlled density equal to 2.13 g/cm^3. Subsequently, the temperature of specimen is allowed to decrease until lower than 60^{o}C. Then, the specimen was removed from the mould and each specimen was cured, at least, for 16 hours before usage referring ASTM D 6927-06. After curing, a layer of asphaltic concrete was obtained as shown in Fig. 3.6.

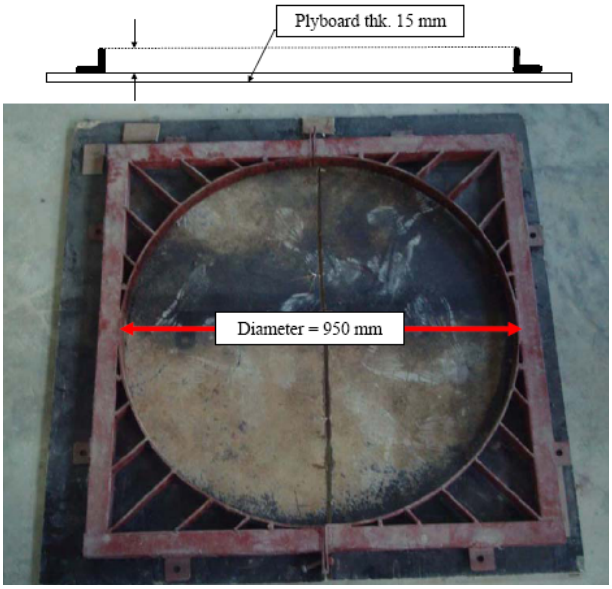

Figure 3.5 Mold for preparing asphaltic concrete layer specimen.

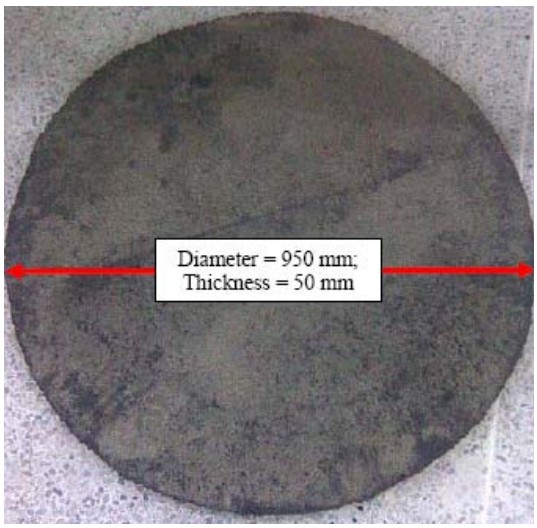

Figure 3.6 Asphaltic concrete specimen for modeling asphaltic concrete layer.

3.4.4 Index Tests of Pavement Materials

The consistency limits and index properties of pavement materials were determined by techniques guided by ASTM standard. The index tests of each pavement materials were summarized in Table 3.2.

Table 3.2 Summarized index tests of pavement materials.

Index properties	ASTM standards	Performed Materials
Minimum void ratio	ASTM D 4253-00	KMUTT sand
Maximum void ratio	ASTM D 4254-00	KMUTT sand
Specific gravity	ASTM D 854-00	KMUTT sand
Particle-size analysis	ASTM D 422-63	KMUTT sand Gravel Aggregates
Compaction test *Standard compaction test *Modified compaction test	ASTM D 698-07 ASTM D 1557-07	KMUTT sand

3.5 Experimental Equipments

3.5.1 Container

A container was used for scaled-down modeling of the pavement structures for testing in laboratory, as shown in Fig. 3.7. It was made from a cylindrical-shape concrete-tube that

has 1,000 mm in inner-diameter, 900 mm in height, and 50 mm in thickness in the radial direction. Each pavement material was filled in this container for modeling each layer of pavement structure from field full scale to laboratory scale.

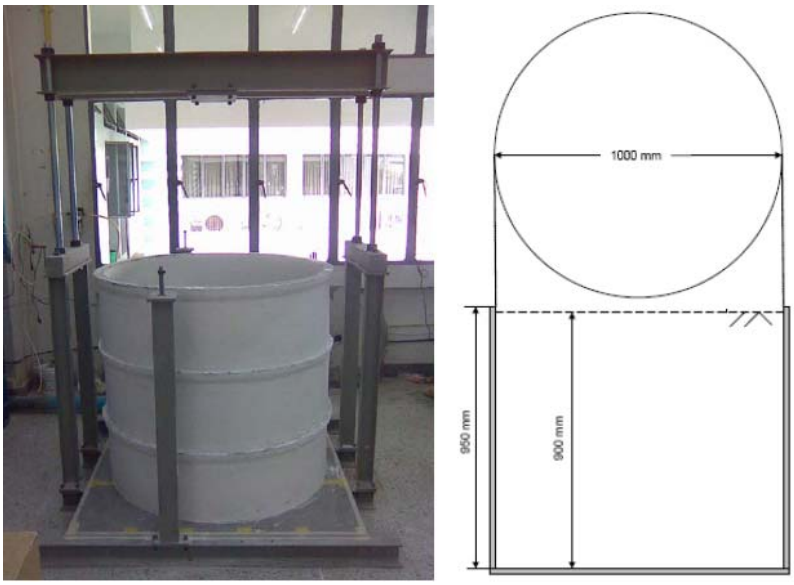

Figure 3.7 Container for modeling pavement structures.

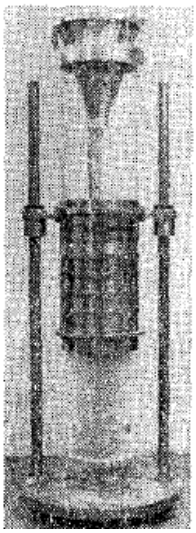

Figure 3.8 Typical pluviation manner in preparing triaxial sand specimen (after Miura and Toki, 1982).

3.5.2 Multiple Sieving Pluviation Apparatus

When preparing layers of KMUTT sand by compaction method, not only it is difficult to control the homogeny of sand layer but also it is possible that sand particles be broken which results in variation of particle-size distribution. In place of compaction, the multiple sieving pluviation apparatus was used to prepare subgrade layer by pluviating air-dried

KMUTT sand through air into the container. In this research, multiple sieving pluviation apparatus was modified and made based on the typical pluviation manner in preparing triaxial sand specimen as shown in Fig. 3.8 (Miura and Toki, 1982).

The multiple sieving pluviation apparatus has 500 mm in width, 1,200 mm in length, and 600 mm in height, as shown in Fig. 3.9. The flow rate of air-dried KMUTT sand was controlled by the drawer that places on the top of sieving. By this method, layer of KMUTT sand was successfully prepared uniformly and density.

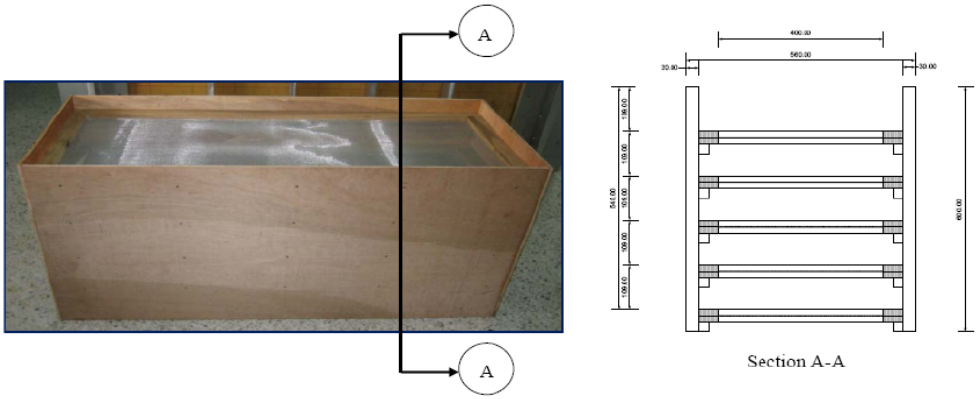

Figure 3.9 Multiple sieving pluviation apparatus for preparing subgrade layer.

3.5.3 Falling Weight Deflectometer (FWD) Device

A light-weight FWD device was newly produced to perform experiments in this research, by modifying from the original one made by Hirakawa et al. (2008). This small-size FWD can be easily carried to be manually operated on many locations. Impact loads and consequent deflections was respectively directly measured by a load cell and indirectly measured by accelerometers. The hammer can be lift with human power or simple equipment and used to generate impulse load. The outline of FWD is shown in Fig. 3.1. Moreover, the configurations of this small FWD device is shown in Table 3.3.

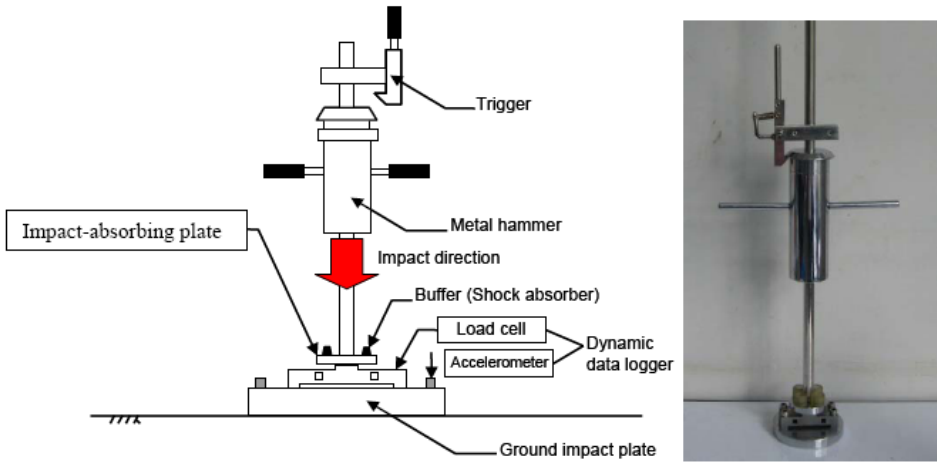

Figure 3.10 Schematic diagram showing detail of small FWD device.

Table 3.3 Configuration of a light-weight FWD device.

Items	Values
Weight of metal hammer	10 kg
Maximum falling height	500 mm
Maximum impulse load	20 kN
Loading plate diameter	150 mm
Impact load measurement	Load cell
Displacement measurement	Accelerometer
Measurement sampling	~ 5 kHz
Total weight	19.23 kg

3.5.4 Loading Frame

A loading frame was used for performing PLT tests. Fig 3.11 shows a schematic diagram of the loading frame. A reference beam was installed on the base of the loading frame for installations of displacement measuring devices.

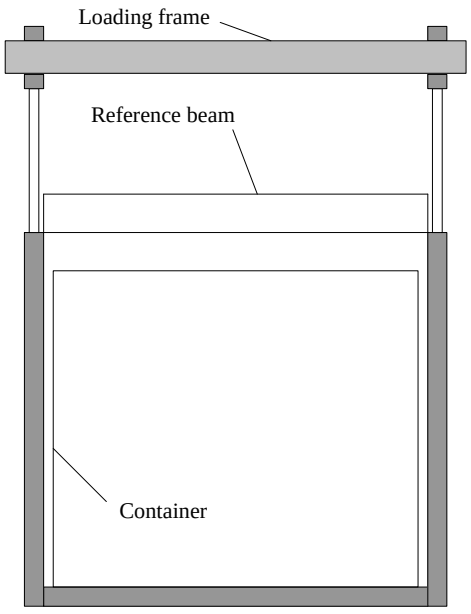

Figure 3.11 Schematic diagram showing detail of loading frame set.

3.5.5 Hydraulic Lifter

In PLT tests, a constant-rate-of-loading can be manually controlled by hydraulic lifter. The hydraulic lifter used in this research is a manually operated with separated units of hydraulic piston and handle as shown in Fig. 3.12, which is excellent in accuracy, performance, and safety. Authorized capacity is 120 % or more of the allowable maximum load.

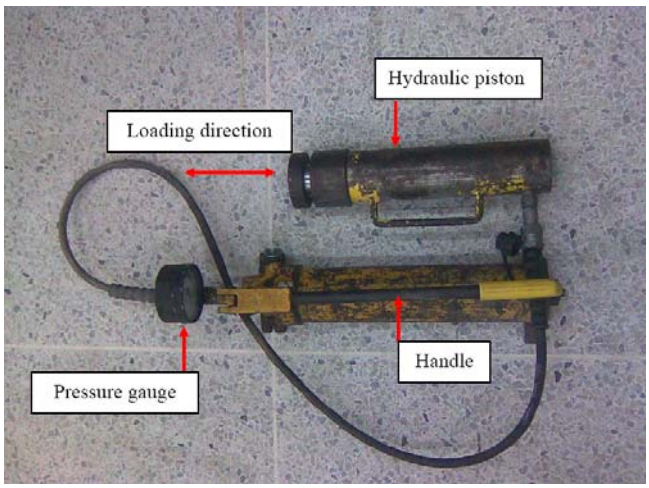

Figure 3.12 Photo showing hydraulic lifter.

3.6 Measuring Devices

3.6.1 Accelerometer

Accelerometer (Fig. 3.13) was used for measuring the surface settlement of pavement layer and transient deformations inside the backfill when subjected to impulse load by double-integration of acceleration with respect to time. In this research, three accelerometers having measuring capacity of 20g, 50g, and 100g, when g is the gravitational acceleration (equal to 9.81 m/s^2), were used.

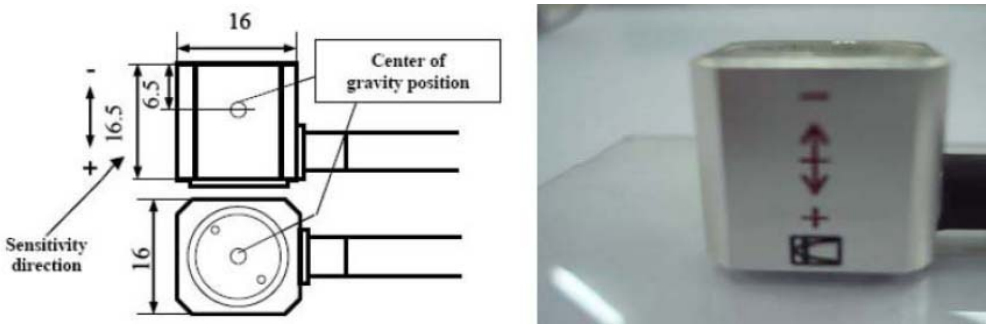

Figure 3.13 Illustration of accelerometer.

3.6.2 Laser Displacement Transducer

A laser displacement transducer (Fig. 3.14) is an optical sensor which measures a displacement based on an optical interference method by the wavelength of a light beam. A laser displacement transducer was used in this research to measure displacements in the vertical direction on the loading plate of PLT test.

Figure 3.14 Illustration of laser displacement transducer.

3.6.3 Gap Sensor

Gap sensor is a non-contact device. Its working mechanism is based on the reflection of electromagnetic wave between an electromagnetic probe head and an aluminum sheet for measuring displacement as shown in Fig. 3.15. Two gap sensors were used in this research for measuring the vertical displacement of damper to perform the stiffness of this one in UC test.

Figure 3.15 Illustration of gap sensor.

3.6.4 Load Cell

Load cell is used to measure axial load (both impulse and static) as shown in Fig. 3.16. In this research, the maximum capacity of load cell used in model test is 50 kN. Any bending moment mobilized between the plate and the piston when performing plate load test was removed by using universal joint. The load cell is a device that converts the load to the resistance changes of the attached strain gauge. As resistance changes of strain gauge are usually very small, four strain gauges attached on the load cell were formed a full Wheatstone bridge to magnify the response. Then, measurements were displayed by means of a digital voltmeter.

Figure 3.16 Illustration of load cell.

3.6.5 Dynamic Data Logger

For operating FWD and PLT tests, the 'strain value' and the 'voltage value' type of data loggers were used to dynamically record and then transfer data to a computer as shown in Fig. 3.17. Eight channels can be synchronized together by combining two 4-channel data loggers together. The sampling frequencies were selected at 5 kHz for FWD tests and 1 Hz for PLT tests.

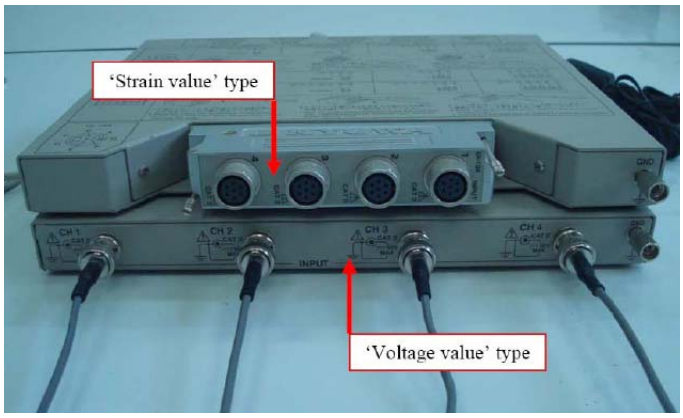

Figure 3.17 Illustration of dynamic data logger.

3.6.6 Linear Variable Differential Transformer (LVDT)

A linear variable differential transformer, LVDT (Fig 3.18) was used for the external measurement of the axial displacement of the loading piston in triaxtial tests. Because the data measured by LVDT has a low accuracy due to the LVDT-measured displacement values are combining values between displacements in specimen and errors consisting of system compliance, bedding errors and so on. In this research, a high- resolution measurement using 'LDT' (explained in Section 3.6.7). The measuring range of LVDT is about 20 mm and its resolution is 10 μm.

Figure 3.18 Illustration of LVDT.

3.6.7 Local Deformation Transducer (LDT)

A Local Deformation Transducer, LDT (Fig. 3.19) can axially measure the local displacement between two points located by two hinges attached on the specimen being measured. Then, LDT is placed on two hinges, LDT itself bends a little and elastic force is generated to hold LDT with hinges. When being used, a LDT is placed between two hinges bonded directly on the membrane or the side surface of specimen with the adhesive.

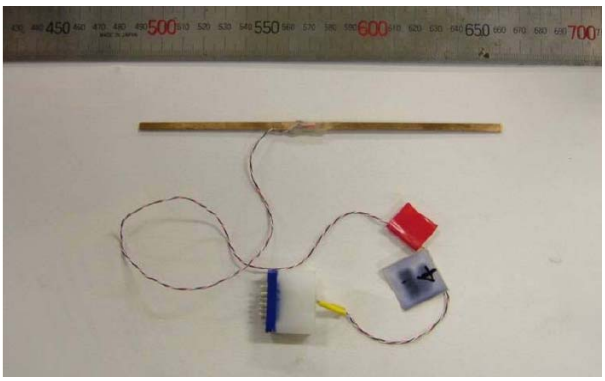

Figure 3.19 Illustration of LDT.

3.6.8 Clip Gauge

Clip Gauge (Fig. 3.20) consists of a phosphor bronze strip fixed at one arm of a U-shape aluminium frame. Four-strain gauges, forming a full Wheatstone bridge, were attached on the phosphor bronze strip, similar to the ones of LDT. Because LDT was not able to be installed to measure the lateral deformation of cylindrical-shape specimen, clip gauge was used.

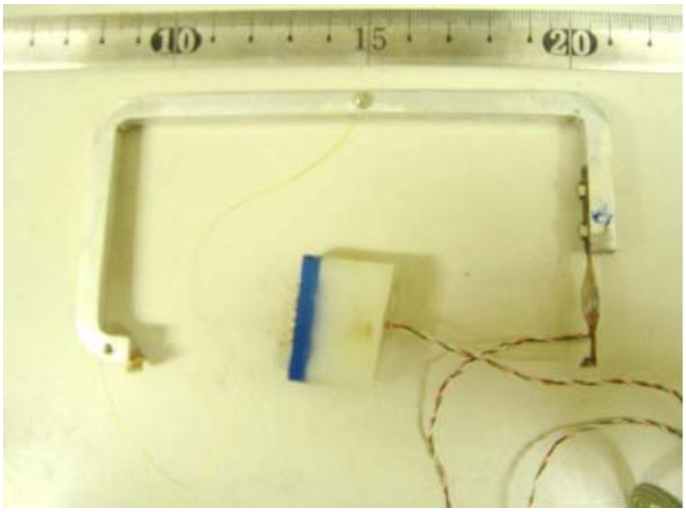

Figure 3.20 Illustration of clip gauge.

3.7 Pavement Structure Preparation

This section described the method to prepare the pavement structures in laboratory scaled. The pavement structures prepared in this research are single structure and two-layer structures that modeled from field pavement conditions.

3.7.1 Subgrade Layer

The subgrade layer (Fig 3.21) was modeled by KMUTT sand as a homogeneous layer. This layer was simulated by pluviated air-dried KMUTT sand into the container. Figure 3.22 shows the method to prepare the modeled subgrade layer by the multiple sieving pluviation apparatus. Because of the multiple sieving pluviation apparatus is smaller than the diameter of container. The multiple sieving pluviation apparatus was moved side-by-side on the container when KMUTT sand layer has a relative on one side higher than the other side for about 50 mm when preparing the sand layer. The KMUTT sand was pluviated until the modeled subgrade has a depth of 900 mm. Then, the surface of subgrade must be smoothened by small sieving pluviation apparatus to pluviate KMUTT sand for leveling the subgrade surface.

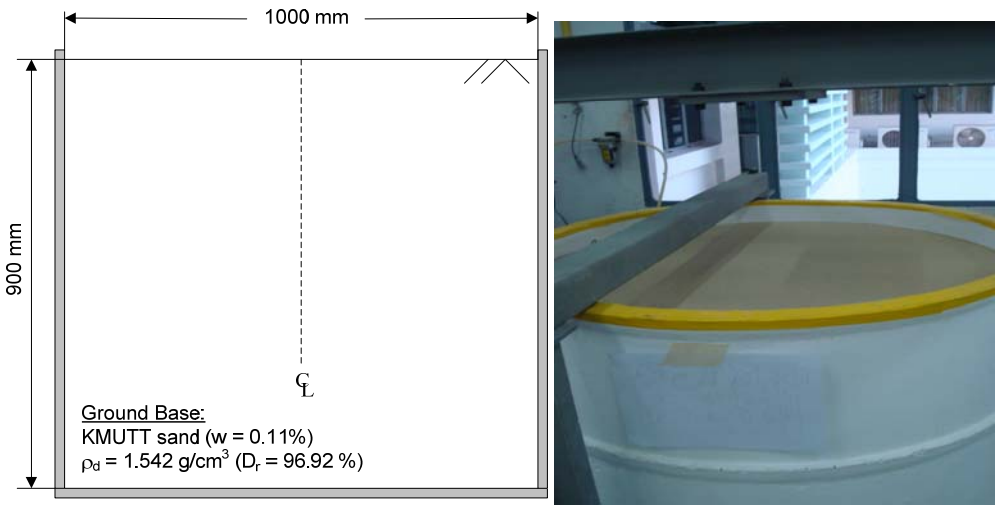

Figure 3.21 Illustration of ground base (subgrade layer).

Figure 3.22 Preparation of the modeled subgrade layer by the multiple sieving pluviation apparatus.

3.7.2 Unpaved Surface in-Two Layer Structure

Two-layer structure in unpaved surface (Fig 3.23) was modeled by laying a gravel layer on the subgrade layer. In this research, the subgrade layer was prepared as same as in Section 3.7.1 until modeled subgrade has a depth of 650 mm. Then, the subgrade surface was smoothened, gravels were pluviated by passing through the sieve with opening of 1/2 in. (12.5 mm) to model a the gravel layer of 250 mm in thickness as shown in Fig. 3.24.

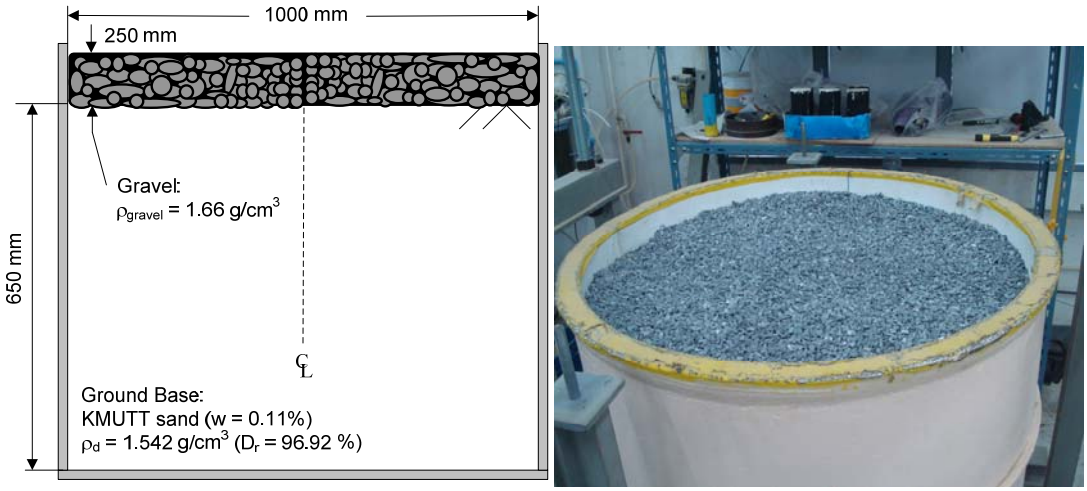

Figure 3.23 Illustration of ground base with gravel layer (unpaved surface).

Figure 3.24 Preparation of the modeled gravel layer by sieve opening 1/2 in.(12.5 mm).

3.7.3 Paved Surface in Two-Layer Structure

Two-layer structure in paved surface (Fig 3.25) was modeled by laying the asphaltic concrete layer on the subgrade layer. The subgrade layer having a depth of 850 mm was prepared as same as in Sections 3.7.1 and 3.7.2. The asphaltic concrete layer having thickness of 50 mm was laid on the subgrade layer to model the asphaltic concrete layer.

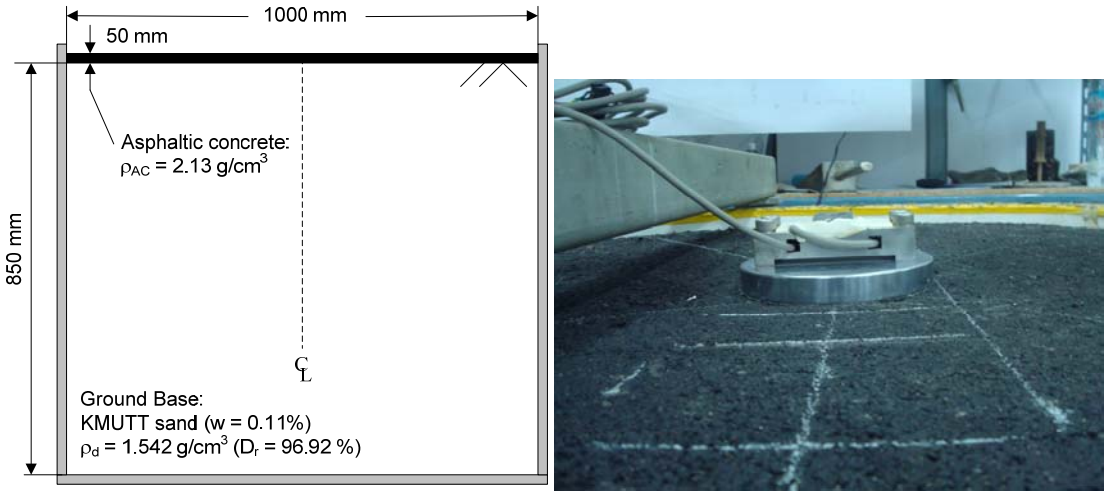

Figure 3.25 Illustration of ground base with asphaltic concrete layer (paved surface).

3.8 Static Plate Load Test and Analytical Method for Evaluating Modulus of Subgrade Reaction on Pavement Structure

AASHTO (1972) defined the modulus of subgrade reaction (k value) as the pressure on a loaded area divided by the average deflection of that loaded area as:

$$k_{PLT} = \frac{p}{s} \tag{3.3}$$

where:

k_{PLT} **= the modulus of subgrade reaction by PLT test (kPa/mm),**

p **= the load on a loaded area (kPa), and**

s **= the settlement of the loaded area (mm).**

The scales for k_{PLT} value presented in the AASHTO design charts are correlated with values obtained by PLT test performed in accordance with AASHTO designation T 222 using a circular loading plate having a diameter of 762 mm (30 in.).

In this research, PLT tests were performed to investigate the modulus of subgrade reaction on the three flexible pavement structure conditions as described in Section 3.7. All PLT tests were performed by a circular loading plate having 150 mm (5.9 in.) in diameter. Test procedures were in accordance with ASTM D 1195-93, Standard Test Method for Repetitive Static Plate Load Tests of Soils and Flexible Pavement Components (ASTM, 2004). Figure 3.26 shows the schematic of PLT set up including the hydraulic lifter for applying a constant rate of loading to the plate. The settlement of

loading plate was measured by laser displacement transducers installed on the reference beam and the load acting on the circular loaded area generated by hydraulic piston by a load cell installed on the loading plate. These measured values were recorded by dynamic data logger at the sampling frequency of 1 Hz. The PLT tests were performed by applying steps of loading and unloading as global for about seven cycles (Fig. 3.27) until the peak of plate pressure on loaded area exhibited. In order to do so, the settlement of loading plate was manually controlled at a constant rate of about 0.03 mm/min as shown in Fig. 3.38.

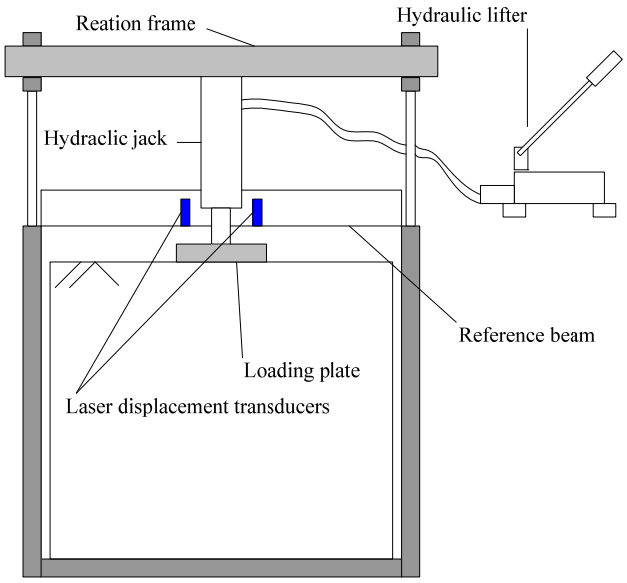

Figure 3.26 Schematic diagram showing detail of PLT set up.

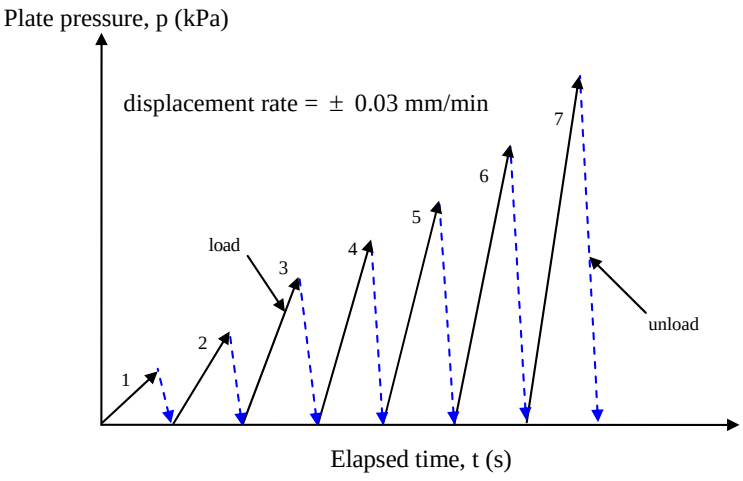

Figure 3.27 Schematic diagram showing time history of plate pressure during a PLT test.

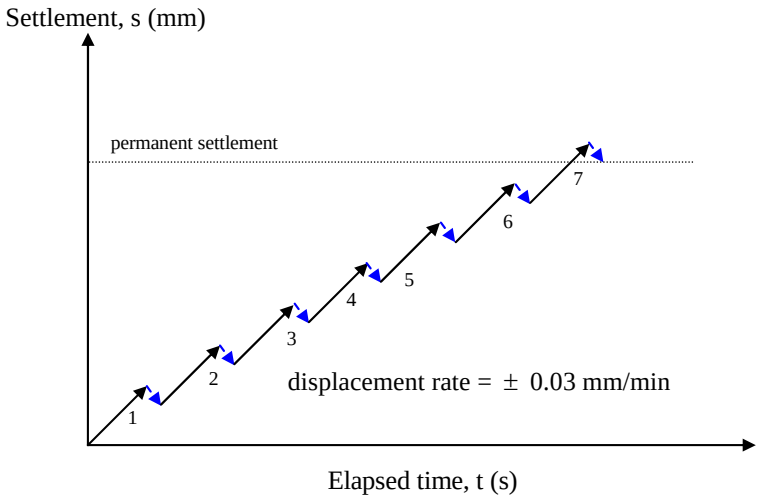

Figure 3.28 Schematic diagram showing time history of plate pressure during a PLT test.

From PLT test result, the relationship between the pressure on loading plate and settlement of soils beneath the loading plate was thus obtained a 4th-degree polynomial function was best fitted to the post-yielding segments of $p-s$ curve to obtain the nonrepetitive relation as shown in Fig. 3.29 in compliance with the procedures given in ASTM D 1196-93, Standard Test Method for Nonrepetitive Static Plate Load Tests of Soils and Flexible Pavement Components (ASTM, 2004) to evaluate the modulus of subgrade reaction.

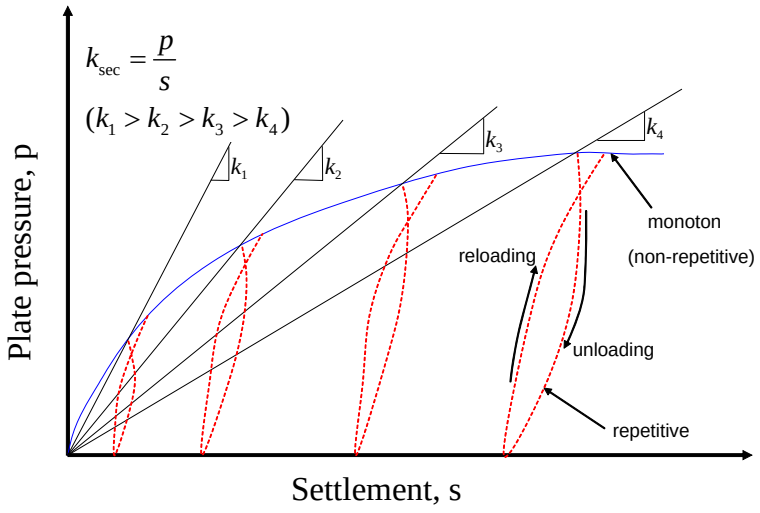

Figure 3.29 Schematic diagram showing an analytical method to calculate the modulus of subgrade reaction.

Following Eq. 3.3, it is clearly seen that the modulus of subgrade reaction is depended only upon p and s values (i.e., it is the secant slope value of a line from the origin $(0,0)$ to coordinate (s,p) on the monotonic $p-s$ relation). Figure 3.29 shows the values of modulus of subgrade reaction computed at different pressure levels from the $p-s$ curve according to Eq. 3.3. Generally, the modulus of subgrade reaction decreases with the increasing load level. It is necessary to select the values for p and s to reliably reflect the stiffness of the soils to determine the modulus of subgrade reaction for various types of soil at the same load level or settlement (Ping et al., 2002).

In this research, two analytical methods were selected for choosing the values of p and s to determine the modulus of subgrade reaction ($k_{sub,\,PLT}$) whereas the effect of size of loading plate is assumed to be negligible as:

AASHTO Method: The 1986 American Association of State Highway and Transportation Officials (AASHTO), *Guide for design of pavement structures* (AASHTO, 1986, 1993) adopted the modulus of subgrade reaction to reflect the stiffness for pavement structure by determining the s value of a 762 mm-(30 in.) diameter rigid loading plate under a given p of 68.9 kPa (10 psi.), as shown in Fig. 3.30.

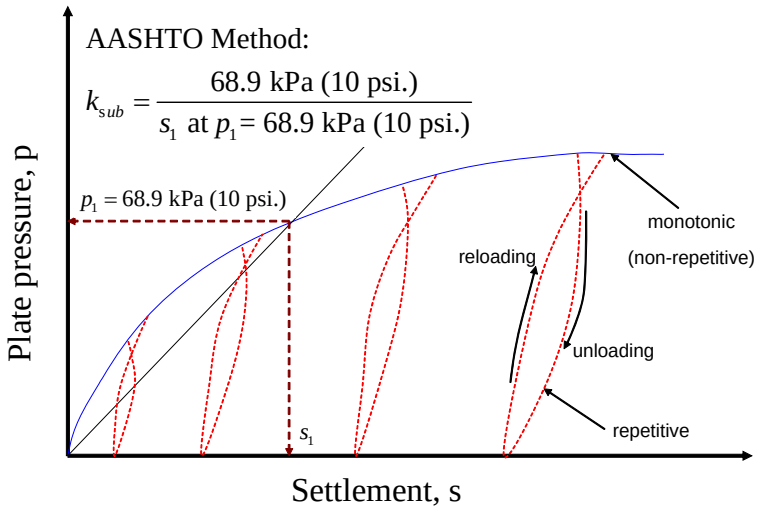

Figure 3.30 Schematic diagram showing the AASHTO designation method to calculate the modulus of subgrade reaction.

Florida Method: The Florida Department of Transportation, *Manual of Florida sampling and testing methods* (1988), specified the s value of 1.27 mm (0.05 in.) for the rigid loading plate having 152 to 762 mm (6 to 30 in.) in diameter, as in the determination of the modulus of subgrade reaction of pavement structure, as shown in Fig. 3.31.

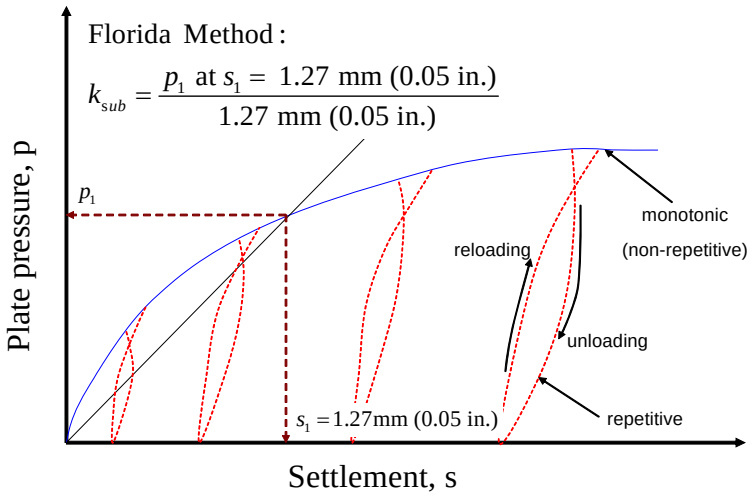

Figure 3.31 Schematic diagram showing the Florida designation method to calculate the modulus of subgrade reaction.

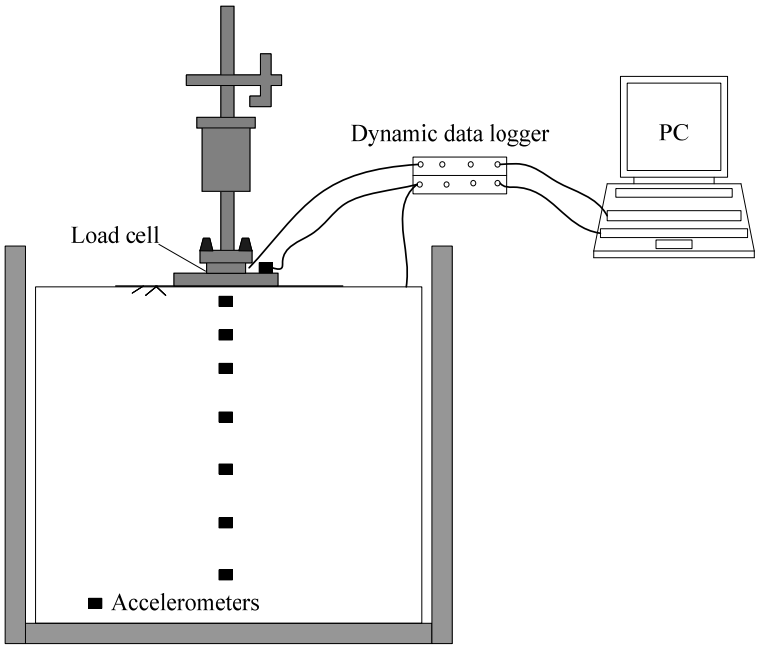

Figure 3.32 Schematic diagram showing detail of FWD set up.

3.9 Falling Weight Deflectometer (FWD) Test

Three pavement conditions described in Section 3.7 were employed in this research which can be classified into two pavement structure systems. That is, single-layer structure (subgrade) and two-layer structures (unpaved surface and paved surface), respectively.

3.9.1 Falling Weight Deflectometer Test on Subgrade

Subgrade layer were modeled by KMUTT sand only as described in Section 3.7.1 and were then performed by FWD device. This device has a 150-mm diameter loading plate

and 98.1 N-(10 kg) hammer. The hammer was released to free fall and then impact to a set of dampers which are connected to the loading plate. The generated impact load could reach about 20 kN when the falling height is 500 mm. FWD tests were performed by increasing the falling heights in the same test series, which were 10, 25, 50, 100, 200, 300, 400 and 500 mm for all pavement conditions. The impact load was measured by a load cell installed between the dampers and the loading plate. The accelerometers were used to measure the vertical settlement under loading plate by double-integration the respective time histories of acceleration. All measured values were recorded by dynamic data logger at sampling frequency of 5 kHz. FWD set up was presented in Fig. 3.32.

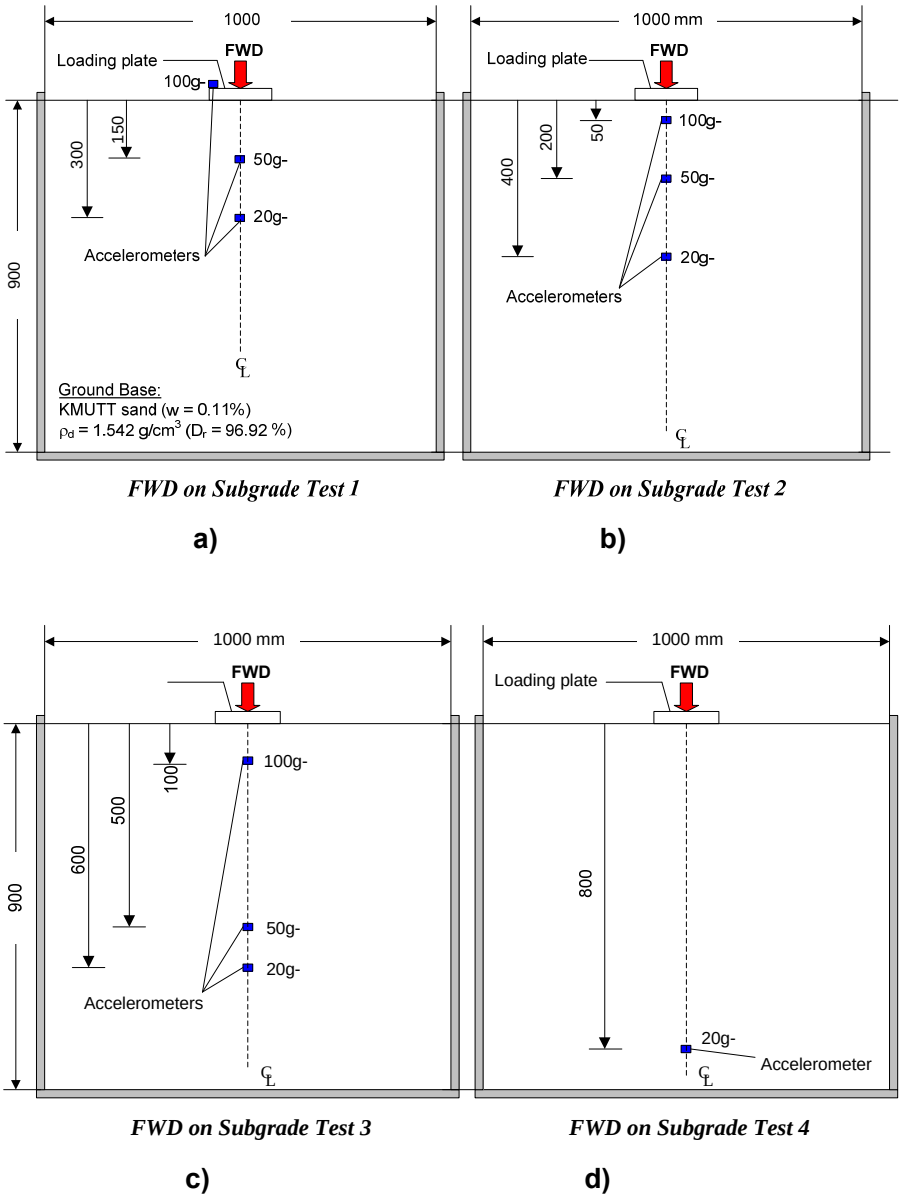

FWD on Subgrade Test 1 a)

FWD on Subgrade Test 2 b)

FWD on Subgrade Test 3 c)

FWD on Subgrade Test 4 d)

Figure 3.33 Illustration of four different configurations of FWD test on ground base (subgrade layer).

Figure 3.34 Photo showing method to install the accelerometers on the loading plate and inside the ground.

***FWD on Subgrade Test 1*: The 100g-accelerometer was installed on the top of the loading plate while the 50g- and 20g-accelerometers were inside the ground at the depth of 150 mm and 300 mm measured from the ground surface, respectively (Fig. 3.33a). Figure 3.34 shows the method to install the accelerometer on the top of loading plate and inside the ground.**

***FWD on Subgrade Test 2*: The 100g- 50g- and 20g-accelerometers were installed inside the ground at the depth of 50 mm, 200 mm and 400 mm measured from the ground surface, respectively (Fig. 3.33b).**

***FWD on Subgrade Test 3*: The 100g- 50g- and 20g-accelerometers were installed inside the ground at the depth of 100 mm, 500 mm and 600 mm measured from the ground surface, respectively (Fig. 3.33c).**

***FWD on Subgrade Test 4*: Only the 20g-accelerometer was installed inside the ground at the depth of 800 mm measured from the ground surface, respectively (Fig. 3.33d).**

3.9.2 Falling Weight Deflectometer Test on Two Layer Structures

Two-layer structures including unpaved surface and paved surface were described in Sections 3.7.2 and 3.7.3, respectively. The procedures for FWD test performed on this two-layer system were significantly similar to the ones described in Section 3.9.1, except the installation of accelerometers. That is, only the 100g-accelerometer was used to be installed on the top of the loading plate and tests were performed as a series for each condition.

3.10 Unconventional Consolidation Drained Triaxial Compression (CDTC) Test on KMUTT Sand

In this research, a series of unconventional consolidated drained triaxial compression (CDTC) tests were performed on KMUTT sand in an advanced laboratory at the Tokyo University of Science (TUS) - Japan.

Figure 3.35 shows the triaxial apparatus was used to perform CDTC test. This apparatus can apply different rates of displacement along a monotonic loading, immediately increase/decrease in displacement rate and allow switching between load-controlled and displacement-controlled modes. The specimen used initially has 70 mm in diameter, 150 mm in height and a relative density D_r is 93.90 %. The measuring devices include two LDTs to locally measure the axial deformation and three Clip Gauges to locally measure the radial deformation of specimen. For observing the increase or decrease the speed of displacement in vertical direction, a LVDT was installed on the reaction frame and pointed to the loading piston. The axial stress can be measured by a load cell that was directly connected to the top cap.

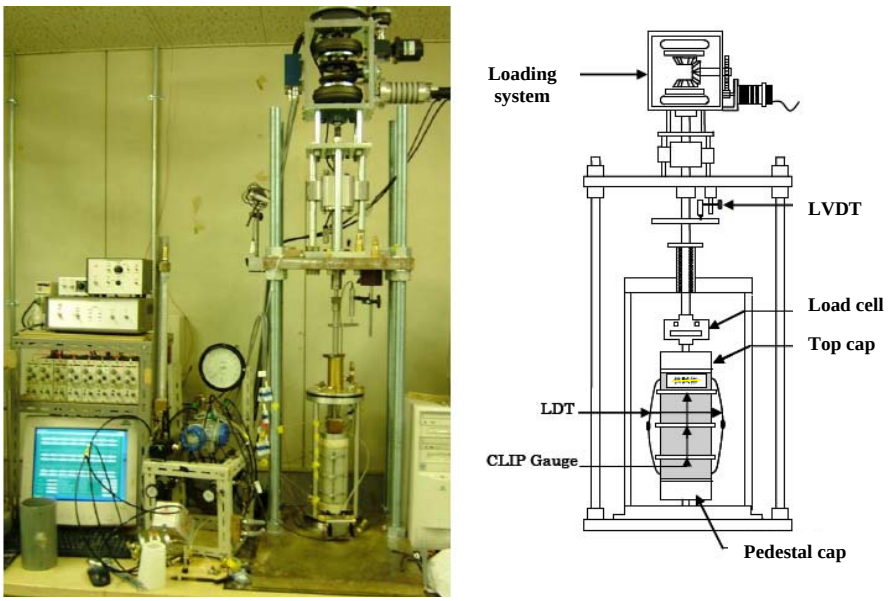

Figure 3.35 Illustration of CDTC test performed on KMUTT sand at the Tokyo University of Scinece (TUS).

Before shearing, the specimen must be fully saturating (B value must be greater than 0.95). The effective confining stress of 200 kPa was isotropic consolidated to the specimen. For triaxial compression loading test, during shearing, the confining stress was constant and a slope of path in $q - p'$ plot is 3 as shown in Fig. 3.36 (Wood, 1990).

The initial strain rate of compressing the specimens for shearing was 0.0045 mm/min (ε_0 = 0.003 %min). The strain rate was changed many times by increasing or decreasing in orders of 100 or 0 of the initial strain rate until the specimen failure.

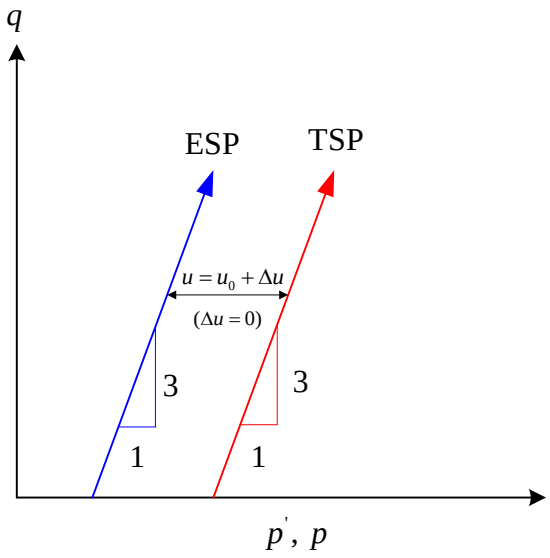

Figure 3.36 Stress path in $q : p'$ space of CDTC test (modified after Wood, 1990).

The objective of performing the CDTC tests in this research is to investigate the rate-sensitivity coefficient (β) of KMUTT sand. The β value is a constant for a given material to represent its rate-dependent behavior. Thai is, this value was obtained by measuring the stress jumps upon stepwise increase/decrease in the strain rate. From CDTC tests, the normalized stress ratio values were plotted with the logarithm of ratio of strain rate increase/decrease for the respective stress jumps as described in Figs. 3.39a and 3.39b, respectively. The slope of the linear relation fitted to the measured data is called the rate-sensitivity coefficient (β) and calculated by Eq. 2.10.

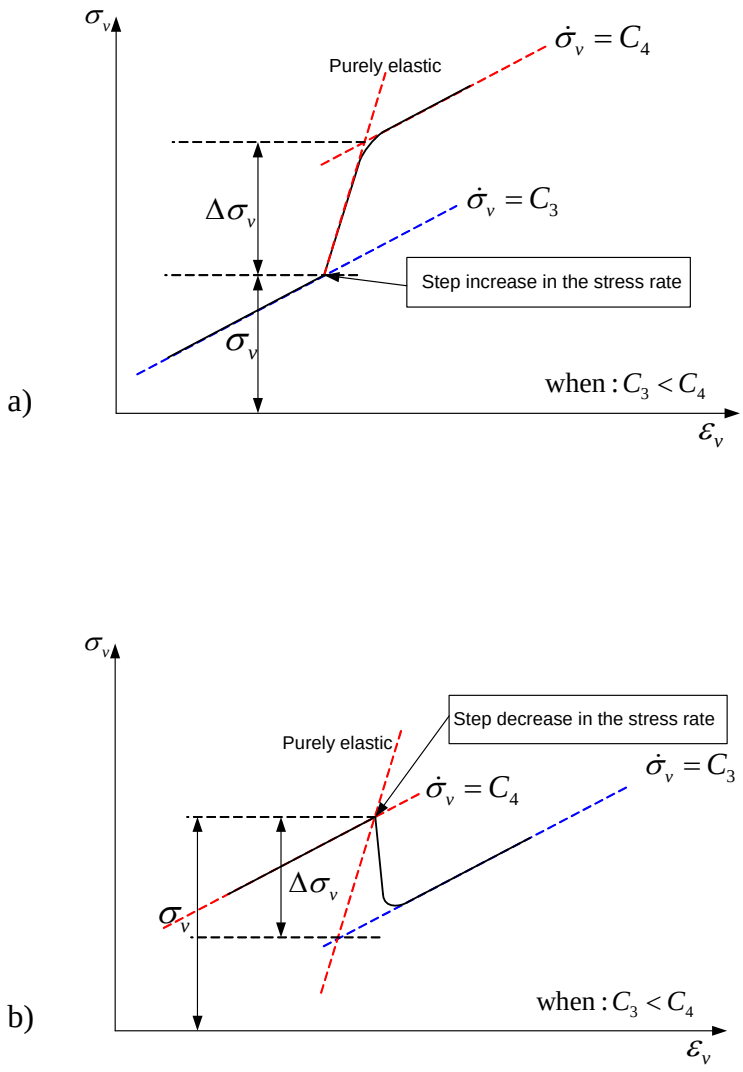

Figure 3.37 a) Stress jump upon a step increase in the vertical strain rate; and b) Stress jump upon a step decrease in the vertical strain rate (modified after Masuda, 2007).

3.11 Analytical Method for Evaluating Modulus of Subgrade Reaction by Falling Weight Deflectometer Test on Pavement Structure

For assumptions of rigid plate pressure, the E value of any Poisson's ratio can be calculated by Burmister's equation (e.g., Bermister, 1943, 1945, 1947; Ping, et al., 2002) as follows:

$$E = \frac{\pi \cdot \left(1 - \nu^2\right) \cdot a \cdot \sigma_0}{2 \cdot d_0} \tag{3.4}$$

where:

ν **= the Poisson's ratio.**

By the definition of k value was presented in Eq. 3.3, it can be seen from Eq. 3.4 that E value depends on the value of σ_0 divided by d_0 or a secant modulus of subgrade reaction ($k_{sec,\ FWD}$ value). Therefore, Eq. 3.4 can be re-written as Eq. 3.5.

$$E = \frac{\pi \cdot \left(1-\nu^2\right) \cdot a \cdot k_{sec,\ FWD}}{2} \quad (3.5)$$

Form AASHTO designation, the k value to be used with the AASHTO design equations and charts is the static k value. This static k value may be approximated form the dynamic k value (e.g., AASHTO, 1993; Huang, 2003) as:

$$\text{Static } k \text{ value} = \frac{\text{Dynamic } k \text{ value}}{2} \quad (3.6a)$$

Here, the definition of the static k value and the dynamic k value are the secant modulus of subgrade reaction that were obtained by PLT and FWD tests, respectively. The following relationship may be used for the conversion between dynamic and static tests:

$$k_{sec,\ PLT} = \frac{k_{sec,\ FWD}}{2} \quad (3.6b)$$

3.12 Analytical Method for Adjustment on Falling Weight Deflectometer Test Result on Subgrade

Generally, the stiffness values obtained by dynamic method are higher than static method. In this research, the following two effects were found responsible to the differences of stiffness values:

i) dynamic behavior of tested material, and

ii) viscous behavior of tested material.

3.12.1 Analytical Method for Adjustment for Dynamic Effects

When the falling weight drops onto a surface of material, an impulse enters the material beneath and creates body wave. This results in the different occurrences of peak acceleration when measured at different depths beneath from the center of the loading plate along the vertical direction. The elapsed time measured when the peak acceleration

at a location exhibited to the peak acceleration at the next location exhibited is called 'time-lag' (Fig. 3.38). Time-lag usually comprises of two components: a) time-lag due to the propagation of the waves (V_p) from the applied load; and b) time-lag due to material damping of the waves (Lytton and Michalak, 1979).

In this research, the effects of damping of material were assumed negligible. As a result, the influence of time-lag can be seen by that the settlement under loading plate by FWD test at the same of p pressure is less than the one by PLT test as shown in Fig. 3.39.

The accelerometers were used to measure the acceleration inside the ground at specified depths from the ground surface. The settlement inside the ground can be calculated by double-integration of time histories of accelerations measured at different depths as follows:

$$u_z = \int_0^{t_1}\int_0^{t_1} \ddot{u}_z \cdot \partial t \cdot \partial t \qquad (3.7)$$

where:

u_z = the settlement inside the ground at depth z, and

$\ddot{u}_z$ = the acceleration inside the ground measured at depth z by the accelerometer.

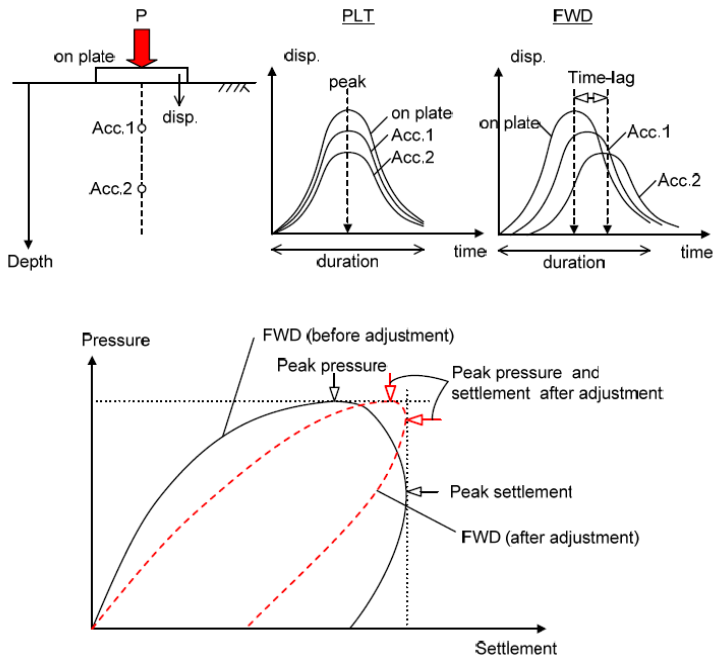

Figure 3.38 Schematic diagram showing the effects of dynamic behavior of material (modified after Hirakawa et al., 2008).

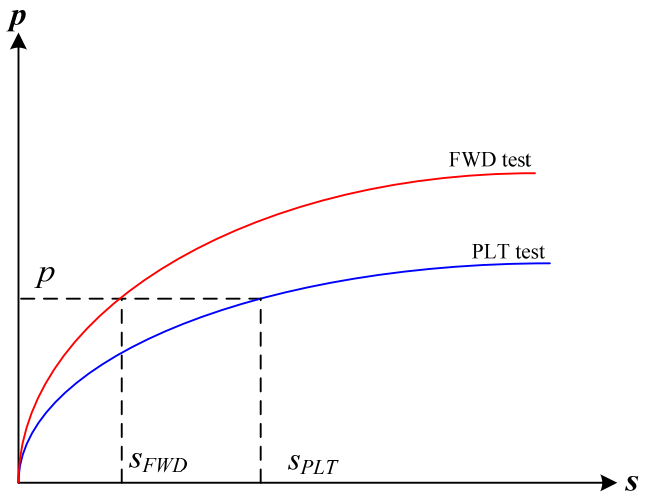

Figure 3.39 Schematic diagram showing the difference of settlement under loading plate between FWD and PLT tests (modified after Masuda, 2007).

Following Eq. 3.7, different settlements measured from accelerations at different depths in the ground in a FWD test can be plotted in Fig. 3.40. Then, the average vertical strain at the each depth can be plotted in Fig. 3.41 and calculated as:

$$\bar{\varepsilon}_z = \frac{u_{(z,\,t)} - u_{(z+\Delta z,\,t)}}{\Delta z} \tag{3.8}$$

where:

$\bar{\varepsilon}_z$ **= the average vertical strain inside the ground,**

$u_{(z,\,t)}$ **= the settlement inside the ground at depth** z **at time** t**,**

$u_{(z+\Delta z,\,t)}$ **= the settlement inside the ground at depth** $z+\Delta z$ **at time** t**, and**

Δz **= the distance between the accelerometer at depths** z **and** $z+\Delta z$**.**

From Fig. 3.40, it can be seen that the moments when the respective peak settlements at different depths exhibited were not the some. To adjust this effect, the velocity of wave propagation must be investigated to quantitatively the time-lag. When the velocity of wave propagation is known, the relationship between the average vertical strains and time at different depths can be plotted as shown in Fig. 3.42 and written as follows:

$$\bar{\varepsilon}_z\left(t,\ z\right) = \bar{\varepsilon}_z\left(t - \frac{z}{V_p},\ z\right) \tag{3.9}$$

where:

$\overline{\varepsilon}_z$ = the average vertical strain inside the ground,

V_p = the velocity of wave propagation inside the ground,

z = the depth from the ground surface, and

t = the elapsed time.

Then, the surface settlement from a FWD test at time = t_1 can be accurately obtained by correcting for the time-lag (Hirakawa et al., 2008) as:

$$[S]_{(t_1)} = \int_{z=0}^{\infty} \left[\int_{t=0}^{t_1} \overline{\varepsilon}_z \left(t - \frac{z}{V_p}\right) \cdot dt \right] \cdot dz \qquad (3.10)$$

where:

$[S]_{(t_1)}$ = the surface settlement from a FWD test at time = t_1.

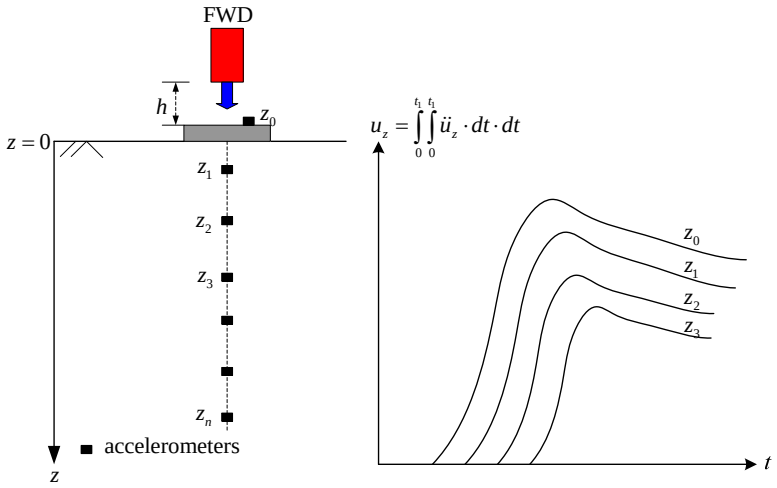

Figure 3.40 Schematic diagram showing different settlements measured from accelerations at different depths inside the ground in a FWD test (modified after Masuda, 2007).

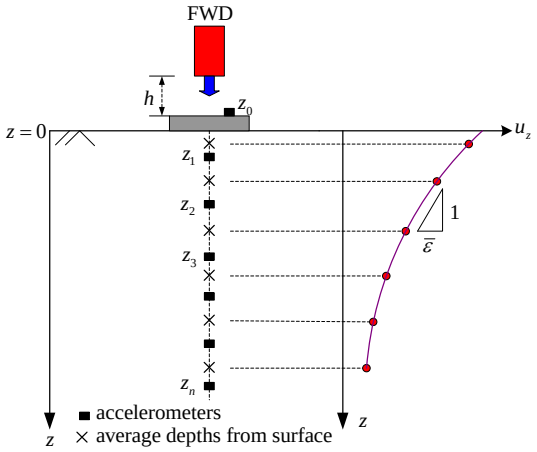

**Figure 3.41 Schematic diagram showing the average vertical strain at the each depth inside the ground in a FWD tests (modified after Masuda, 2007). **

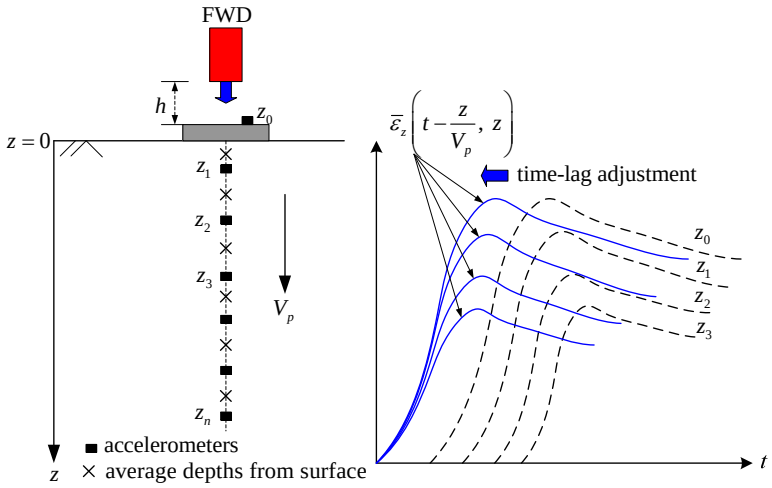

Figure 3.42 Schematic diagram showing the differences of settlement after time-lag adjustment of FWD tests (modified after Masuda, 2007).

3.12.2 Analytical Method for Adjustment for Loading Rate Effects

Loading rate effect is herein defined as a time-dependent stress-strain response of a given type of geomaterial due to its viscous property. A basic structure of viscous property of geomaterials is described by a non-linear three-component model as shown in Fig. 2.33 (e.g., Kongkitkul et al., 2008; Tatsuoka et al., 2008). Following this model, the total stress (σ) is composed of the inviscid stress component (σ^f) and the viscous component (σ^v). The σ^v component is a function of the instantaneous irreversible (or visco-plastic) strain rate ($\dot{\varepsilon}^{ir}$ or $\dot{\varepsilon}^{vp}$) and other relevant parameters, not by time. Therefore, the higher $\dot{\varepsilon}^{ir}$ results in the higher σ^v. This also explains why the plate pressure value by a FWD test, at the same value of plate settlement, is higher than the

one by PLT test, as the value of $\dot{\varepsilon}^{ir}$ encountered in FWD test is noticeably higher than the one encountered in PLT. The viscosity of material can be quantitatively defined in Eq. 2.10 (e.g., Kongkitkul et al., 2008; Tatsuoka, 2007; Tatsuoka et al., 2008).

In this research, it is first necessary, to know how much differences in the settlement rates between FWD and PLT tests. Then, the consequent amount of plate pressure difference between FWD and PLT tests at a given settlement value (Fig. 3.43) can be determined. That is, the influence of loading rate can be represented by that the pressure on the loading plate by FWD test is higher than the one by PLT test at the same of s value as shown in Fig. 3.44.

From Fig. 3.43, compare and adjust test results from FWD and PLT tests in this research, Eq. 2.10 was re-written as follows:

$$\beta = \frac{\dfrac{p_B - p_A}{p_A}}{\log_{10}\left\{\dfrac{\dot{u}_{z,\,FWD}}{\dot{u}_{z,\,PLT}}\right\}} \tag{3.11}$$

where:

p_A = the load at the moment when the change in the settlement rate (in this case p_A is the pressure from the self-weight of FWD apparatus),

p_B = the load upon change in the settlement rate (measured by FWD test),

$\dot{u}_{z,\,FWD}$ = the settlement rate of loading plate by FWD test, and

$\dot{u}_{z,\,PLT}$ = the settlement rate of loading plate by PLT test.

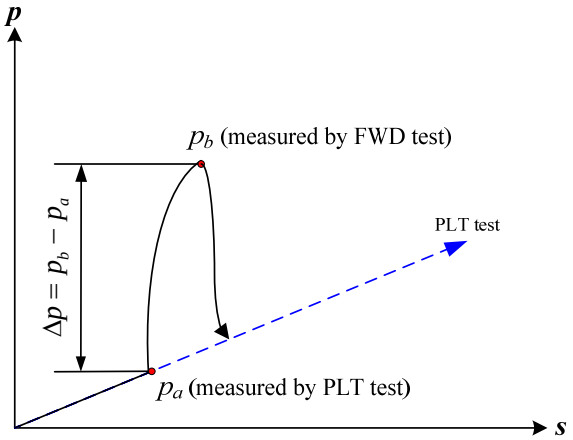

Figure 3.43 Schematic diagram showing load jump upon a step increase in settlement rate from a FWD test compared with PLT tests.

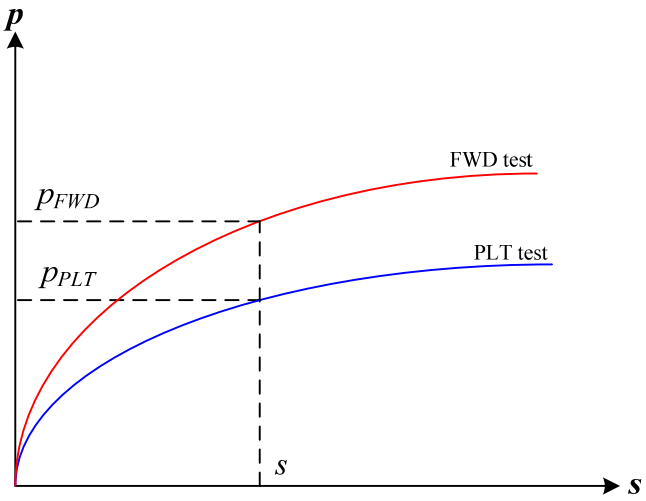

Figure 3.44 Schematic diagram showing the different measured plate pressure between FWD and PLT tests (modified after Masuda, 2007).

3.13 Analytical Method by Undamped Harmonic Motion for Evaluating Modulus of Subgrade Reaction on Falling Weight Deflectometer Test

In this section, a method for evaluating modulus of subgrade reaction from a FWD test considering loading condition is described. This method considers the relationship between load and vertical displacement of loading plate and is described by the Newton's law of motion or undamped harmonic motion (UHM).

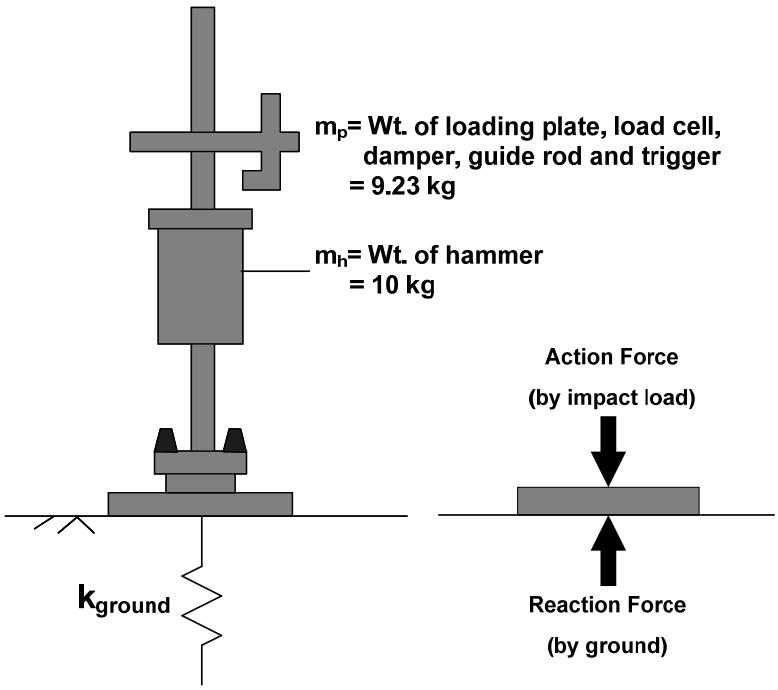

Figure 3.45 Illustration of action force and reaction force from a FWD test on ground.

Calculation of Spring Constant of the Ground: The Falling Weight Deflectometer (FWD) test whose loading plate is subjected to impulse loads of short duration, referred to as impact. Figure 3.45 shows a resting loading plate on a spring. Let the spring represents the elastic properties of the ground. The load F represents the impulse load on the loading plate due to the impaction of the released hammer. If the loaded area is A_p, the intensity of load transmitted to the ground (Das, 1992) can be given by

$$p = \frac{F}{A_p} \tag{3.12}$$

where:

p = the value of impulse pressure on the loading plate,

F = the value of impulse load on the loading plate, and

A_p = the area of loading plate.

Due to the impulse load F, a static vertical displacement u will develop. By definition, the following equation can be written:

$$k_{ground} = \frac{F}{u} \tag{3.13}$$

If the loading plate is disturbed from its static equilibrium position, the system will vibrate for a single-action dropped hammer. The equation of motion of the loading plate when it has been disturbed through a vertical displacement u can be written from Newton's law of motion (undamped harmonic equation) (e. g., Das, 1992; Hirakawa et al., 2008) as:

$$\ddot{u} \cdot m_p + k_{ground} \cdot u = 0 \tag{3.14a}$$

or

$$\ddot{u} + \left(\frac{k_{ground}}{m_p} \right) \cdot u = 0 \tag{3.14b}$$

where:

u = the vertical displacement,

$\ddot{u}$ = the vertical acceleration,

m_p = the mass of the loading plate, and

k_{ground} = the spring constant of the ground.

In order to solve Eq. 3.14b, let the vertical displacement u as:

$$u = A_1 \cdot \cos \omega_n t + A_2 \cdot \sin \omega_n t \tag{3.15}$$

where:

A_1 and A_2 = the constants,

ω_n = the undamped natural circular frequency, and

t = the elapsed time.

Substitution of Eq. 3.15 into Eq. 3.14b yields:

$$-\omega_n^2 \cdot (A_1 \cdot \cos \omega_n t + A_2 \cdot \sin \omega_n t) + (\frac{k_{ground}}{m_p}) \cdot (A_1 \cdot \cos \omega_n t + A_2 \cdot \sin \omega_n t) = 0 \tag{3.16}$$

when,

$$\omega_n = \sqrt{\frac{k_{ground}}{m_p}} \tag{3.17}$$

The unit of ω_n is in radians per second (rad/s). Hence,

$$u = A_1 \cdot \cos(\sqrt{\frac{k_{ground}}{m_p}} \cdot t) + A_2 \cdot \sin(\sqrt{\frac{k_{ground}}{m_p}} \cdot t) \tag{3.18}$$

In order to determine the values of A_1 and A_2, one must substitute the proper boundary conditions. At time $t = 0$, let

Vertical displacement $u = u_0$

and

Vertical velocity $= \frac{du}{dt} = \dot{u} = v_0$

Substituting the first boundary condition in Eq. 3.18, we obtained:

$$u_0 = A_1 \tag{3.19}$$

Again, from Eq. 3.18, we obtained:

$$\dot{u} = -A_1 \cdot \sqrt{\frac{k_{ground}}{m_p}} \cdot \sin(\sqrt{\frac{k_{ground}}{m_p}} \cdot t) + A_2 \cdot \sqrt{\frac{k_{ground}}{m_p}} \cdot \cos(\sqrt{\frac{k_{ground}}{m_p}} \cdot t) \tag{3.20}$$

Substituting the second boundary condition in Eq. 3.20, we obtained:

$$\dot{u} = v_0 = A_2 \cdot \sqrt{\frac{k_{ground}}{m_p}} \tag{2.21a}$$

or

$$A_2 = \frac{v_0}{\sqrt{\frac{k_{ground}}{m_p}}} \tag{3.21b}$$

At t = 0, the vertical displacement rate at the moment of impaction of the weight freely dropped from the height = h can be defined by the conservation of energy law (Walker, 2004) as:

$$\frac{1}{2} \cdot m_h \cdot v_b^2 = \frac{1}{2} \cdot m_h \cdot v_a^2 + \frac{1}{2} \cdot m_p \cdot v_0^2 \tag{3.22a}$$

or

$$v_0 = \sqrt{\frac{m_h}{m_p} \cdot (v_b^2 - v_a^2)} \tag{3.22b}$$

where:

m_h **= the mass of the hammer,**

v_a **= the velocity of the hammer after impact to damper,**

v_b **= the velocity of the hammer before impact to damper, and**

v_0 **= the velocity of the loading plate.**

The velocity of the hammer after impact to damper v_a can not be measured directly from testing. In this research, we assumed the velocity of the hammer after impact to damper equal to zero ($v_a = 0$) and the loss of the velocity of the hammer after impact to damper is represented by the efficiency value E_f ($0 \le E_f \le 1$) remained after impact. Eq. 3.22b can be newly defined as:

$$v_0 = E_f \cdot \sqrt{\frac{m_h}{m_p} \cdot (v_b)^2} \tag{3.23}$$

The velocity of the hammer at the moment before impaction to damper by the weight freely dropped from the height = h is:

$$v_b = \sqrt{2 \cdot g \cdot h} \tag{3.24}$$

Substituting Eqs. 3.23 and 3.24 into Eq. 3.21b yields

$$A_2 = \frac{E_f \cdot \sqrt{\frac{m_h}{m_p} \cdot (2 \cdot g \cdot h)}}{\sqrt{\frac{k_{ground}}{m_p}}} = E_f \cdot \sqrt{\frac{2 \cdot g \cdot h \cdot m_h}{k_{ground}}} \tag{3.25}$$

where:

E_f **= the remain efficiency values after impact,**

g **= the gravitational acceleration, and**

h **= the falling height.**

Substituting Eqs. 3.19 and 3.25 into Eq. 3.18 yields

$$u = u_0 \cdot \cos\left(\sqrt{\frac{k_{ground}}{m_p}} \cdot t\right) + \left(E_f \cdot \sqrt{\frac{2 \cdot g \cdot h \cdot m_h}{k_{ground}}}\right) \cdot \sin\left(\sqrt{\frac{k_{ground}}{m_p}} \cdot t\right) \tag{3.26a}$$

or

$$u = u_0 \cdot \cos(\omega_n t) + \left(E_f \cdot \sqrt{\frac{2 \cdot g \cdot h \cdot m_h}{k_{ground}}}\right) \cdot \sin(\omega_n t) \tag{3.26b}$$

For the boundary conditions of u = 0 when t = 0, we obtain:

$$u_0 = 0$$

Then

$$u = E_f \cdot \sqrt{\frac{2 \cdot g \cdot h \cdot m_h}{k_{ground}}} \cdot \sin(\omega_n t) \qquad \textbf{(3.27)}$$

From Eq. 3.27, we obtain the vertical load acting on the ground F, as:

$$F = k_{ground} \cdot u = k_{ground} \cdot E_f \cdot \sqrt{\frac{2 \cdot g \cdot h \cdot m_h}{k_{ground}}} \cdot \sin(\omega_n t) \qquad \textbf{(3.28a)}$$

or

$$F = E_f \cdot \sqrt{2 \cdot g \cdot h \cdot k_{ground} \cdot m_h} \cdot \sin(\omega_n t) \qquad \textbf{(3.28b)}$$

Therefore, the loading rate dF/dt, can be expressed as:

$$\frac{dF}{dt} = E_f \cdot \omega_n \cdot \sqrt{2 \cdot g \cdot h \cdot k_{ground} \cdot m_h} \cdot \cos(\omega_n t) \qquad \textbf{(3.29)}$$

From Eq. 3.29, the peak value of vertical load can be obtained as:

$$F_{peak} = E_f \cdot \sqrt{2 \cdot g \cdot h \cdot k_{ground} \cdot m_h} \qquad \textbf{(3.30a)}$$

or

$$F_{peak} = E_f \cdot \sqrt{\frac{2 \cdot g \cdot h \cdot k_{ground} \cdot m_h}{1000}} \qquad \textbf{(3.30b)}$$

where:

F_{peak} **= the peak value of vertical load on the loading plate (kN),**

E_f **= the remain efficiency values after impact (** $0 \le E_f \le 1$ **),**

g **= the gravitational acceleration (m/s^2),**

h **= the falling of drop (mm),**

k_{ground} = the spring constant of ground (kN/mm), and

m_h = the mass of the hammer (in this case m_h = 10 kg).

Remain Efficiency due to Damper for FWD Test: In condition of FWD test without the shock absorber (no damper), it is assumed that the impaction of hammer to loading plate is elastic collisions. Therefore, the remain efficiency value in Eq. 3.23 is equal to 1 (E_f = 1). The velocity of loading plate after impaction in Eq. 3.23 in this condition can be re-written as follows:

$$v_{0,\,nd} = \sqrt{\frac{m_h}{m_p} \cdot (v_b)^2} \tag{3.31}$$

where:

$v_{0,\,nd}$ = the velocity of rate of loading plate after impact without damper.

In general condition of FWD test with damper, if the assumption described above is the same as the condition of FWD test without damper, the displacement under loading plate can be determined by Eqs. 3.23, 3.24, 3.25 and 3.26a, and Eq. 3.26b can be re-written for this condition as follows:

$$u = u_0 \cdot \cos(\omega_n t) + \left(\frac{v_{0,\,d}}{\sqrt{\bar{k} / m_p}} \right) \cdot \sin(\omega_n t) \tag{3.32}$$

where:

$v_{0,\,d}$ = the velocity of loading plate after impact with damper,

$\bar{k}$ = the summation of the spring coefficients of damper and ground.

For the boundary conditions of u = 0 when t = 0, we obtain:

$$u_0 = 0$$

then

$$u = \left(\frac{v_{0,\,d}}{\sqrt{\bar{k} / m_p}} \right) \cdot \sin(\omega_n t) \tag{3.33}$$

From Eq. 3.33, we obtain the vertical load acting on ground F, as:

$$F = \bar{k} \cdot u = \bar{k} \cdot \left(\frac{v_{0,d}}{\sqrt{\bar{k} / m_p}} \right) \cdot \sin(\omega_n t) \quad \textbf{(3.34a)}$$

or

$$F = v_{0,d} \cdot \sqrt{m_p \cdot \bar{k}} \cdot \sin(\omega_n t) \quad \textbf{(3.34b)}$$

Therefore, the loading rate, dF / dt, can be expressed as:

$$\frac{dF}{dt} = v_{0,d} \cdot \omega_n \cdot \sqrt{m_p \cdot \bar{k}} \cdot \cos(\omega_n t) \quad \textbf{(3.45)}$$

From Eq. 3.35, the peak value of vertical load can be obtained as:

$$F_{peak} = v_{0,d} \cdot \sqrt{m_p \cdot \bar{k}} \quad \textbf{(3.46a)}$$

or

$$v_{0,d} = \frac{F_{peak}}{\sqrt{m_p \cdot \bar{k}}} \quad \textbf{(3.46b)}$$

where:

$v_{0,d}$ = the velocity of loading plate after impact with damper (m/s),

F_{peak} = the peak value of vertical load on the loading plate (kN),

$\bar{k}$ = the summation of the spring coefficients of damper and ground (kN/mm), and

m_p = the mass of the loading plate (in this case m_p = 9.23 kg).

The definition of the remain efficiency value due to the impact of hammer to loading plate between the condition of FWD tests with damper and without damper is the velocity of loading plate after impact with damper divided by the velocity of loading plate after impact without damper. By this definition, we can calculate the remain efficiency due to damper for FWD test as follows:

$$E_f = \frac{v_{0,\,d}}{v_{0,\,nd}} \tag{3.37}$$

From Eqs, 3.31 and 3.36b, we can re-write the remain efficiency value as:

$$E_f = \frac{F_{peak} / (\sqrt{m_p \cdot \bar{k}})}{\sqrt{(m_h / m_p) \cdot (2 \cdot g \cdot h)}} \tag{3.38}$$

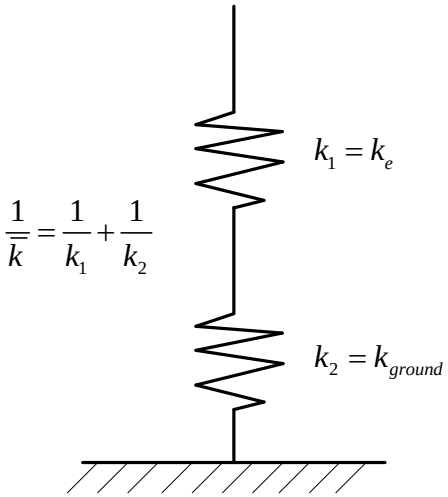

Figure 3.46 Illustration of a series of spring.

$\bar{k}$ **value is the summation of the spring coefficients of damper and ground (Fig. 3.46). This value is calculated by a series of spring constant in Fig. 3.46 as follows:**

$$\frac{1}{\bar{k}} = \frac{1}{k_{ground}} + \frac{1}{k_e} \tag{3.39}$$

where:

k_e **= the spring constant value of damper.**

From Eq. 3.39, when FWD test is performed onto the very stiff pavements (e.g., concrete slab) and when it can be ensured that the spring constant of the ground (k_{ground} **value) is substantially higher than the spring constant value of damper (**k_e **value),** k_{ground} **value can be treated to be equal to infinity and Eq. 3.39 came be re-written as:**

$$\frac{1}{\overline{k}} = \frac{1}{\infty} + \frac{1}{k_e} \quad \textbf{(3.40a)}$$

or

$$\overline{k} = k_e \quad \textbf{(3.40b)}$$

Substituting k_e value instead of the $\overline{k}$ value into Eq. 3.38 yields:

$$E_f = \frac{F_{peak} / (\sqrt{m_p \cdot k_e})}{\sqrt{(m_h / m_p) \cdot (2 \cdot g \cdot h)}} \quad \textbf{(3.41)}$$

The capacity of FWD device can be reached by assumed E_f is equal to 1 and substituting k_{ground} value with k_e value in Eq 3.30b yields:

$$F_{peak} = \sqrt{\frac{2 \cdot g \cdot h \cdot k_e \cdot m_h}{1000}} \quad \textbf{(3.42)}$$

***Calculation of the Modulus of Subgrade Reaction*: The modulus of subgrade reaction was defined as:**

$$k_{sub} = \frac{p}{u} \quad \textbf{(3.43)}$$

For Falling Weight Deflectometer test, we can obtain the peak value of vertical pressure on the loading plate by measuring from load cell and calculated the k_{ground} value from the test. We can back-calculate the modulus of subgrade reaction, k_{sub} following:

Combination Eqs. 3.12 and 3.13 into Eq 3.43 gives

$$k_{sub} = \frac{F / A_p}{u} \quad \textbf{(3.44a)}$$

or

$$k_{sub} = \frac{k_{ground}}{A_p} \quad \textbf{(3.44b)}$$

where:

p = the value of impulse pressure on the loading plate (kPa),

u = the vertical displacement under the loading plate (mm),

F = the value of impulse load on the loading plate (kN),

A_p = the area of loading plate (m^2),

k_{sub} = the modulus of subgrade reaction of the ground (kPa/mm), and

k_{ground} = the spring constant of the ground (kN/mm).

3.14 Uniaxial Test on Damper

Damper in FWD device was served to lengthen the impulse duration time and to decrease the load magnitude (Mooney and Miller, 2009). In this research, the spring constant of damper was investigated to determine the remain efficiency value and the capacity of FWD device by Eqs. 3.41 and 3.42, respectively.

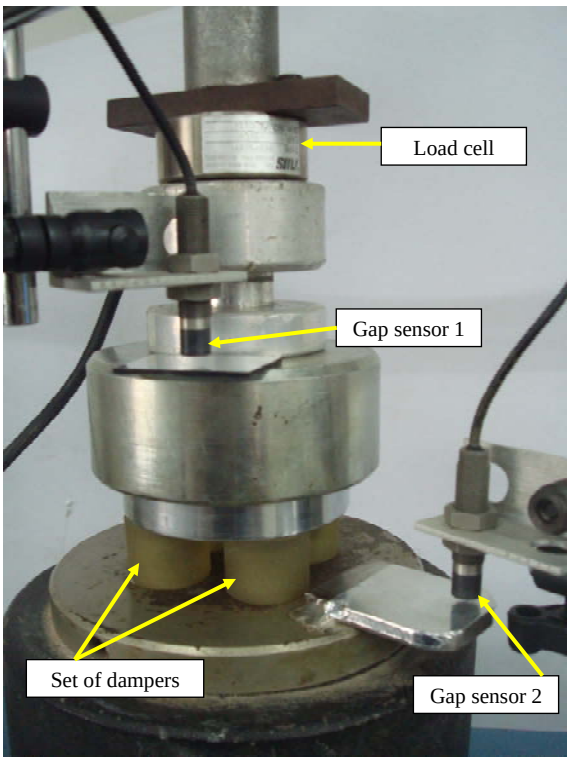

Figure 3.47 Photo showing method to determine a spring constant value of damper by UC test.

Figure 3.47 shows the method to perform the spring constant by unconfined compression (UC) test on one of the four dampers of FWD device. Two gap sensors were used to measure the displacement in vertical direction of damper and axial load was measured by a load cell. The spring constant value was defined as axial load divided by vertical displacement as follows:

$$k_e = \frac{F_a}{\Delta} \quad (3.45)$$

where:

k_e = the spring constant value of damper (kN/mm),

F_a = the axial load by UC test (kN), and

Δ = the vertical displacement of damper (mm).

3.15 Evaluation of Remain Efficiency of Damper

The remain efficiency test was performed to investigate the remain efficiency value due to the absorption of impulse load by damper in FWD test.

In this research, FWD tests were performed on a rigid pavement (i.e., reinforced concrete deep-beam) (Fig. 3.48) and the impact load was measured by a load cell. These tests were performed by increasing the falling heights in series of tests, which are 10, 25, 50, 75, 100, 150, 200, 250, 300, 350, 400, 450, 500, 550 and 600 mm. From this test, the peak impact load was measured and the remain efficiency value was determined by Eq. 3.41.

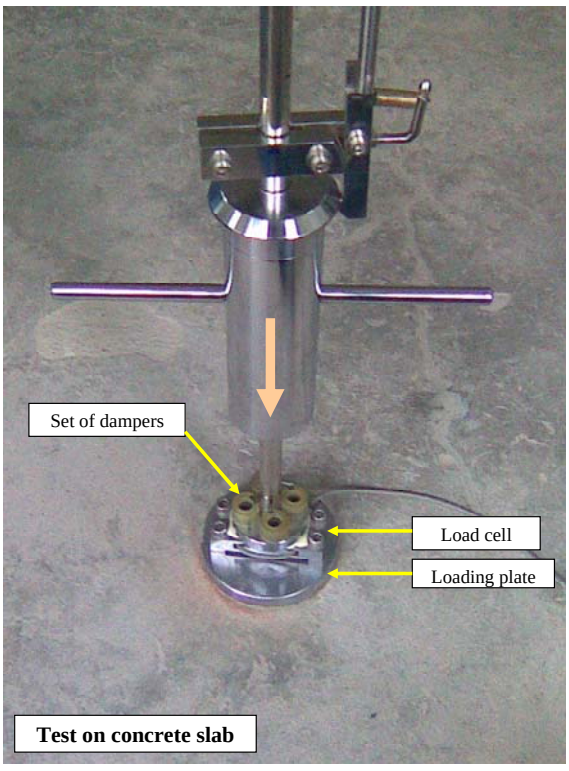

Figure 3.48 Photo of method to perform a remain efficient value of FWD due to damper on concrete slab.

4 RESULTS

4.1 Introduction

Generally, the stiffness values of pavement structure obtained by the dynamic method are higher than the ones by the static method. In this chapter, test results by dynamic method were compared with respective test results by static method and adjustments on dynamic test results were proposed to obtain reliable modulus of subgrade reaction (k value). In addition, an analytical method by undamped harmonic motion to predict the modulus of subgrade reaction from Falling Weight Deflectometer (FWD) test result was proposed and compared with the ones from other methods.

4.2 Basic tests of Materials

4.2.1 KMUTT Sand (for Subgrade)

The index property tests of KMUTT sand conducted in this research consisted of specific gravity test, sieve analysis, maximum and minimum void ratio determination and compaction test. The results of this various index property tests are summarized in Table 4.1. The specific gravity of the KMUTT sand sample was observed to be 2.64.

The grain-size distribution curve from sieve analysis performed on KMUTT sand was compared with the one on the original river-bed sand as presented in Fig. 4.1. The KMUTT sand contains 0.38 percent passing through the No. 200 sieve (0.075 mm). The uniformity coefficient C_u and the coefficient of gradation C_c were equal to 1.879 and 0.946, respectively. Based on the Unified Soil Classification System (USCS), the KMUTT sand can be classified as poorly-graded-sand (SP). In this research, subgrade was prepared by pluviating KMUTT sand through air by a multiple sieving pluviation apparatus in order to obtain the average density of about 1.542 g/cm^3 (D_r = 96.92 %).

Table 4.1 Index properties of KMUTT sand used in this research.

Properties	Characteristics Values
Maximum void ratio, e_{max}	1.06
Minimum void ratio, e_{min}	0.71
Air-dried water content, w_a (%)	0.11
Specific gravity, G_s	2.64
Maximum particle size, d_{max} (mm)	0.425
Minimum particle size, d_{min} (mm)	0.150
Mean particle size, d_{50} (mm)	0.285
Coefficient of uniformity, C_u	1.879
Coefficient of gradation, C_c	0.946
Angularity	Sub-angular

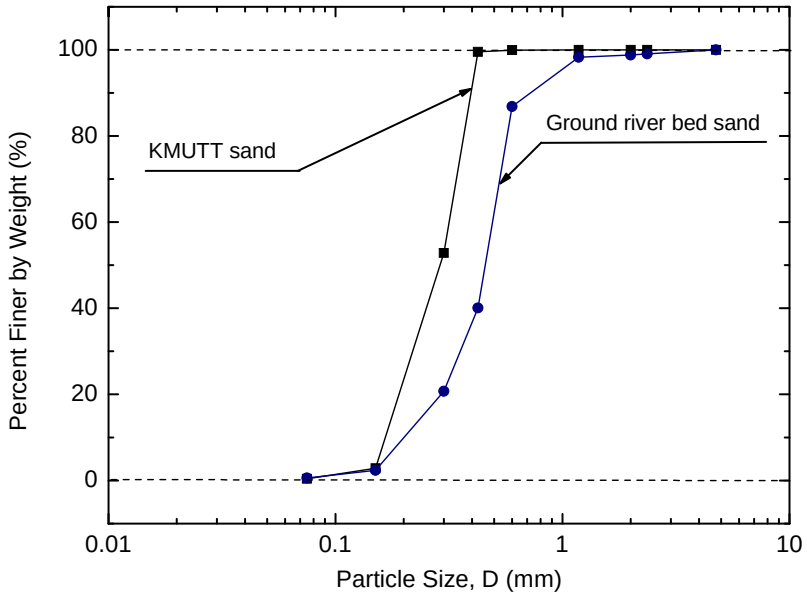

Figure 4.1 Comparison of gradation curves of KMUTT-sand between before and after sieving.

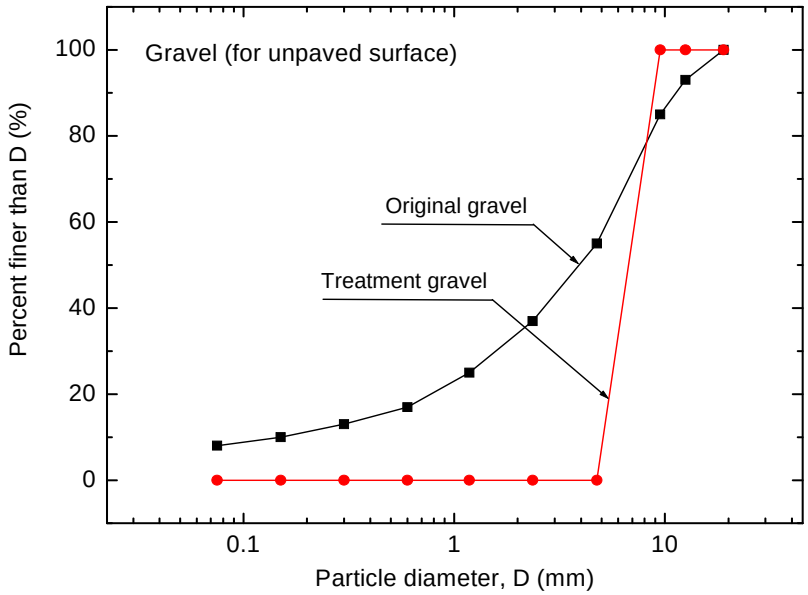

Figure 4.2 Gradation curves of gravel between before and after sieving.

4.2.2 Gravel (for unpaved surface)

Gravel layer was modified by coarse aggregates for modeling the gravel road. It was prepared by sieving the coarse aggregate to pass through sieve with opening size of 3/8 in. (9.50 mm) and to retain on sieve No.4 (4.75 mm). Then, gravel were pluviated by a sieve with opening size of 1/2 in. (12.5 mm) for modeling the gravel layer of 250 mm in thickness.

Gradation curve of gravel for modeling unpaved surface layer is presented in Fig. 4. 2. The uniformity coefficient C_u and the coefficient of gradation C_c were equal to 1.421 and 0.930, respectively. Based on the Unified Soil Classification System (USCS), this modeled gravel can be classified as poorly graded gravel (GP). The average dry density of gravel layer is about 1.66 g/cm^3 and the other properties were summarized in Table 4.2.

Table 4.2 Index properties of gravel for modeling unpaved surface.

Properties	Characteristics Values
Maximum particle size, d_{max} (mm)	9.50
Minimum particle size, d_{min} (mm)	4.75
Mean particle size, d_{50} (mm)	6.73
Coefficient of uniformity, C_u	1.421
Coefficient of gradation , C_c	0.930

4.2.3 Asphaltic Concrete (for paved surface)

4.2.3.1 Aggregates

The particle distribution curves and sizes of aggregate for wearing course layer of which the size name was called "the 12.5 mm (1/2 in.)" were selected based on standard test number DRR 209-2545 of the Department of Rural Roads (DRR)-Thailand and Job Mix Formula (JMF) for a state mix No.4 of the Department of Transportation (DOT)-USA as shown in Fig. 4.3 and Table 4.3, respectively. In this research, the particle size was reduced by a factor of 1.5 while the gradation was kept the same as the standard one. The results of various index property tests on this scaled-down aggregate were summarized in Table 4.4.

The uniformity coefficient, C_u, and the coefficient of gradation, C_c, were equal to 38.070 and 3.352, respectively. Comparing the values of C_u and C_c, it was found that the gradation of scaled-down aggregates was nearly close to the well-graded gravel (C_u > 4; C_c = 1-3), reported by Head (1982).

Table 4.3 The particle size of aggregates scaled-down from DRR 209-2545 and Job Mix Formula (JMF) for a State Mix No.4.

Sieve size	Percent passing (by weight)			
	Upper boundary	Lower boundary	Aggregate by DRR 209-2545 and state mix No.4 by JMF	Scaled-down aggregate
(3/4") - (1/2")	100	100	100	100
(1/2") - (3/8")	85	100	93	100
(3/8") - (#4)	72	88	85	96
(#4) - (#8)	48	66	55	73
(#8) - (#16)	30	47	37	48
(#16) - (#30)	21	37	25	33
(#30) - (#50)	15	27	17	22
(#50) - (#100)	9	21	13	16
(#100) - (#200)	6	16	10	13
finer than No.200	4	10	8	9

Table 4.4 Index properties of scaled-down aggregate used in this research.

Properties	Characteristics Values
Maximum particle size, d_{max} (mm)	12.50
Mean particle size, d_{50} (mm)	2.51
Minimum particle size, d_{min} (mm)	finer than 0.075 mm
Coefficient of uniformity, C_u	38.07
Coefficient of gradation , C_c	3.35

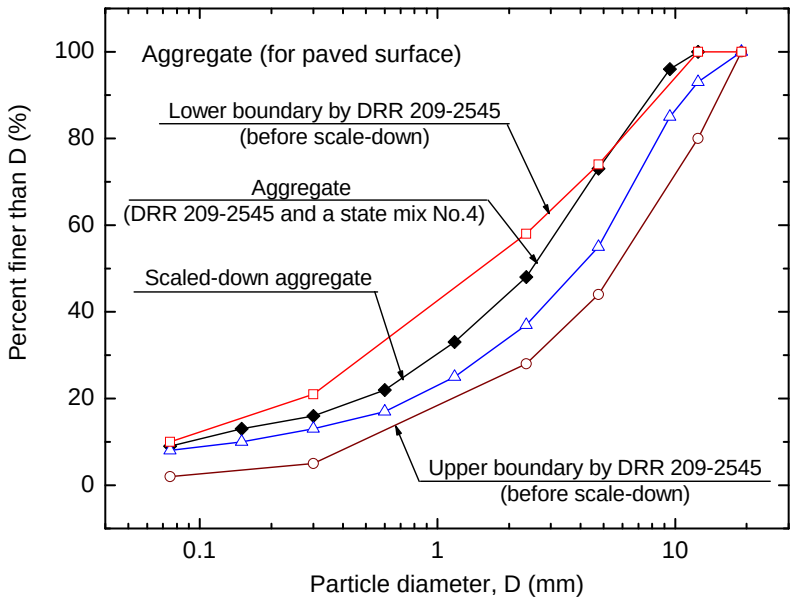

Figure 4.3 Gradation curve of aggregates scaled down from DRR 209-2545 and Job Mix Formular (JMF) for a State Mix No. 4.

4.2.3.2 Asphaltic Cement

The physical properties of asphaltic cement of 60/70 grade that is specified for hot-mixed asphaltic concrete by standard test number DRR 230-2545, are controlled in industrial process.

4.3 Rate-sensitivity Coefficients of KMUTT Sand

A series of unconventional consolidated drained triaxial compression (CDTC) tests were performed on KMUTT sand. The specimens used initially have 70 mm in diameter and 150 mm in height before consolidation. Then, they were isotropic consolidated to the effective confining stress of 200 kPa before shearing by compressing the specimens at the strain rate values that were changed many times during shearing process until failure.

The relationship between effective stress ratio ($R = \sigma_1'/\sigma_3'$) and axial strain (ε_a) obtained by a CDTC test is shown in Fig. 4.4a. Figure 4.4b shows the stress jump by an increase in the instantaneous strain rate. From Figs. 4.4a and 4.4b, the normalized stress ratio can be plotted with the logarithm of strain rate changes for the respective stress jumps as shown in Fig. 4.5. Subsequently, the slope of the linear relation fitted to the data plotted in Fig. 4.5 which is called the rate-sensitivity coefficient (β) was defined. The β value of 0.02682 was derived for KMUTT sand.

Due to the global stress paths employed in FWD and PLT test are different from CDTC test in which only the major principal stress increases while the minor one is kept constant, the β value for a given type of material increases from the value obtained by CDTC to the value that would be described by Fig. 4.6. Here, it is assumed that the stress path *R* in Fig. 4.6 is the global stress path of sand underneath the loading plate. If stress paths *R* is performed by FWD or PLT test under general stress conditions, there would be no viscous effects developed along *R* is kept constant stress paths. To understand the relationship between stress paths *R* and stress paths by TC test, the shear and compression yield loci illustrated in Fig. 4.6 are introduced. The two types of yield loci described in total stress components are considered to expand and shrink upon an increase and decrease in $\dot{\varepsilon}^{ir}$ at a fixed $\dot{\varepsilon}^{ir}$. Then, the fact that the β values in FWD and PLT test are larger than in TC test can be understood.

a)

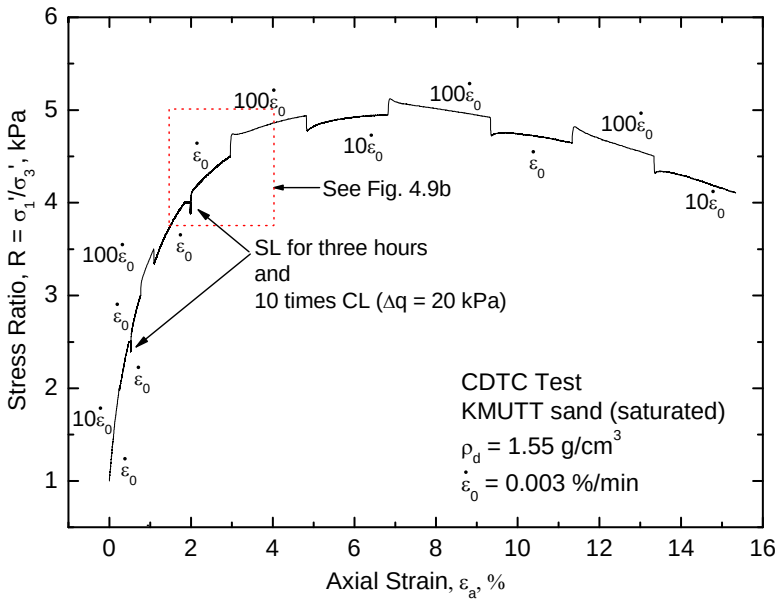

b)

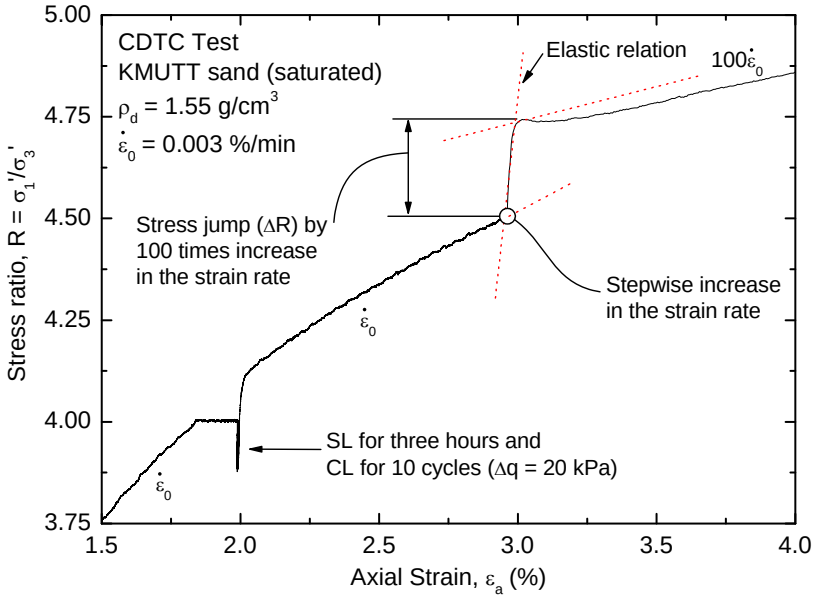

Figure 4.4 a) Stress-strain behavior of KMUTT sand performed by CDTC test; and b) Stres jump by increase in the change of instantaneous strain rate (Kawabe, 2008).

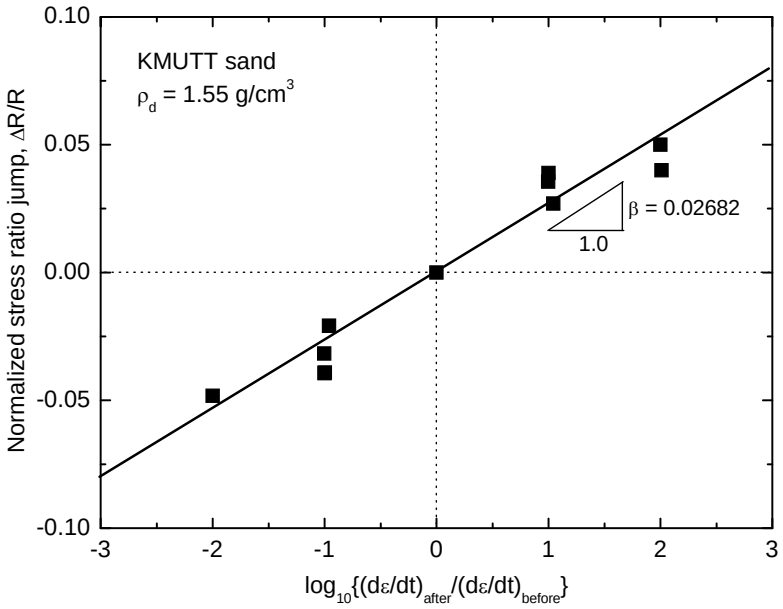

Figure 4.5 Rate-sensitivity coefficient (β) values of KMUTT sand evaluated by CDTC test. (Kawabe, 2008).

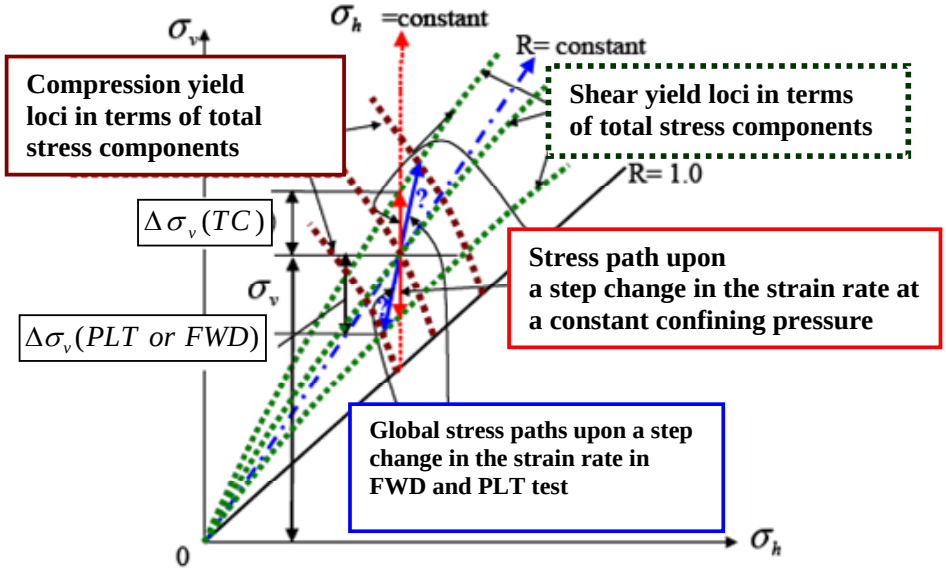

Figure 4.6 Inferred global stress paths by FWD and PLT test compared with TC test (modified after Tatsuoka et al., 2003b).

It is the vital drawback of the present FWD and PLT tests that the horizontal stress was not measured, so it was not possible to analyse this issue based on the yield loci. It seems that the stress ratio *R* is not kept constant upon a step change in the strain rate in FWD and PLT tests. To investigate the β value along stress path *R* in FWD and PLT tests would be performed as:

a) To perform settlement rate changes in PLT test (Hirakawa, 2003; Hirakawa et al., 2008).

b) To perform settlement rate changes and analyse in Finite Element Method (FEM) by computing programming.

By comparing the β value obtained by PLT with the one by CDTC test on the same material reported by (Hirakawa et al., 2008), the β value by PLT was higher than the one by CDTC test by a factor of 1.346. In this research, this ratio was assumed to be independent of types of geomaterial. Therefore, the equivalent β value for PLT with KMUTT sand is:

$$\beta_{KMUTT,PLT} = 1.346 * \beta_{KMUTT,CDTC}$$
$$= 1.346 * 0.02682$$
$$= 0.03610$$

4.4 Uniaxial Test on Damper

Figure 4.7 shows the test result by unconfined compression (UC) test on a set of the four dampers of FWD apparatus. The relationship between axial load (F_a) and settlement (Δ) value is essentially linear, showing a spring constant (k_e) equal to 3.439 kN/mm.

The capacity of FWD device determined from the impact load by dropping hammer from the falling height of 500 mm (specified as the maximum falling height of this device used in this research) following Eq. 3.48 is 18.37 kN.

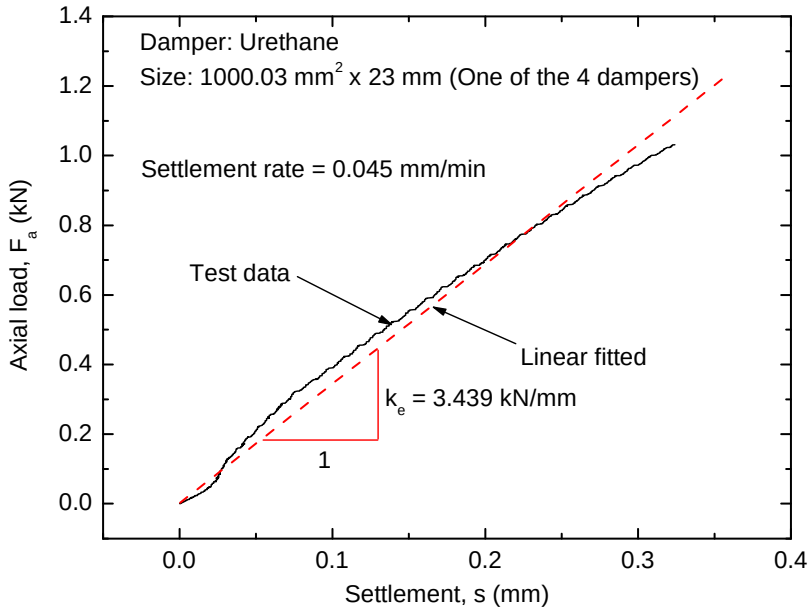

Figure 4.7 Spring constant value of damper performed by UC test.

4.5 Discussions on Evaluated Modulus of Subgrade Reaction by Static Plate Load Test on Pavement Structure

In this section, test results of the repetitive PLT test were analyzed to obtain the relationship between plate pressure and settlement that would be obtained from nonrepetitive PLT test. The values of modulus of subgrade reaction by PLT tests (k_{PLT} -values) were evaluated into three different values following different determining definitions as follows:

a) the secant modulus ($k_{\text{sec, }PLT}$) obtained by dividing the pressure on loading plate p (or $p_{\max}$) with settlement s (or $s_{\max}$) at the post-yielding immediately before unloading each loop of repetitive PLT test.

b) the modulus of subgrade reaction ($k_{sub,\ PLT}$) calculated by AASHTO method. This value was obtained by dividing the pressure on loading plate (p) when it is equal to 68.9 kPa (10 psi.) with respective settlement (s) from the nonrepetitive $p-s$ relation.

c) the modulus of subgrade reaction ($k_{sub,\ PLT}$) calculated by Florida method. This value was obtained by dividing the respective pressure on loading plate (p) on the nonrepetitive $p-s$ relation with the settlement (s) is of 1.27 mm (0.05 in.).

For subgrade, the relationship between plate pressure and settlement of repetitive PLT test is shown in Fig. 4.18. Figure 4.19 shows the recorded average settlement rate of loading plate by a controlled nominal rate of 0.237 mm/min during testing. A 4th-degree polynomial function was fitted to the post-yielding regimes of $p-s$ relation from repetitive tests to obtain the non-repetitive one (Fig. 4.8). Then, the values of modulus of subgrade reaction ($k_{sub,\ PLT}$) were obtained as: 98.15 and 85.96 kPa/mm following respectively AASHTO and Florida methods, as shown in Figs. 4.10 and 4.11.

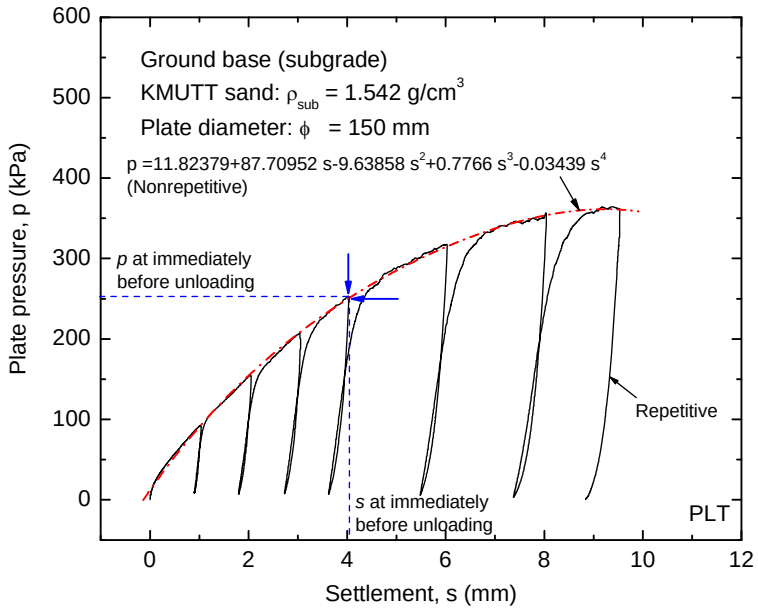

Figure 4.8 Repetitive PLT test result and a 4th-degree polynomail function fitted to nonrepetitive PLT test result on subgrade.

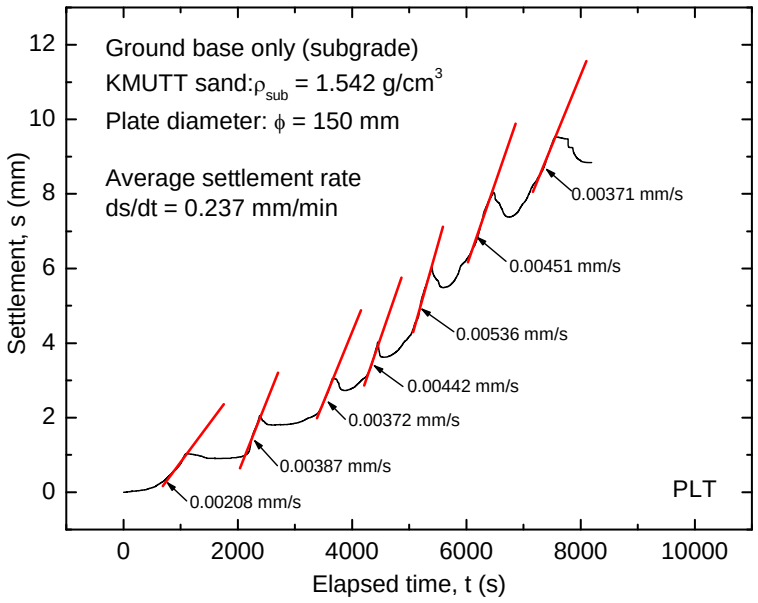

Figure 4.9 Time history of plate settlement in repetitive PLT test and the derived settlement rates during loading on subgrade.

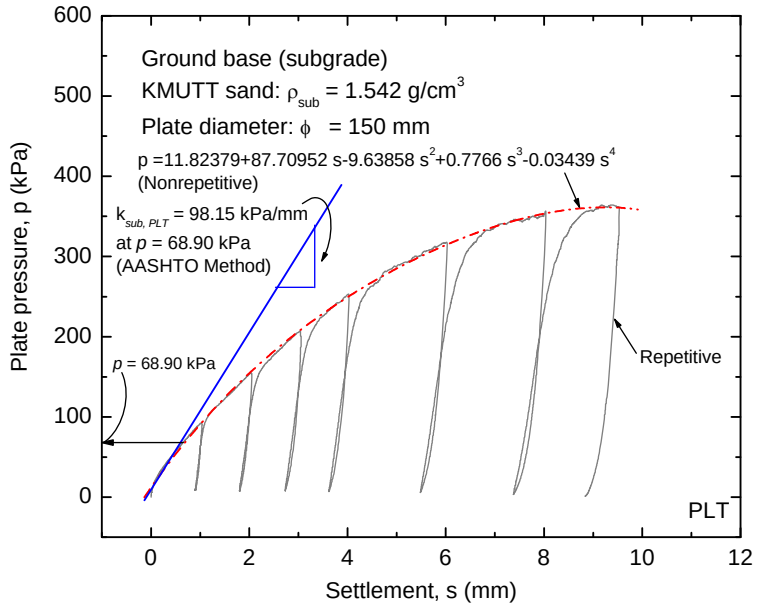

Figure 4.10 The $k_{sub,\ PLT}$ value of subgrade from a PLT test evaluated following AASHTO designation method.

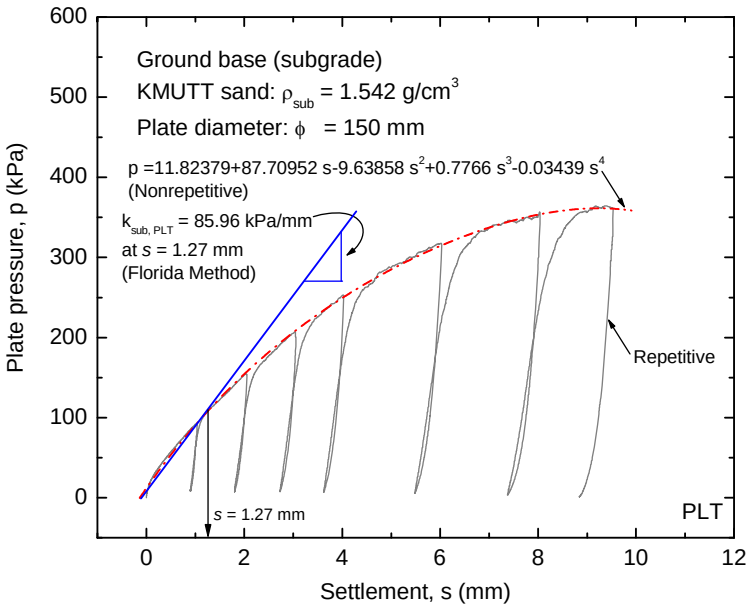

Figure 4.11 The $k_{sub,\,PLT}$ value of subgrade from a PLT test evaluated following Florida designation method.

For unpaved surface, a 250-mm thick gravel layer was laid on the top of subgrade layer for modeling an unpaved gravel road. The PLT test result on unpaved surface and the average settlement rate of loading plate at a nominal controlled value of 0.187 mm/min are shown in Figs. 4.12 and 4.13, respectively. The values of modulus of subgrade reaction ($k_{sub,\,PLT}$) evaluate following respectively AASHTO and Florida methods are equal to 78.55 and 73.30 kPa/mm as shown in Figs. 4.14 and 4.15.

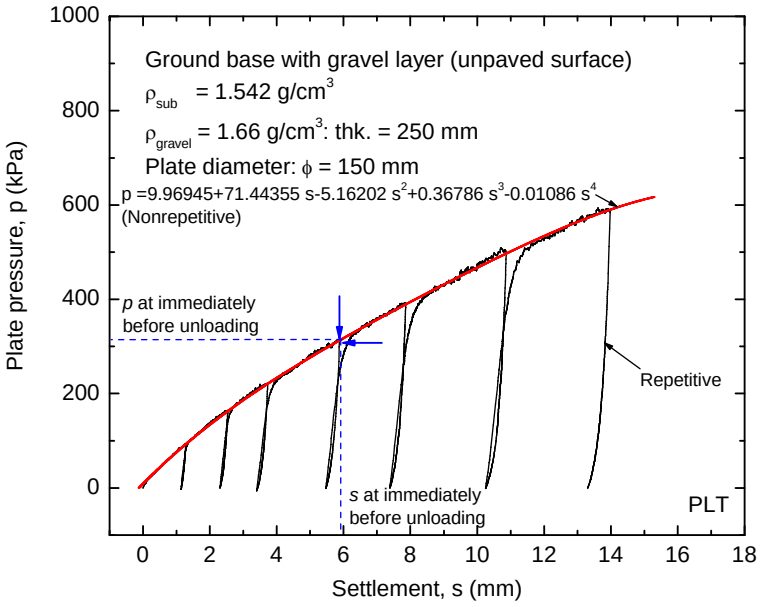

Figure 4.12 Repetitive PLT test result and a 4th-degree polynomail function fitted to nonrepetitive PLT test result on unpaved surface.

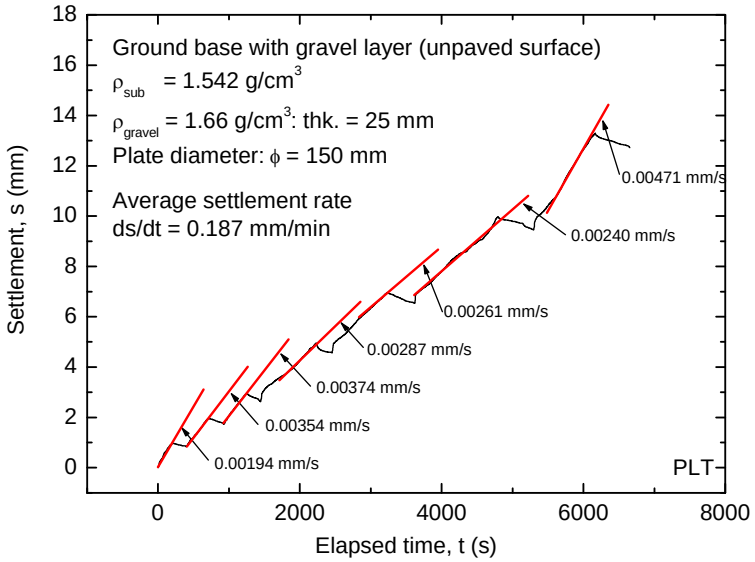

Figure 4.13 Time history of plate settlement in repetitive PLT test and the derived settlement rates during loading on unpaved surface.

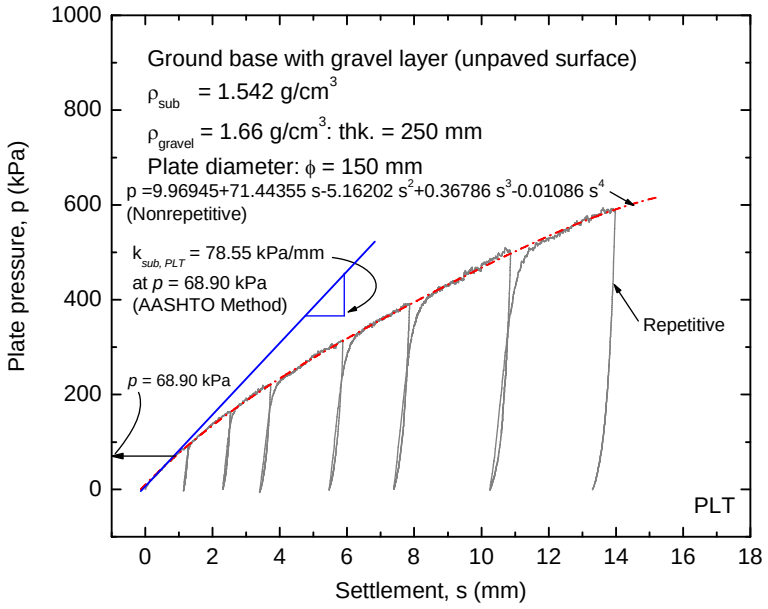

Figure 4.14 The $k_{sub,\ PLT}$ value of unpaved surface from a PLT test evaluated following AASHTO designation method.

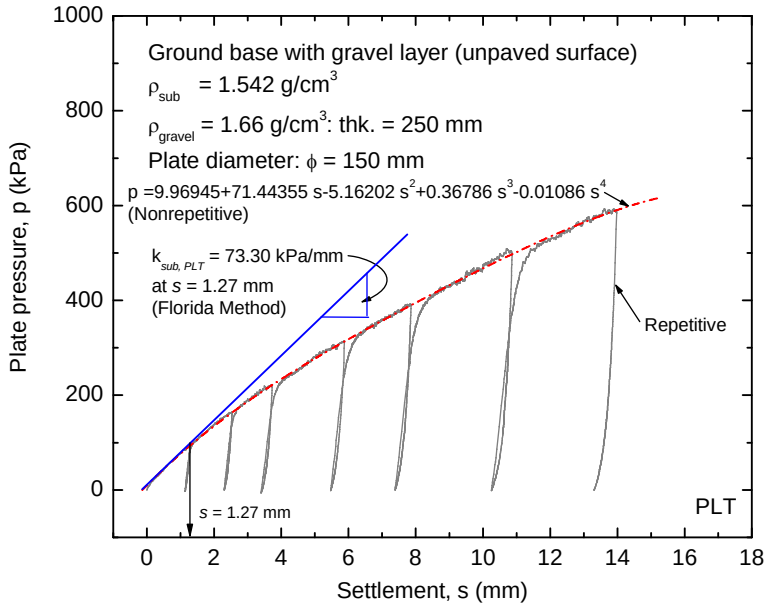

Figure 4.15 The $k_{sub,\ PLT}$ value of unpaved surface from a PLT test evaluated following Florida designation method.

For paved surface, an asphaltic concrete layer having thickness of 50 mm was laid on the subgrade layer to model the layer stiffer than subgrade layer. The PLT test result on paved surface and the average settlement rate of loading plate at a controlled nominal value of 0.122 mm/min are shown in Figs. 4.16 and 4.17, respectively. The values of modulus of subgrade reaction ($k_{sub,\ PLT}$) evaluate following respectively AASHTO and Florida methods are equal to 281.45 and 203.08 kPa/mm as shown in Figs. 4.18 and 4.19.

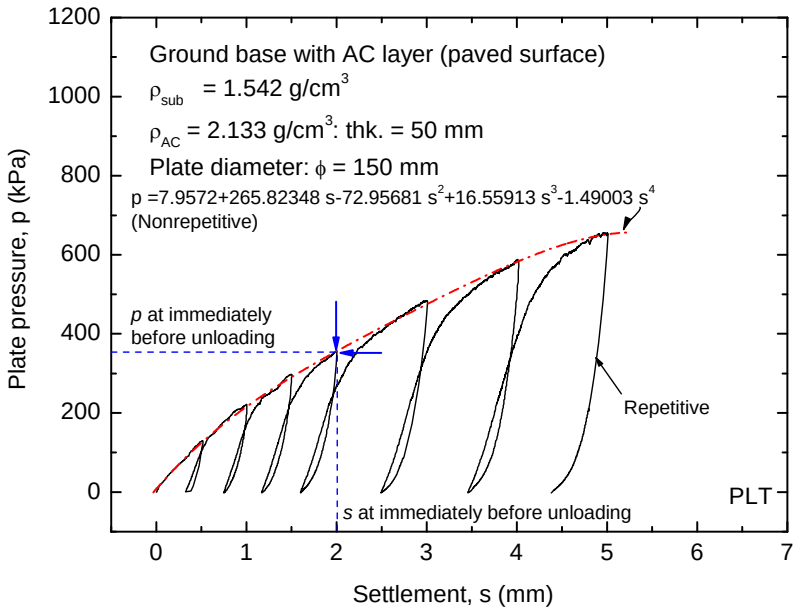

Figure 4.16 Repetitive PLT test result and a 4th-degree polynomail function fitted to nonrepetitive PLT test result on paved surface.

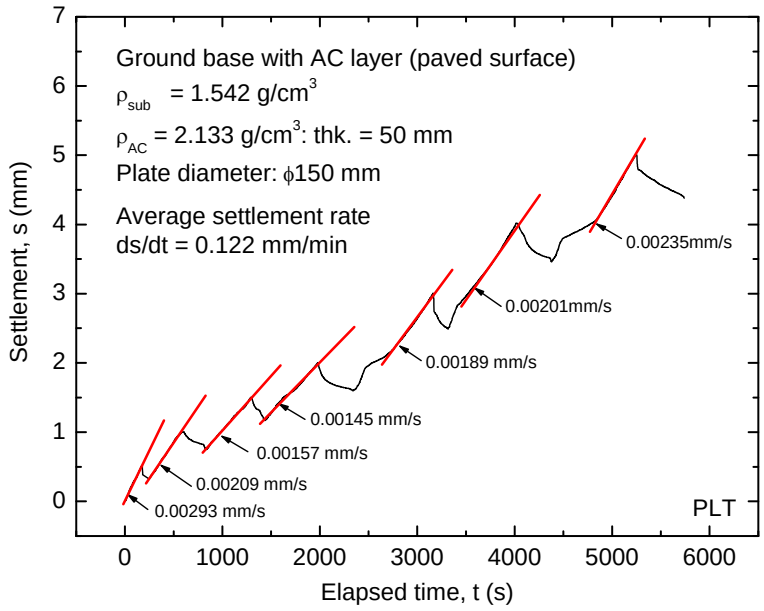

Figure 4.17 Time history of plate settlement in repetitive PLT test and the derived settlement rates during loading on paved surface.

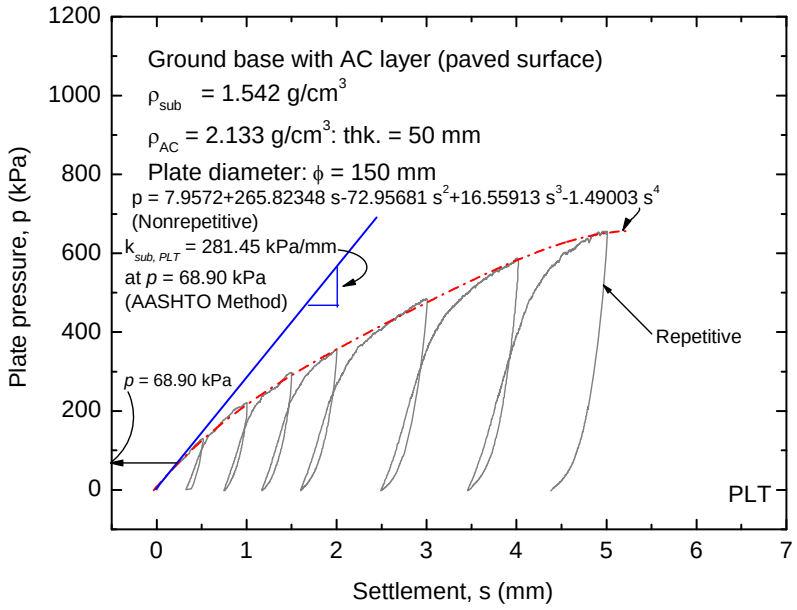

Figure 4.18 The $k_{sub,\ PLT}$ value of paved surface from a PLT test evaluated following AASHTO designation method.

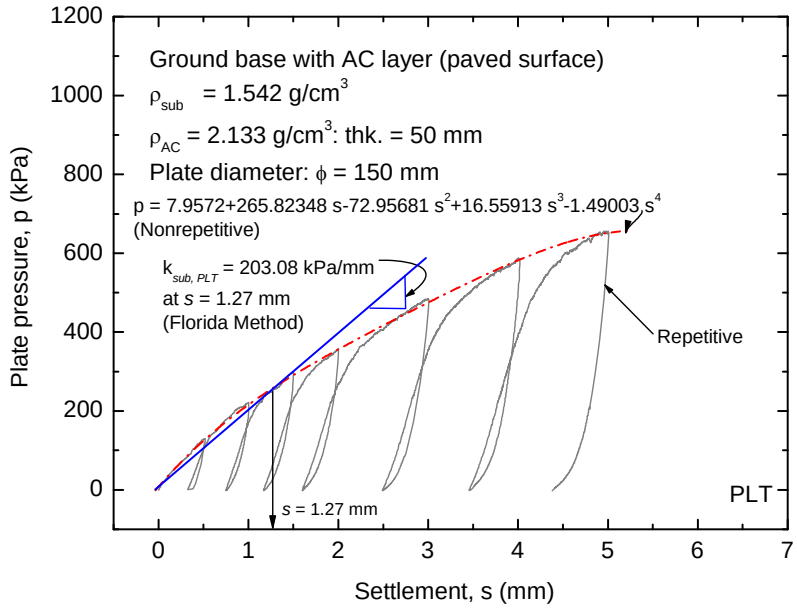

Figure 4.19 The $k_{sub,\ PLT}$ value of paved surface from a PLT test evaluated following Florida designation method.

4.6 Discussions on Evaluated Modulus of Subgrade Reaction by Falling Weight Deflectometer Test on Pavement Structure

In this section, test procedures to evaluate the modulus of subgrade reaction (k_{FWD} values) by FWD tests are presented into two forms as follows:

a) a series of drop in FWD test to evaluate the secant modulus of subgrade reaction ($k_{\text{sec},\ FWD}$) value.

b) a single drop in FWD test to evaluate the modulus of subgrade reaction ($k_{sub,\ FWD}$) value.

4.6.1 Falling Weight Deflectometer Test by a series of drops

A series of drop in FWD test were performed to obtain relationship between the plate pressure on loading plate and were settlement from each falling height (each loop) and then settlements measured for subsequent falling heights (loops) were accumulated to the precedent value. The modulus of subgrade reaction can be considered as a secant modulus ($k_{\text{sec},\ FWD}$) obtained as the maximum value of p ($p_{\max}$) divided by the maximum value of s ($s_{\max}$) for a respective loop of loading (falling height).

Test results of a series of drops in FWD test for three different pavement conditions (subgrade, unpaved surface and paved surface) are shown in Figs. 4.20, 4.271 and 4.22, respectively.

At each falling height, the evaluated $k_{\text{sec, }FWD}$ values from three different pavement conditions seem to be higher for stronger surface and smaller for weaker surface. These results are consistent with the $k_{sub,\ PLT}$ values described in section 4.5.

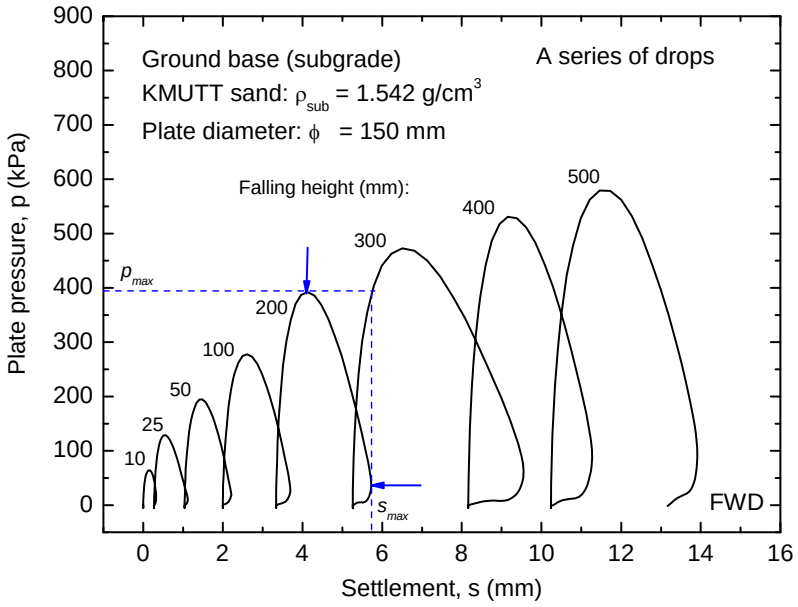

Figure 4.20 Test result of a FWD test by a series of drops on subgrade.

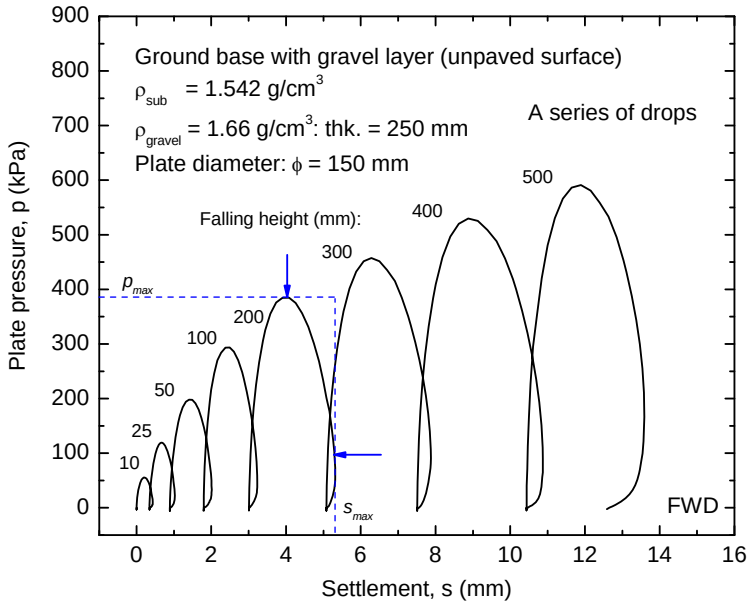

Figure 4.21 Test result of a FWD test by a series of drops on unpaved surface.

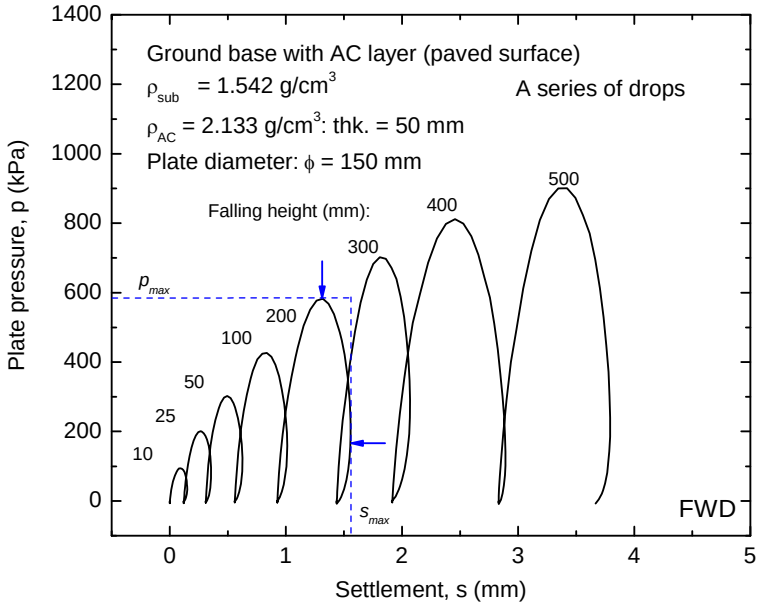

Figure 4.22 Test result of a FWD test by a series of drops on paved surface.

4.6.2 Falling Weight Deflectometer Test by a single drop

A single of drop in FWD test was performed to obtain relationship between the plate pressure on loading plate and settlement at each falling height (each loop) without accumulating the settlement values from respective subsequent loops. The modulus of subgrade reaction can be considered as a secant modulus ($k_{\text{sec, }FWD}$) obtained as the maximum value of p ($p_{\max}$) divided by the maximum value of s ($s_{\max}$) for each loop of loading (falling height).

Fig. 4.23 shows the relationship between plate pressure on loading plate (p) and settlement (s) obtained from FWD test by many single drops from different falling heights on subgrade. Figure 4.24 shows the $p-s$ relation when the falling height = 200 mm was used then, a modulus of subgrade reaction ($k_{sub,\ FWD}$) of 162.82 kPa/mm was obtained. Fig. 4.25 shows the $(s_{\max}, p_{\max})$ data, presented as solid squares, obtained from different loops of a single drop in FWD test performed at different falling heights. A linear having a slope of 162.63 kPa/mm was fitted to the test data (Fig. 4.25).

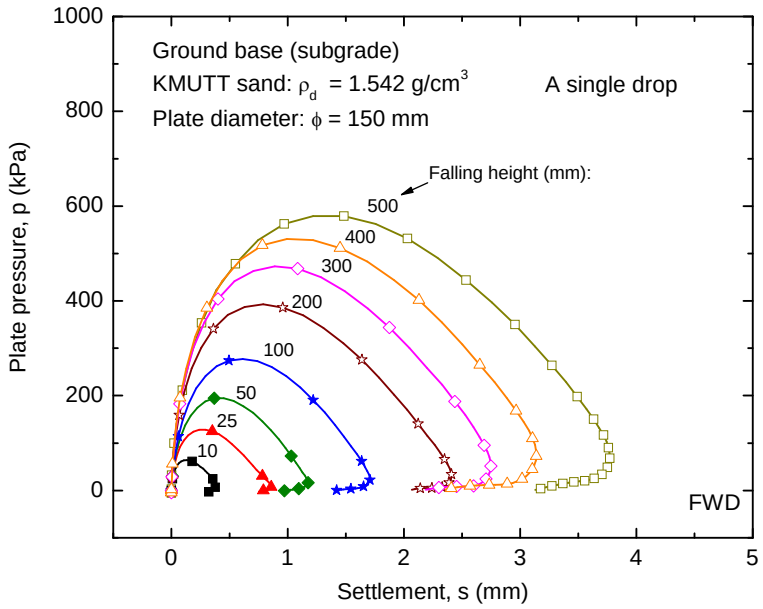

Figure 4.23 Test result of a FWD test by a single drop on subgrade.

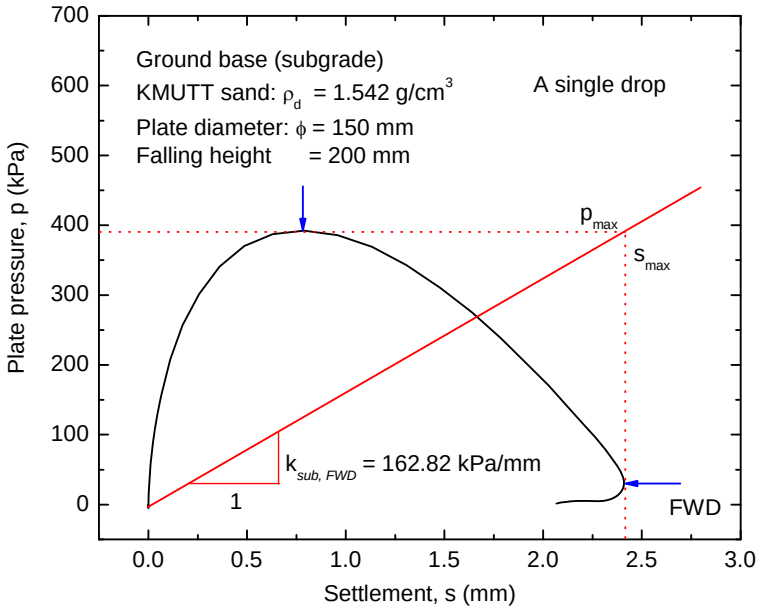

Figure 4.24 $k_{sub,\,FWD}$ **value of subgrade by a single drop at falling height = 200 mm in a FWD test calculated by dividing** $p_{\max}$ **with** $s_{\max}$ **of the** $p-s$ **relation.**

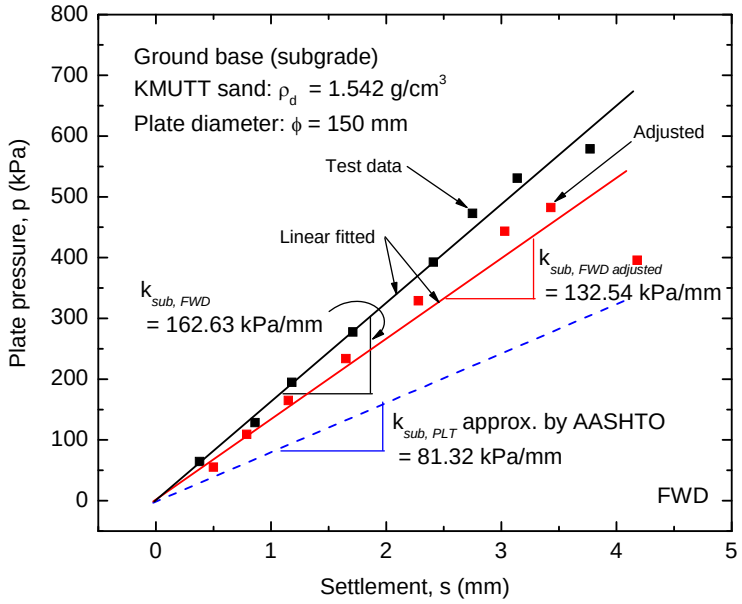

Figure 4.25 $k_{sub,\,FWD}$ **values of subgrade by a single drop in FWD test before and after adjustments for dynamic and loading rate effects and the approximated** $k_{sub,\,PLT}$ **value determined following AASHTO.**

For unpaved surface, the relationships between plate pressure on loading plate and settlement for the each loop and the respective relation for a falling height of 200 mm in a single drop in FWD test are shown in Figs. 4.26 and 4.27, respectively. The $k_{sub,\,FWD}$ value for the falling height of 200 mm is equal to 166.55 kPa/mm. A linear having a slope of 171.05 kPa/mm was fitted to the $(s_{\max}, p_{\max})$ coordinates obtained from different falling heights as shown in Fig. 4.28.

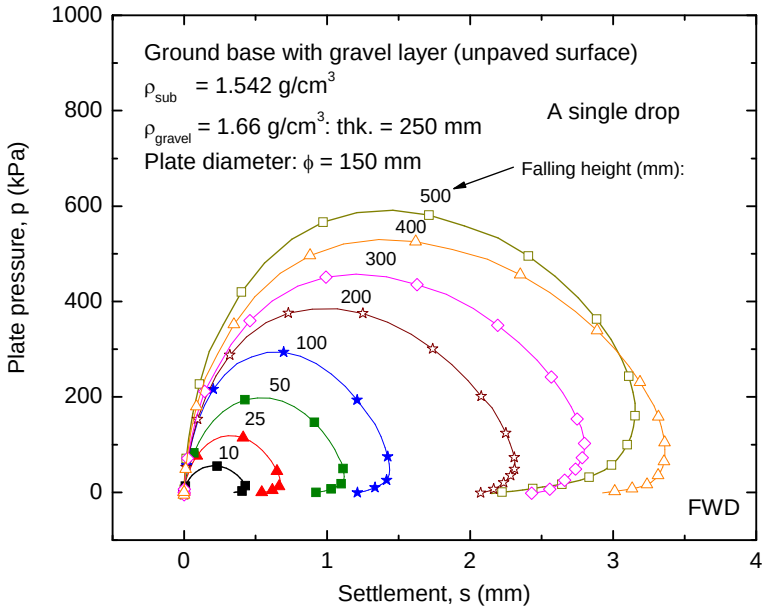

Figure 4.26 Test result of a FWD test by a single drop on unpaved surface.

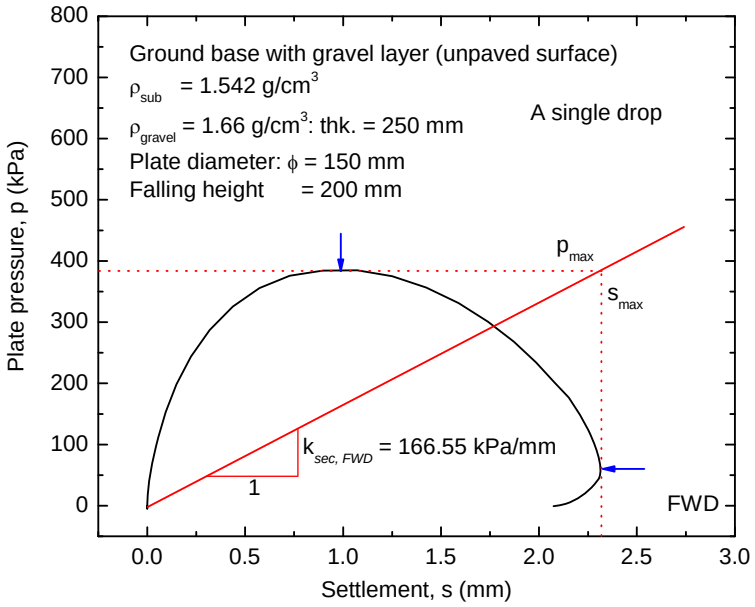

Figure 4.27 $k_{sub,\,FWD}$ value of unpaved surface by a single drop at falling height = 200 mm in a FWD test calculated by dividing $p_{\max}$ with $s_{\max}$ of the $p-s$ relation.

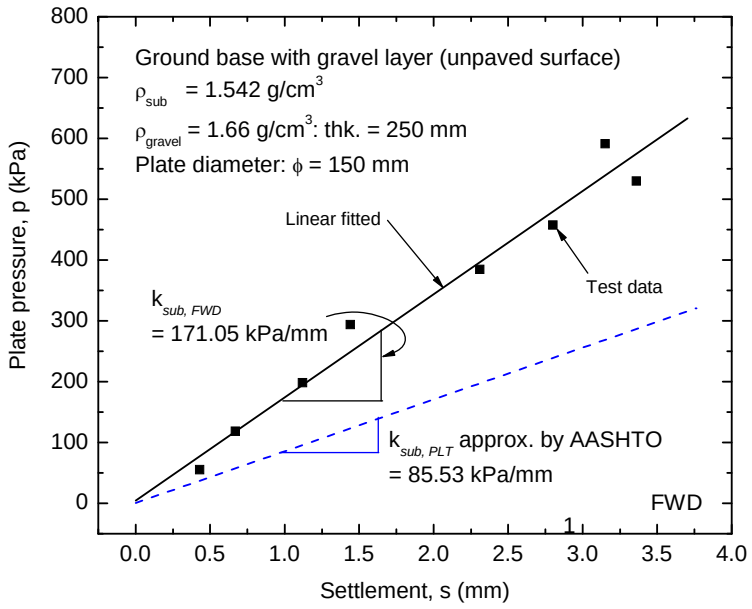

Figure 4.28 $k_{sub,\,FWD}$ values of unpaved surface by a single drop in a FWD test and the approximated $k_{sub,\,PLT}$ value determined following AASHTO.

For paved surface, the relationships between plate pressure on loading plate and settlement for the each loop and the respective relation for a falling height of 200 mm in a single drop in FWD test are shown in Figs. 4.29 and 4.30, respectively. The $k_{sub,\,FWD}$ value for the falling height of 200 mm is equal to 925.08 kPa/mm. A linear having a slope of 922.10 kPa/mm was fitted to the $(s_{\max}, p_{\max})$ coordinates obtained from different falling heights as shown in Fig. 4.31.

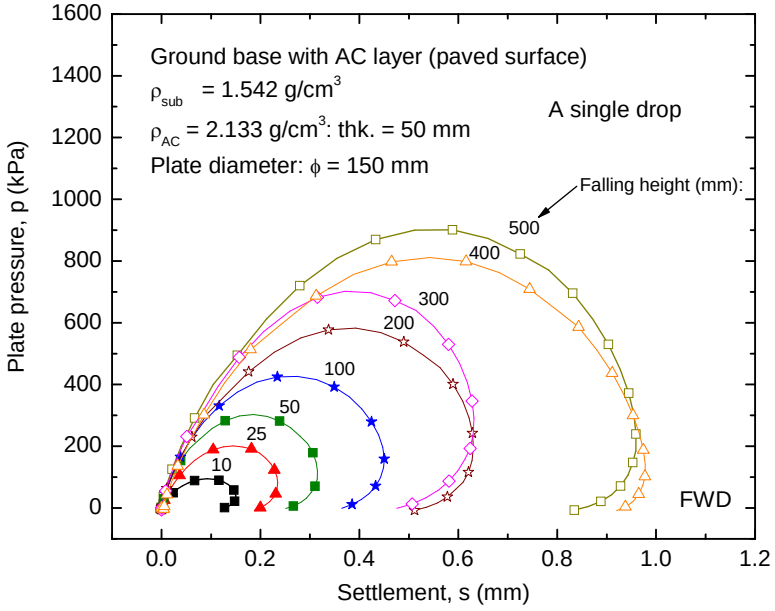

Figure 4.29 Test result of a FWD test by a single drop on paved surface.

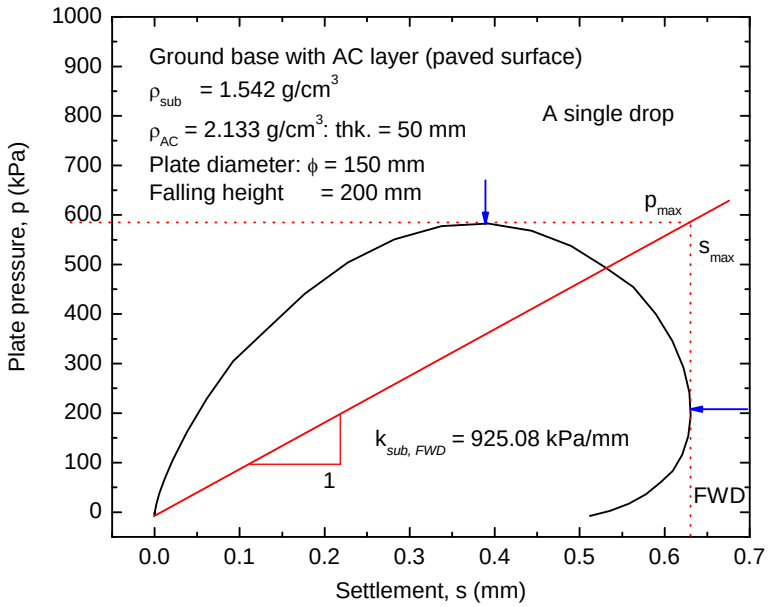

Figure 4.30 $k_{sub,\,FWD}$ value of paved surface by a single drop at falling height = 200 mm in a FWD test calculated by dividing $p_{\max}$ with $s_{\max}$ of the $p-s$ relation.

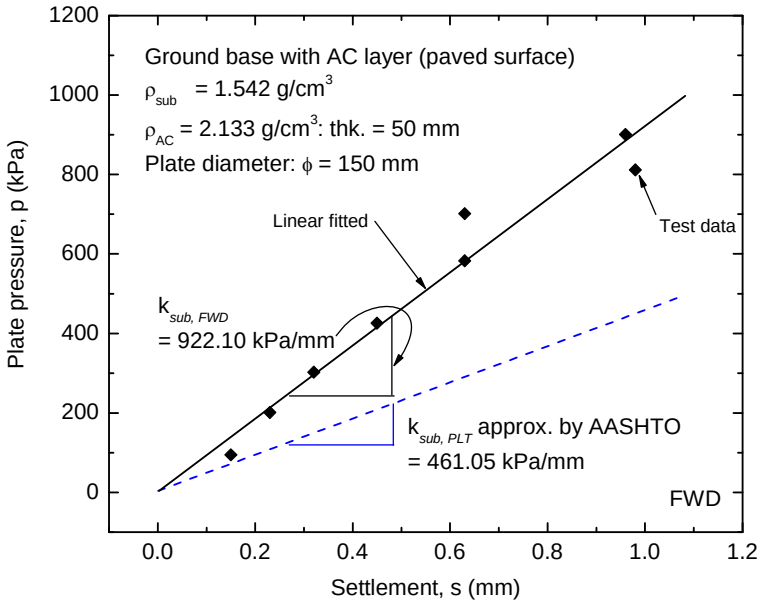

Figure 4.31 $k_{sub,\,FWD}$ values of paved surface by a single drop in a FWD test and the approximated $k_{sub,\,PLT}$ value determined following AASHTO.

The $k_{sub,\,FWD}$ values can be used to approximately determine $k_{sub,\,PLT}$ by following Eq. 3.6b which was proposed by AASHTO (1993). Then, in this manner, the approximated $k_{sub,\,PLT}$ of subgrade, unpaved surface and paved surface are equal to 81.32, 85.53 and 461.05 kPa/mm, respectively. These results were shown in Figs. 4.25, 4.28 and 4.31, respectively.

Comparing the approximated $k_{sub,\,PLT}$ from FWD following AASHTO approximation method with $k_{sub,\,PLT}$ from PLT following AASHTO and Florida designation methods as described in Section 4.5, it was found that the range of differences of $k_{sub,\,PLT}$ from FWD following AASHTO approximation method on the unbound surface (e.g., sand layer in subgrade and gravel layer in unpaved surface) are 5.40 % to 17.15 %. On the other hand, for bound surface (e.g., asphaltic concrete layer in paved surface), the range of differences of $k_{sub,\,FWD}$ are 63.82 % to 127.04 %. Then, it the approximated $k_{sub,\,PLT}$ from FWD following AASHTO approximation method by Eq. 3.6b are not applied for evaluating the k-value for all flexible pavement condition. Comparing of $k_{sub,\,PLT}$ from FWD following AASHTO approximation method with the ones from PLT tests were tabulated in Table. 4.5.

Table 4.5 Summary of the approximated $k_{sub,\,PLT}$ in FWD following AASHTO approximation method compared with the $k_{sub,\,PLT}$ evaluated following AASHTO and Florida designation methods in nonrepetitive PLT test on pavement surface.

Pavement condition	$k_{sub,\,FWD}$ by FWD test (kPa/mm)	$k_{sub,\,PLT}$ approximated by $k_{sta}=\frac{k_{dyn}}{2}$ (kPa/mm)	$k_{sub,\,PLT}$ by AASHTO method (kPa/mm)	$k_{sub,\,PLT}$ by Florida method (kPa/mm)	Range of differences from PLT test (for both AASHTO and Florida methods) (%)
subgrade	162.63	81.32	98.15	85.96	5.40 - 17.15
unpaved surface	171.05	85.53	78.55	73.30	8.89 - 16.68
paved surfaced	922.10	461.05	281.45	203.08	63.81 - 127.03

4.7 Adjustment on Falling Weight Deflectometer Test Result for Subgrade and Discussion

In this section, the analyses for eliminating the dynamic effects were shown. Then, the plate pressure p and settlement s relationships obtained by FWD test were adjusted. Subsequently, the loading rate effects were taken into consideration and the $p-s$ relationships that already have been adjusted for dynamic effects were adjusted again for loading rate effect. For ease of illustration, the $p-s$ relationship of FWD at the falling height of 200 mm was compared with the original FWD test result in a series of drops and a single drop.

4.7.1 Adjustment for Dynamic Effects

The time histories of accelerations measured at the loading plate and inside the ground were shown in Fig. 4.32. From this figure, it is clearly seen that there are time-lags when wave propagated into the ground. Then, for each curve in Fig. 4.32, the vertical displacement at each depth as a function of time can be obtained by double-integration the respective time-histories of acceleration. In this research, the velocities of wave propagation were explained into two parts following the different depths from ground surface as shown in Fig. 4.32. Firstly, the velocities of wave propagation were averaged from the ground surface to the depth equal to twice of loading plate diameter (range of 0 to 300 mm). Secondly, the velocities of wave propagation were averaged again from the depth of 300 mm to the deepest depth where the accelerometers were installed (range of 300 to 800 mm). Subsequently, the vertical strain values at the different average depths were determined by following Eq. 3.8 as shown in Fig. 4.33. By correcting for time-lag by following Eq. 3.9, the new time histories of vertical strain that were corrected to remove time-lag were obtained and calculated. The settlement under loading plate is shown and compared with the original one in Fig. 4.34.

A series of drops and a single drop in FWD tests show that, at the same p, the settlements after time-lag have been removed increase when compared with the original ones as shown in Figs. 4.35 and 4.36, respectively. Figure 4.37 shows the relationship between vertical strain ε_z and depth z inside the ground from the ground surface. From this figure, it may be seen that there are differences between actual vertical strain and theoretical vertical strain shown in Fig. 3. 37.

4.7.2 Adjustment for Loading Rate Effects

Figures 4.38 and 4.39 respectively show the time histories of plate pressure and vertical velocity of plate for different falling heights in a series of FWD tests. On the other hand, Fig. 4.39 shows the time history of vertical settlement of plate measured in a PLT tests. In this figure, the slopes during loading stages in which the settlement increases were

derived to obtain the settlement rates ($\dot{u}_{z,\,PLT} = ds/dt$). Averagely, the $\dot{u}_{z,\,PLT}$ value is about 0.237 mm/min (0.00395 mm/s).

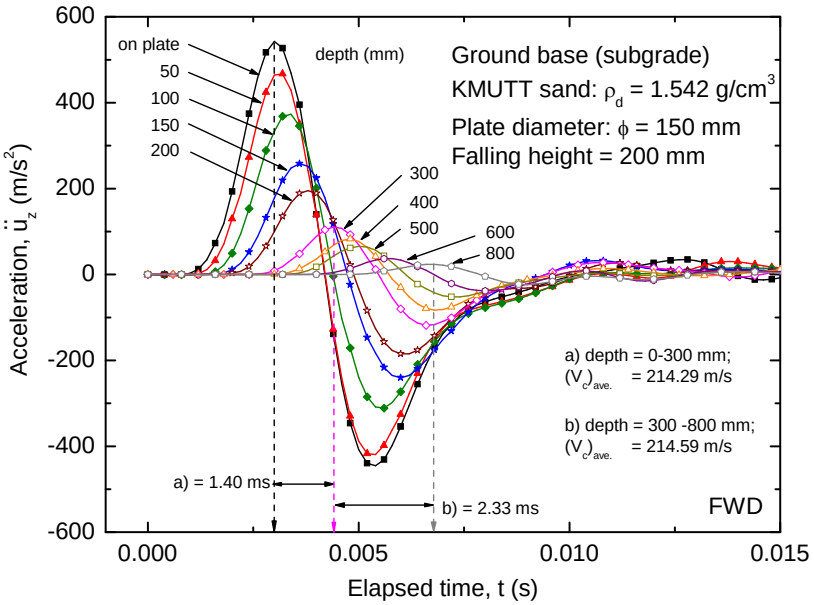

Figure 4.32 Time-lag due to wave propagation in subgrade.

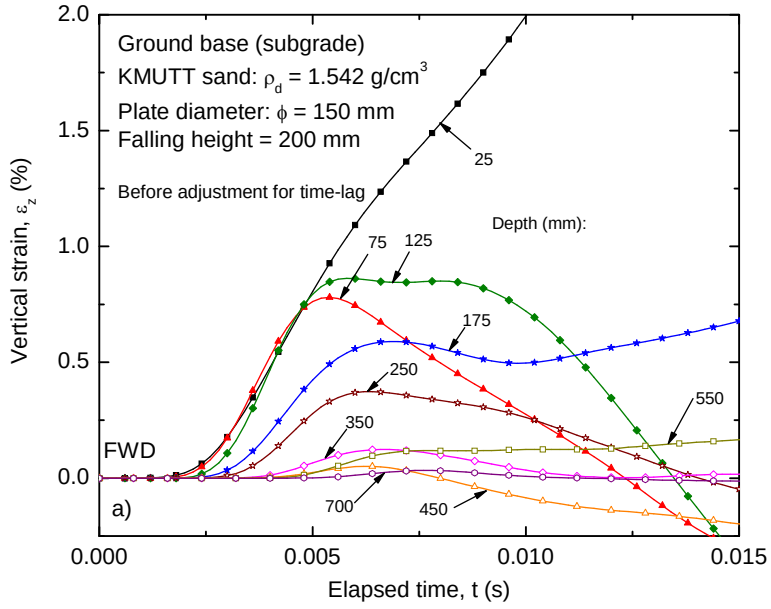

Figure 4.33 Time histories of the different averaged strains at different depths inside the subgrade.

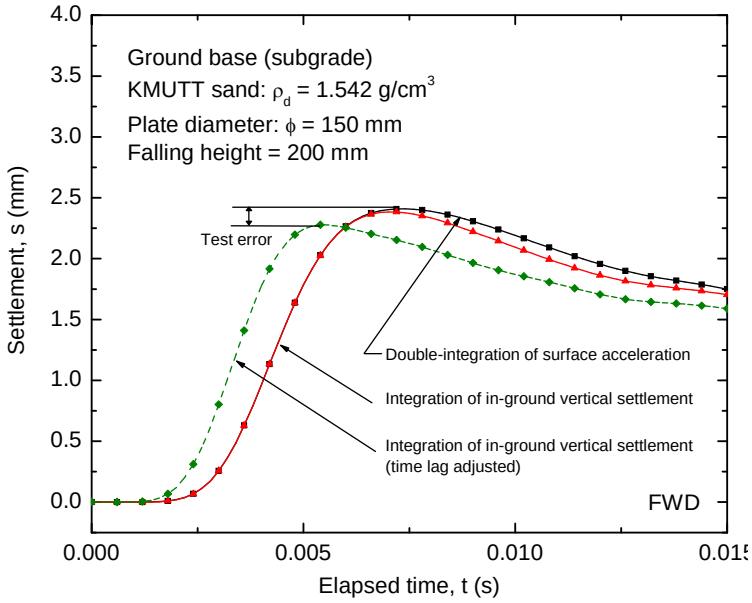

Figure 4.34 Time histories of the settlement beneath the loading plate before and after adjustments for time-lag on subgrade.

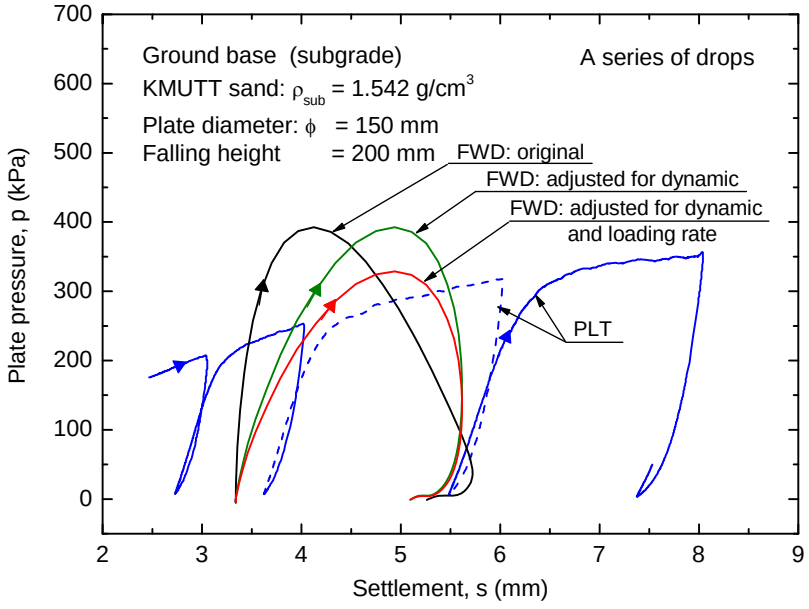

Figure 4.35 Comparison between a series of drops of FWD test results before and after adjustments and PLT test result on subgrade.

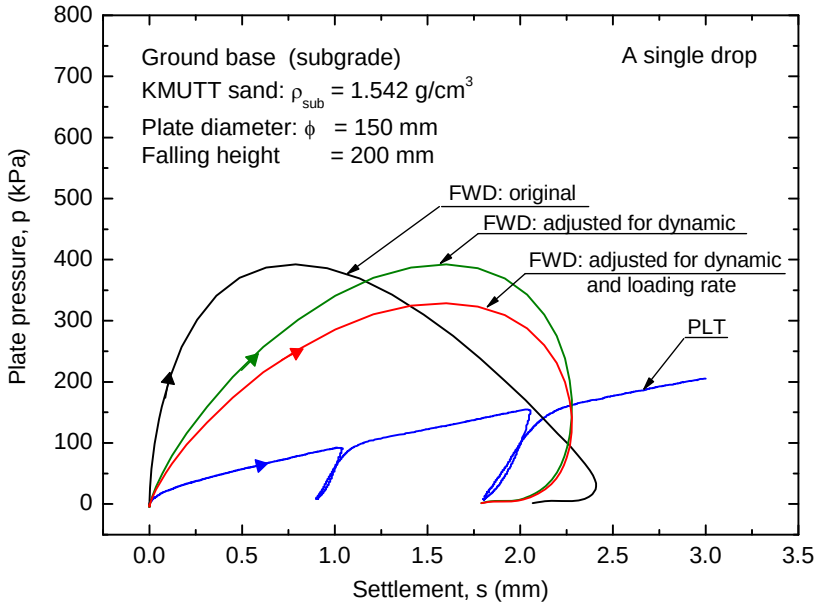

Figure 4.36 Comparison between a single drop of FWD test result before and after adjustments and PLT test result on subgrade.

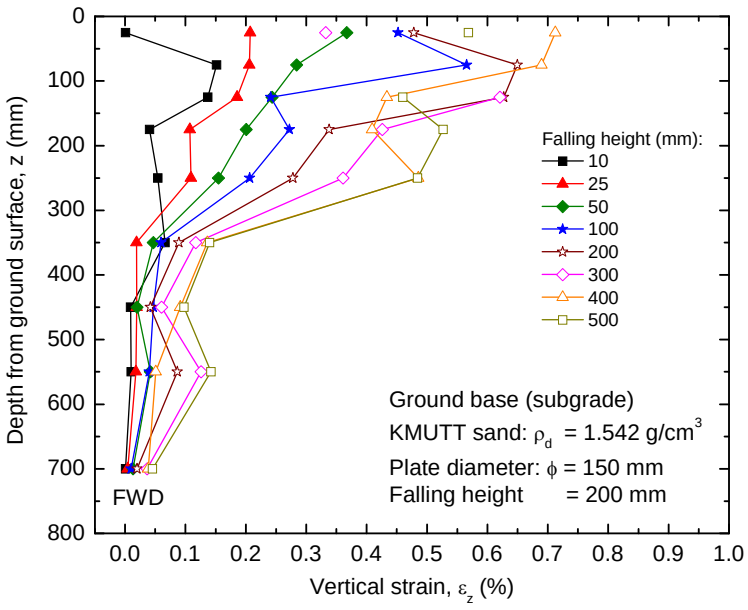

Figure 4.37 Average vertical strains at different depths inside the ground by FWD tests by different falling heights.

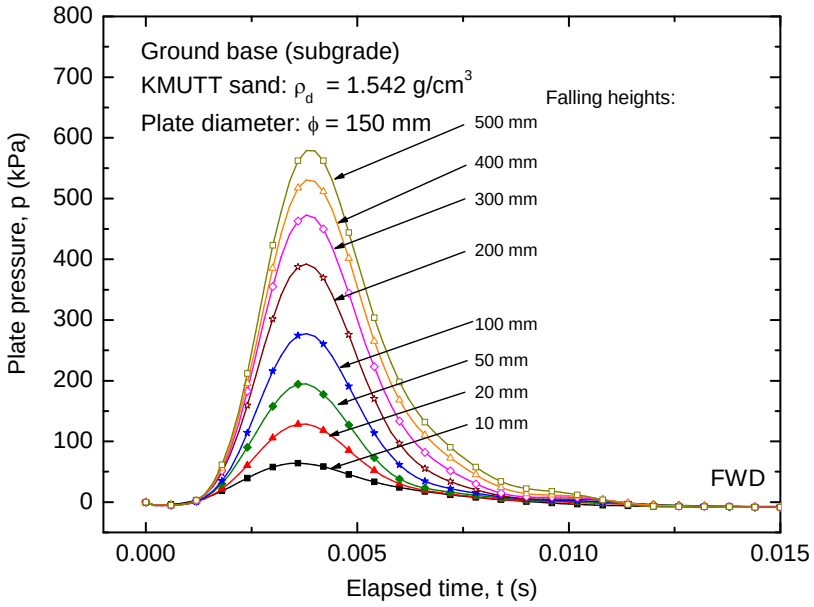

Figure 4.38 Time histories of plate pressure in FWD test for different falling heights on subgrade.

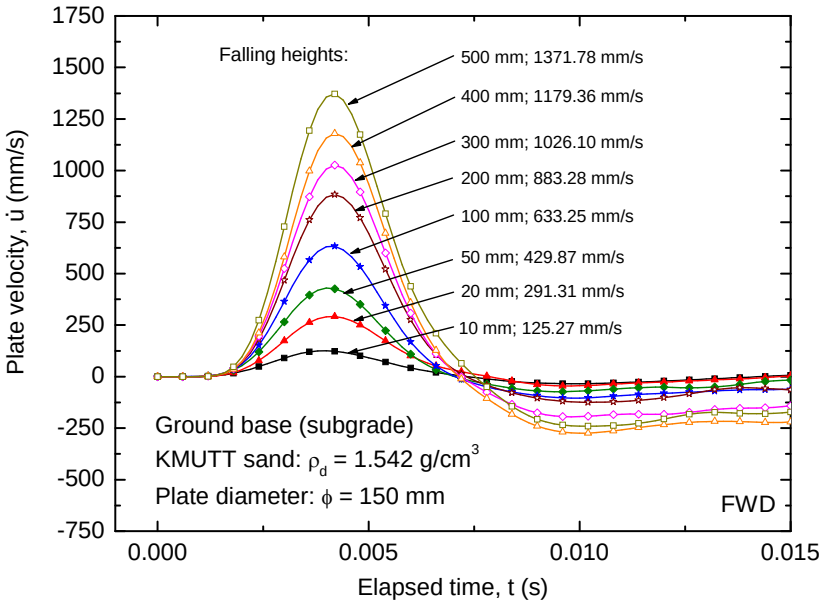

Figure 4.39 Time histories of plate vertical velocities in FWD test for different falling heights on subgrade.

Following Eq. 3.11, the *p*-*s* relationships of a series of drops and a single drop in FWD tests that have been adjusted for dynamic effects were adjusted again for loading rate effect respectively show in Fig 4.36 by using different ratios of $\dot{u}_{z,\,FWD}$ for FWD test to $\dot{u}_{z,\,PLT}$ for PLT test at different elapsed times. Thus, for falling height of 200 mm, the $\dot{u}_{z,\,FWD}$ implemented by FWD is higher than by the one in PLT for 2.24x10^5 times and therefore the plate pressure from FWD is higher than PLT for about 19.31 % due to loading rate effects. On the other hand, Table 4.6 shows that, for different falling heights, the settlement rates in FWD tests are higher than the ones in PLT tests in order of 10^4 to 10^5 and therefore the plate pressure from FWD is higher than PLT for about 18.68 % in average.

Table 4.6 Summary of the decreased plate pressure due to adjustment for loading rate effect for the each drop of loading in FWD test on subgrade.

FWD test			PLT test			Evaluating static pressure by FWD test (p_A) (kPa)	Percent of plate pressure decreasing (%)
Falling height (m)	Peak of plate pressure (p_B) (kPa)	Peak of plate velocity ($\dot{u}_{z,\,FWD}$) (mm/s)	Average settlement rate ($\dot{u}_{z,\,PLT}$) (mm/s)	$\frac{\dot{u}_{z,\,FWD}}{\dot{u}_{z,\,PLT}}$	β - value		
10	64.30	125.27	0.00395	3.17x10^4	0.03610	55.31	16.25
25	128.37	291.31		7.37x10^4		109.18	17.58
50	194.73	429.87		1.09x10^5		164.77	18.18
100	277.53	633.25		1.60x10^5		233.63	18.79
200	392.40	883.28		2.24x10^5		328.89	19.31
300	472.85	1026.10		2.60x10^5		395.54	19.55
400	530.83	1179.36		2.99x10^5		443.23	19.76
500	579.13	1371.78		3.47x10^5		482.60	20.00
average							18.68

4.8 Comparison of Evaluated Moduli of Subgrade Reaction between Falling Weight Deflectometer Test and Static Plate Load Test for Subgrade and their Adjustments

Figures 4.40 and 4.41 compare the $p-s$ relationships of a series of drops and a single drop in FWD test before and after adjustments for dynamic and loading rate effects with the ones by PLT test, respectively. It is clearly seen that the results from FWD test become similar to those of PLT test. It should be noted that any difference remained may be likely due to the fact that there are still effects of other factors in FWD test than the dynamic and loading rate effects that have not been taken into account when adjusting the FWD test results presented in this research. Yet, after having adjusted for dynamic and loading rate effects, FWD test can be used in place of PLT test to accurately obtain the stiffness value of subgrade.

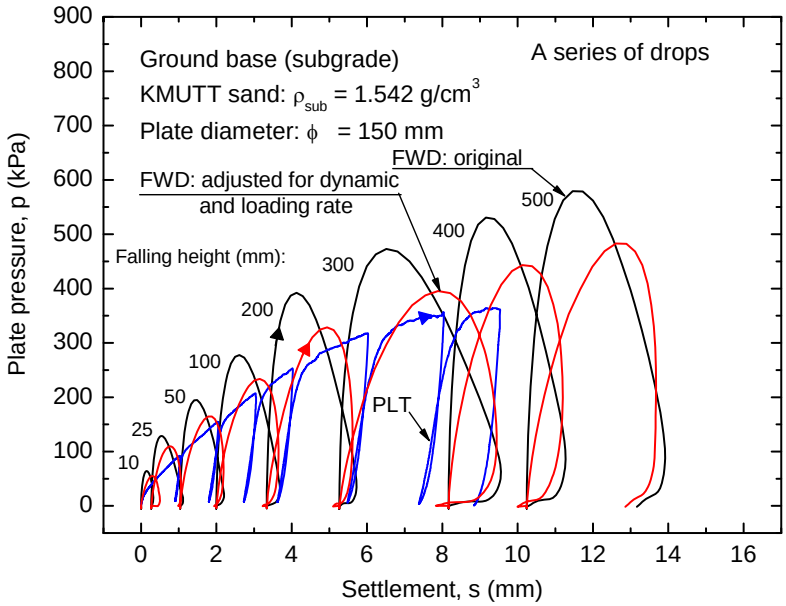

Figure 4.40 Comparison between a series of drops in FWD test results before and after adjustments and PLT test result on subgrade.

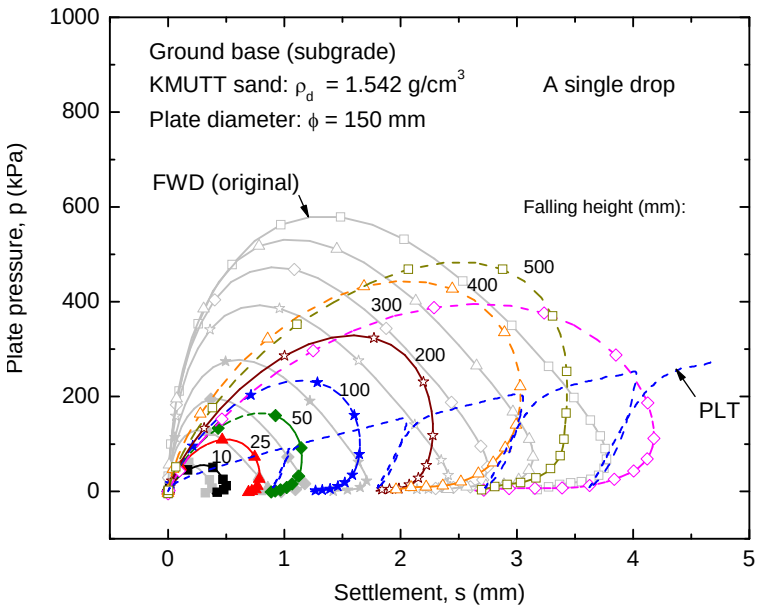

Figure 4.41 Comparison between a single drop in FWD test results before and after adjustments and PLT test result on subgrade.

4.8.1 Comparison of Evaluated Results by a Series of Drops and Adjustments

Figure 4.42 shows the $k_{sec} - p$ relationships from FWD and PLT tests which are also fitted by respective linear relations. Following the AASHTO designation method to determine the k_{sub}- value at the p value of 68.9 kPa (10 psi.) as described in Section 3.8, it was found that the k_{sub} values by FWD test (138.38 kPa) before adjustments for dynamic and loading rate effects are higher than the ones from nonrepetitive PLT test (98.15 kPa) for about 40.99 %. Then, after adjustments for these two effects, the k_{sub} values (102.82 kPa) become higher than the ones by PLT test for only about 4.76 %. On the other hand, the k_{sub} values evaluated by repetitive PLT test (92.22 kPa) is different from the one evaluated by nonrepetitive PLT for about 6.04 %.

Figure 4.43 shows the $k_{sec} - s$ relationships from FWD and PLT tests which are also fitted by respective 1st-degree exponential decay function. Following the Florida designation method to determine the k_{sub}- value at the s value of 1.27 mm (0.05 in.) as described in Section 3.8, it was found that the k_{sub} values by FWD test (119.44 kPa and 99.90 kPa) before and after adjustments for dynamic and loading rate effects are higher than the ones from nonrepetitive PLT test (85.96 kPa) for about 38.95 and 16.22 %, respectively. On the other hand, the k_{sub} value evaluated by repetitive PLT test (84.87 kPa) is different from the one evaluated by nonrepetitive PLT for about 1.27 %.

4.8.2 Comparison of Evaluated Results by a Single Drop and Adjustments

Figure 4.25 shows the $p-s$ relationships of FWD test which were used to determine k_{sub}-value. The original FWD test yields the k_{sub} value of 162.63 kPa/mm. Then, after adjustments for dynamic and load rate effects, the k_{sub} value decreases to 132.54 kPa/mm. Comparing these values with the ones from PLT test by AASHTO (98.15 kPa) and Florida (85.96 kPa) designation methods, it may be seen that these values are higher than the ones by PLT test for about 65.70 % and 89.19 % before adjustments and for about 35.04 % and 54.19 % after adjustments.

By AASHTO determination method to evaluate the $k_{sub,\,PLT}$ value from FWD test following Eq. 3.6b, the approximated $k_{sub,\,PLT}$ equal to 81.32 kPa/mm was obtained as shown in Fig. 4.25. Then, comparing this approximated k_{sub} value with the one directly obtained from PLT test by AASHTO (98.15 kPa) and Florida (85.96 kPa) designation methods, it was found that the differences are 17.15 % and 5.40 %, respectively.

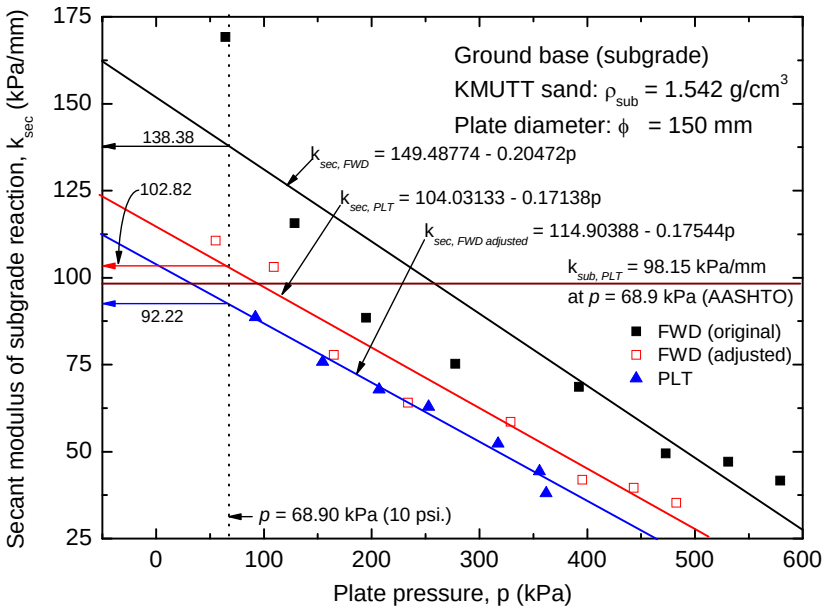

Figure 4.42 Comparison between k_{sub} - values obtained by a series of drops in FWD test results before and after adjustments and PLT test results following AASHTO designation method on subgrade.

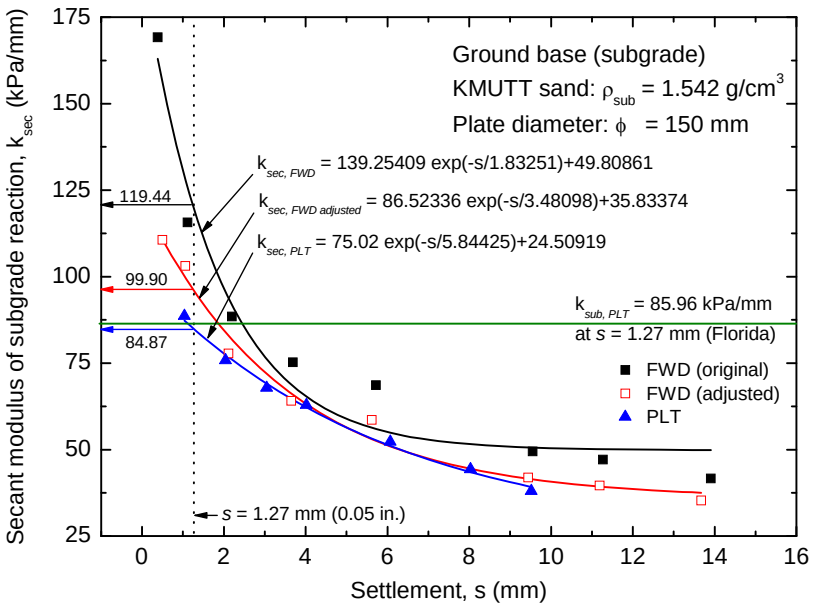

Figure 4.43 Comparison between k_{sub} - values obtained by a series of drops in FWD test results before and after adjustments and PLT test results following Florida designation method on subgrade.

4.9 Limitations of Adjustments on Multilayer Pavement Structures

Nowadays, there is no close-form solution to directly determine the rate-sensitivity coefficients (β) value of a given multilayer pavement structure for adjusting for loading rate effects. Investigating for the β value is complicated and should be performed by Finite Element Method (FEM). For adjusting the dynamic effects, it is clearly seen that investigating the velocity of wave propagation and evaluating the influential zone due to impact load are also the complicated. In practice, $k_{sub,\,FWD}$ value of pavement surface can be calculated by Eq. 3.15 by adjusted only for the loading rate effect. In this manner, the results of the original $k_{sub,\,FWD}$ value become different for about 5.46 % when compared with the result adjusted for both dynamic and loading rate effect for falling height of 200 mm as shown in Fig. 4.44. Therefore, in Sections 4.10 and 4.11, comparisons of the evaluated k_{sub} value between FWD and PLT tests on two-layer structures are only based on original test results.

4.10 Comparison of Evaluated Moduli of Subgrade Reaction between Falling Weight Deflectometer Test and Static Plate Load Test on Unpaved Surface

Figures 4.45 shows the time histories of plate pressure for different falling heights in a series of FWD tests. Then, the $p-s$ relationships of a series of drops and a single drop

in FWD test were plotted and compared with the ones by PLT test as shown in Figs. 4.46 and 4.47, respectively

4.10.1 Comparison of Moduli of Subgrade Reaction Evaluated by a Series of Drops on Unpaved Surface

Figure 4.48 shows the $k_{sec} - p$ relationships from FWD and repetitive PLT tests which are also linear fitted to evaluate the k_{sub} value and to compare with k_{sub} value from PLT evaluated by the AASHTO designation. The k_{sub} value by the original FWD test (123.88 kPa) is higher than the one by nonrepetitive PLT test (78.55 kPa) for about 57.71 %. On the other hand, the k_{sub} value obtained from by repetitive PLT test (72.50 kPa) defined by AASHTO is different from the one evaluated by nonrepetitive PLT for about 7.70 %.

Figure 4.49 shows the $k_{sec} - s$ relationships from FWD and repetitive PLT tests which are also linear fitted by a 1st-degree exponential decay function. Comparing the k_{sub} value by FWD and nonrepetitive PLT tests following the Florida designation method, it was found that the k_{sub} value of original FWD test (112.99 kPa) is higher than nonrepetitive PLT test (73.30 kPa) for about 54.15 %. Then, the k_{sub} value evaluated by repetitive PLT (74.05 kPa) following Florida designation is different from the one evaluated by nonrepetitive PLT for about 1.02 %.

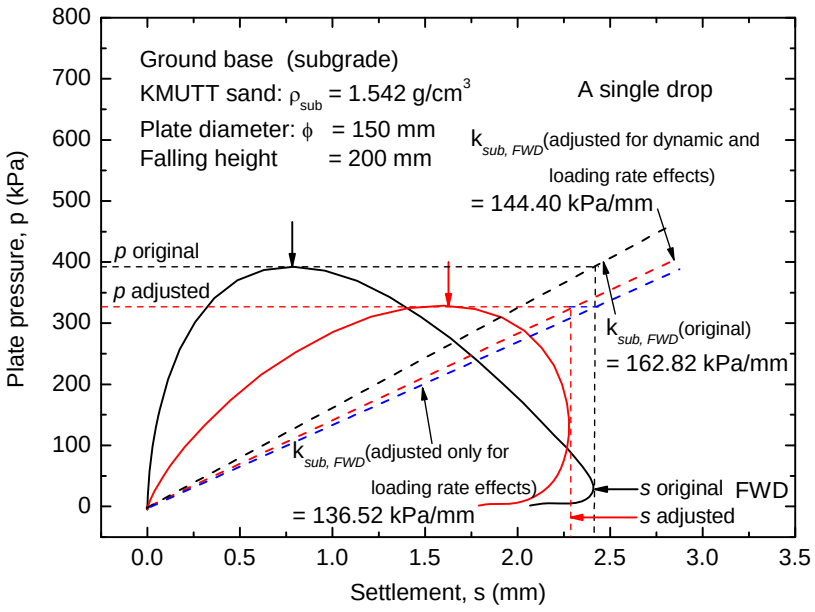

Figure 4.44 Comparison of the $k_{sub,\,FWD}$ values of a single drop in a FWD test results before and after adjustments for both dynamic and loading rate effects, adjusted for loading rate effect only and the approximate $k_{sub,\,FWD}$ value by AASHTO.

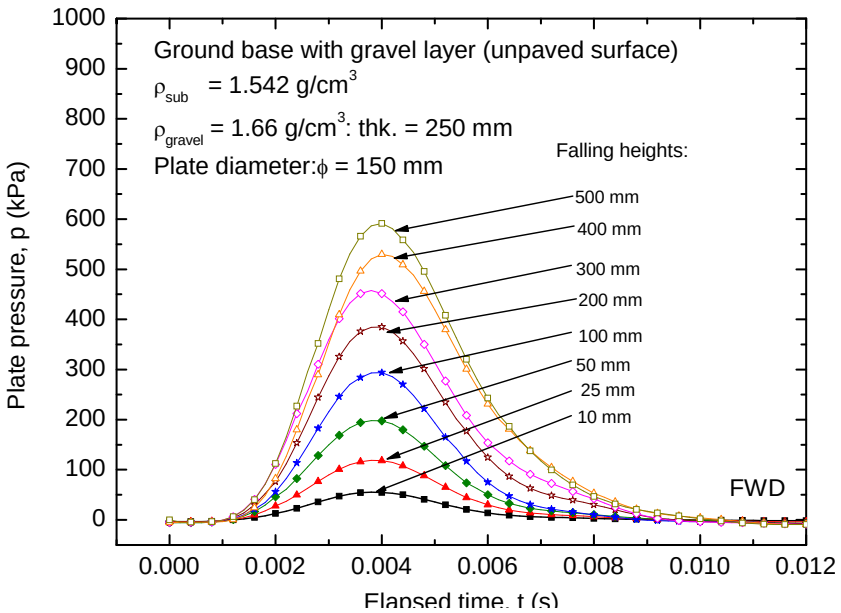

Figure 4.45 Time histories of plate pressure in FWD test for different falling heights on unpaved surface.

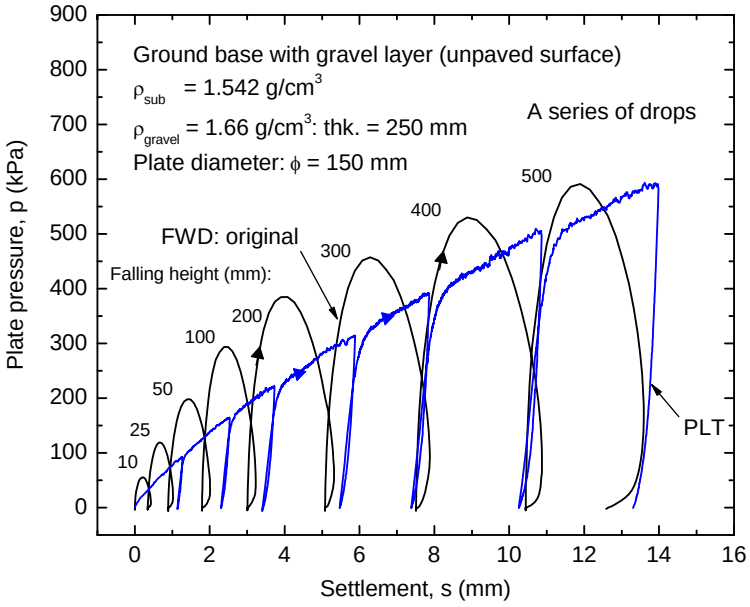

Figure 4.46 Comparison between a series of drops in FWD and PLT test result on unpaved surface.

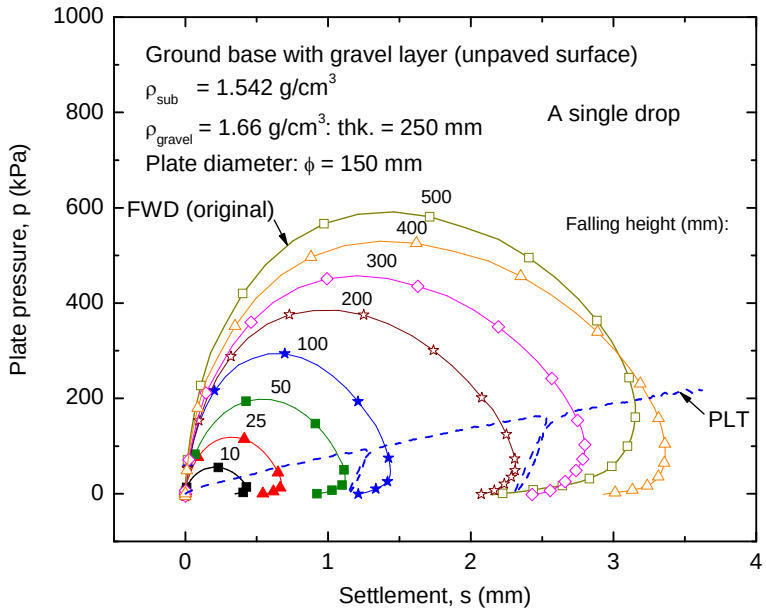

Figure 4.47 Comparison between a single drop in FWD and PLT test result on unpaved surface.

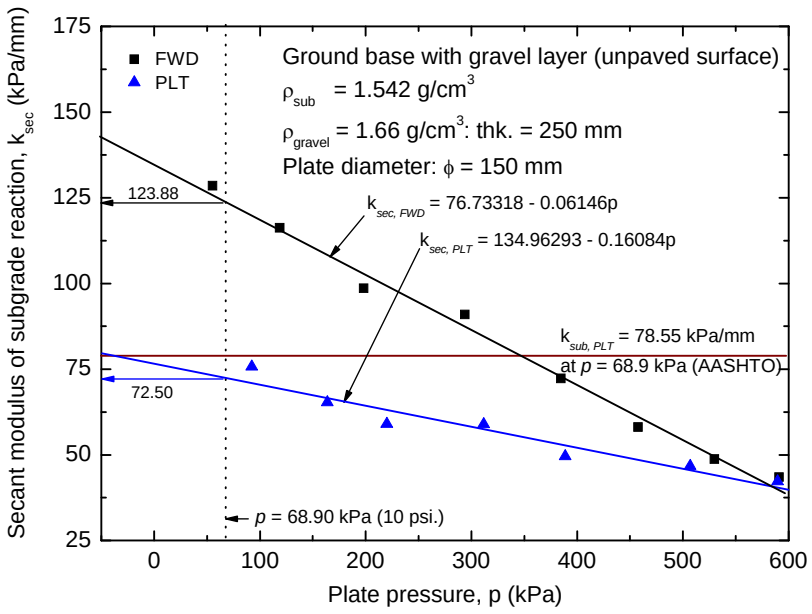

Figure 4.48 Comparison among k_{sub}- values evaluated by a series of drops of FWD, repetitive PLT tests and PLT defined following AASHTO designation on unpaved surface.

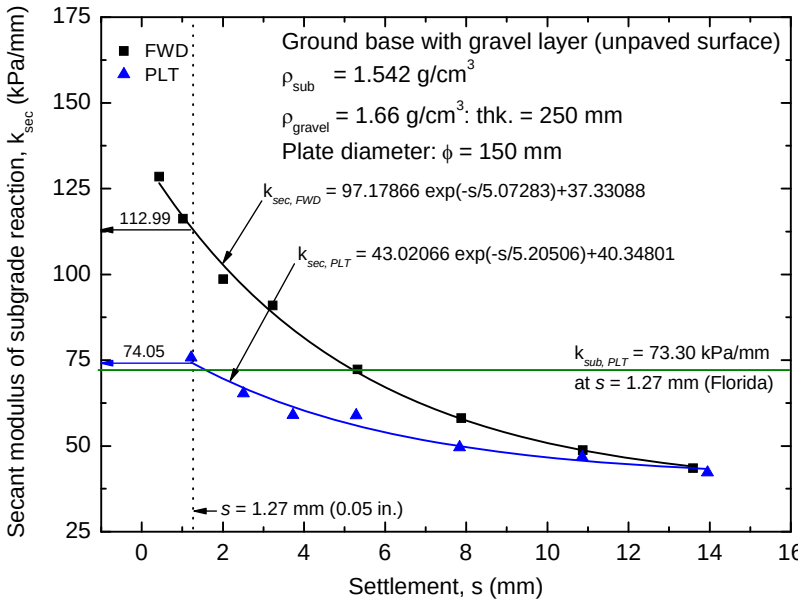

Figure 4.49 Comparison among k_{sub}- values evaluated by a series of drops of FWD, repetitive PLT tests and PLT defined following Florida designation on unpaved surface.

4.10.2 Comparison of Moduli of Subgrade Reaction Evaluated by a Single Drop on Unpaved Surface

Figure 4.47 shows the $p-s$ relationships from a single drop in FWD tests. Figure 4.28 shows the $p-s$ relationship from FWD test which is also linear fitted to obtain the k_{sub} value of 171.05 kPa/mm.

Comparing the $k_{sub,\ FWD}$ value with nonrepetitive PLT test by AASHTO (78.55 kPa) and Florida (73.30 kPa) designation methods, it was found that $k_{sub,\ FWD}$ is higher for about 117.76 % and 133.36 %, respectively. By the AASHTO approximation method to obtain k - value for PLT from FWD, the approximated k_{sub} value is equal to 85.53 kPa/mm. Then, comparing this k_{sub} value (85.53 kPa/mm) with the nonrepetitive PLT test by AASHTO and Florida designation methods it was found that the differences are 8.89 % and 16.68 %, respectively.

4.11 Comparison of Evaluated Moduli of Subgrade Reaction between Falling Weight Deflectometer Test and Static Plate Load Test on Paved Surface

The time histories of plate pressure for different falling heights in a series of FWD tests are shown in Fig. 4.50. Then, the $p-s$ relationships of a series of drops and a single drop in FWD test were plotted and compared with the ones by PLT test as shown in Figs. 4.51 and 4.52, respectively

4.11.1 Comparison of Moduli of Subgrade Reaction Evaluated by a Series of Drops on Paved Surface

Figure 4.53 shows the $k_{sec}-p$ relationships of FWD and repetitive PLT tests which are also linear fitted to evaluate the k_{sub} value and to compare with the one from nonrepetitive PLT test evaluated following AASHTO designation. The k_{sub} value by the original FWD test (612.93 kPa) is higher than nonrepetitive PLT test (281.45 kPa) for about 117.78 %. For the k_{sub} value by repetitive PLT test (251.74 kPa) defined by AASHTO is different from the one evaluated by nonrepetitive PLT for about 10.56 %.

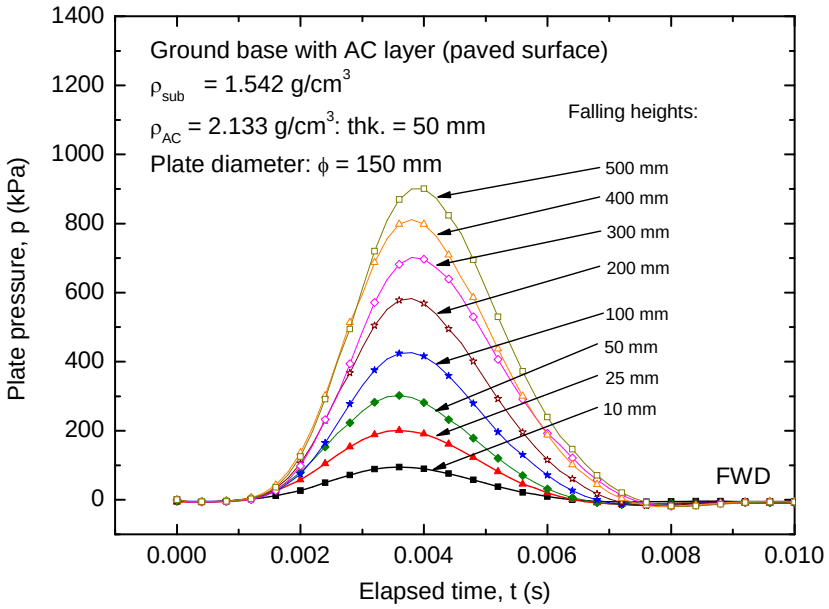

Figure 4.50 Time histories of plate pressure in FWD test for different falling heights on paved surface.

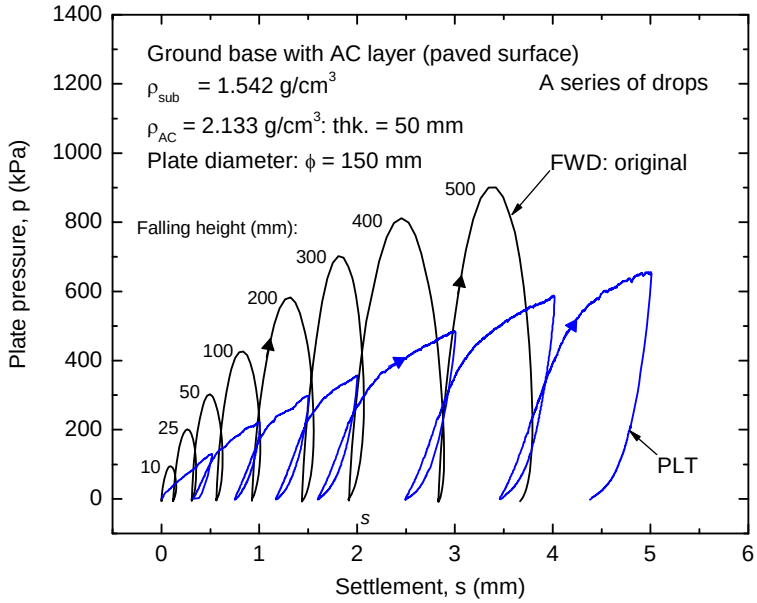

Figure 4.51 Comparison between a series of drops in FWD and PLT test results on paved surface.

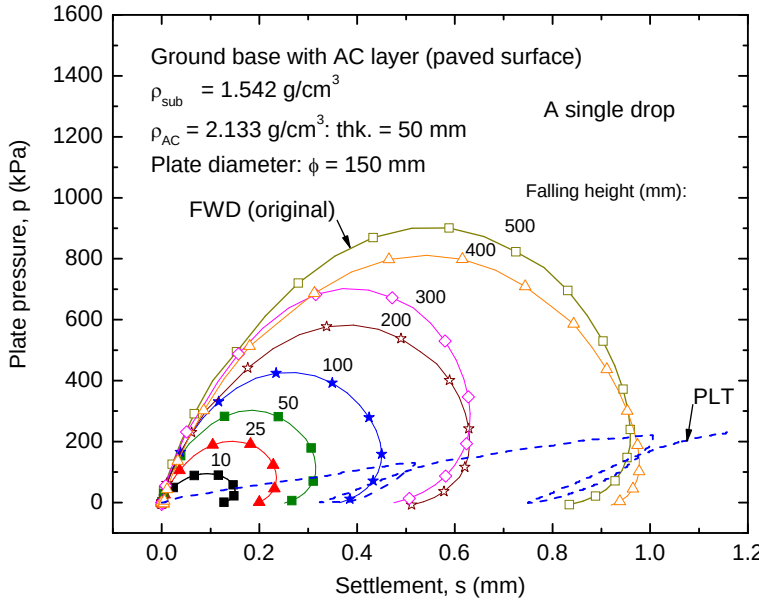

Figure 4.52 Comparison between a single drop in FWD and PLT test results on paved surface.

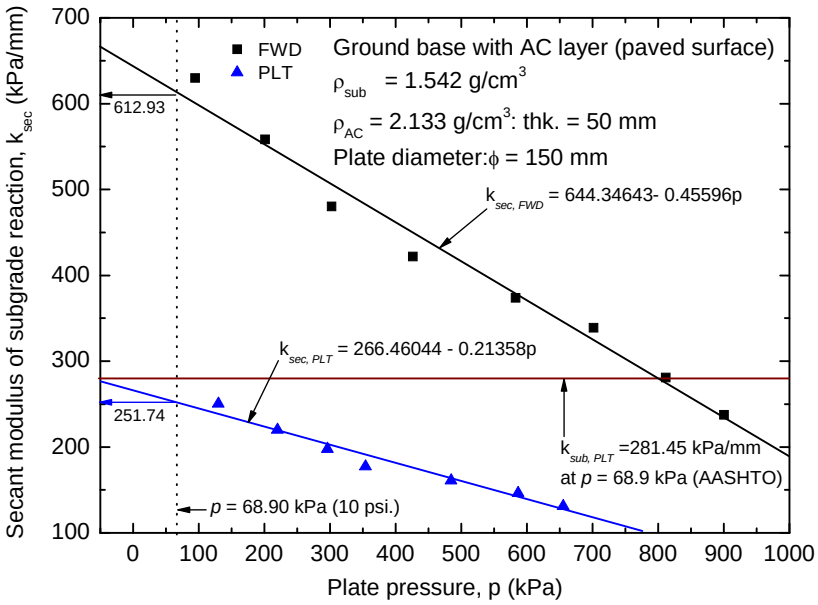

Figure 4.53 Comparison among k_{sub}- values evaluated by a series of drops of FWD, repetitive PLT tests and PLT defined following AASHTO designation on paved surface.

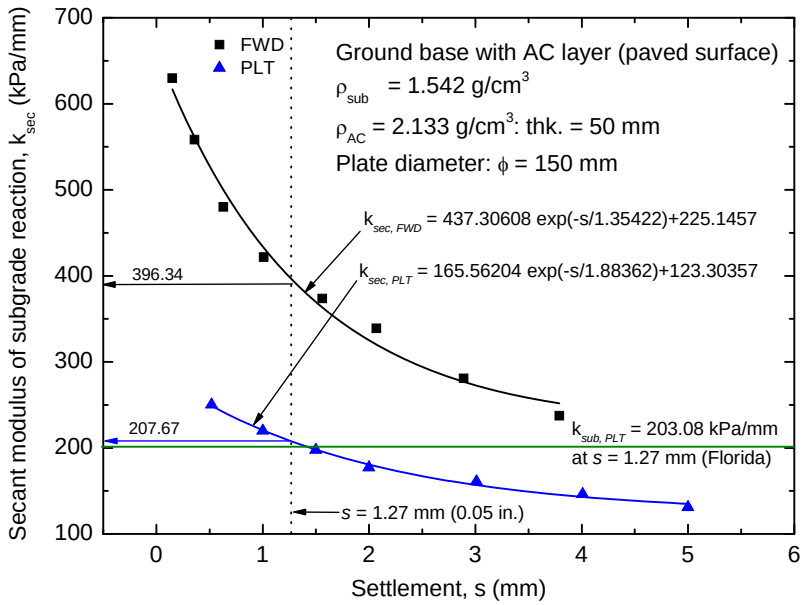

Figure 4.54 Comparison among k_{sub}- values evaluated by a series of drops of FWD, repetitive PLT tests and PLT defined following Florida designation on paved surface.

Figure 4.54 shows the $k_{sec} - s$ relationships from FWD and PLT tests which are also fitted by a 1st-degree exponential decay function. Comparing the k_{sub} value by FWD and nonrepetitive PLT test following the Florida designation method, it was found that the k_{sub} value of original FWD test (396.34 kPa) is higher than nonrepetitive PLT test (203.08 kPa) for about 95.16 %. Then, the k_{sub} value by repetitive PLT (207.67 kPa) evaluated following Florida designation method test is different from the one obtained from nonrepetitive PLT test for about 2.26 %.

4.11.2 Comparison of Moduli of Subgrade Reaction Evaluated by a Single Drop on Paved Surface

Figure 4.52 shows the $p - s$ relationships from a single drop in FWD tests. Figure 4.31 shows the $p - s$ relationship of FWD test which are also fitted to obtain the k_{sub} value of 922.10 kPa/mm.

Comparing the $k_{sub,\,FWD}$ value with nonrepetitive PLT test by AASHTO (281.45 kPa) and Florida (203.08 kPa) designation methods, it was found that $k_{sub,\,FWD}$ is higher for about 227.62 % and 354.06 %, respectively. By the AASHTO approximation method to obtain k value for PLT from FWD, the approximated k_{sub} value is equal to 461.05 kPa/mm. Then, comparing this k_{sub} value (461.05 kPa/mm) with the nonrepetitive PLT test by AASHTO and Florida designation methods it was found that the differences are 63.81 % and 127.03 %, respectively.

Differences in percentage between k-value obtained by FWD compared with PLT are tabulated in Table 4.7. For subgrade, as described in Sections 4.8, it is clearly seen that the k_{sub} values evaluated by FWD test are higher than the ones of PLT test. Then, after adjustments for dynamic and loading rate effects, it is found that the k_{sub} values become close to the ones by PLT test.

For two-layer structures, as described in Sections 4.10 and 4.11, it is clearly seen that the k_{sub} values evaluated by FWD test are higher than the ones of PLT test especially in the paved surface condition. Then, a single drop method shows the percent difference is higher than a series of drops method.

By a single drop method to evaluate the k_{sub} value for unbound surface (subgrade and unpaved surface conditions), it was found that the k_{sub} values by FWD test are higher than the ones by PLT test. Then, the approximation by AASHTO shows that the k_{sub} values by FWD test become close to the ones by PLT test. In contrast, it is clearly seen, for bound surface, the closeness of the approximated k_{sub} to the ones by PLT test is less than the unbound surface.

4.12 Analytical Method by Undamped Harmonic Motion for Falling Weight Deflectometer Test for Evaluation of Moduli of Subgrade Reaction on Pavement Structure and Discussion

From a series of FWD tests as described in Section 3.9, the spring constant of the ground $(k_{ground}$ value$)$ at each falling heights can be calculated by Eq. 3.30b. Then, the modulus of subgrade reaction $(k_{sub}$ value$)$ of each falling heights can be calculated by Eq. 3.44b. On the other hand, the k_{sub} values obtained in this manner are less than the originally obtained values because of assumption of $E_f = 1$ specified in this equation. The use of $E_f = 1$ results in the increase in the vertical displacement under loading plate, and therefore the calculated k_{sub} decreases as described in Eq. 3.30a.

In this research, a special FWD test was perform to determine the remain efficiency value described in Section 3.15. Figure 4.55 shows the time histories of plate pressure for different falling heights in a series of FWD tests on a very stiff pavement (e.g., concrete slab) and the comparison between the velocities of loading plate with damper and without damper are shown in Fig. 4.56. Then, the $E_f - h$ relationships are plotted and fitted by the Extended Freundlich function as shown in Fig. 4.56. From this figure, the remain efficiency values at different heights of 10, 25, 50, 100, 200, 300, 400 and 500 mm in a series of FWD test are 0.8443, 0.9157, 0.9295, 0.9180, 0.8897, 0.8682, 0.8516 and 0.8382, respectively.

Table 4.7 Summary of percent differences in $k-\text{values}$ from the FWD tests compared with the ones from PLT test on pavement surface.

Pavement condition	PLT test		Percent differences of FWD test compared with PLT test by AASHTO designation					Percent difference of FWD test compared with PLT test by Florida designation					UHM method (adjusted for E_f)	
			A series of drops		A single of drop			A series of drops		A single of drop				
	AASHTO designation (kPa/mm)	Florida designation (kPa/mm)	original (%)	adjusted effects (%)	original (%)	adjusted effects (%)	approximate by AASHTO (%)	original (%)	adjusted effects (%)	original (%)	adjusted effects (%)	approximate by AASHTO (%)	different percent from AASHTO designation (%)	different percent from Florida designation (%)
Subgrade	98.15	85.96	40.99	4.76	65.70	35.04	17.15	38.95	16.22	89.19	54.19	5.40	19.20	7.74
Unpaved surface	78.55	73.30	57.71	No	117.76	No	8.89	54.15	No	133.36	No	16.68	1.74	5.29
Paved surface	281.45	203.08	117.78		227.62		63.81	95.16		354.06		127.03	34.57	9.33

Note: 1. AASHTO designation specified the k_{sub} value at p = 68.9 kPa (10 psi.)

2. Florida designation specified the k_{sub} value at s = 1.27 mm (0.05 in.)

3. No means not perform adjustment for effects

4. Approximated k_{sub} by AASHTO was defined as: $k_{sub,\,PLT} = k_{sub,\,FWD} / 2$

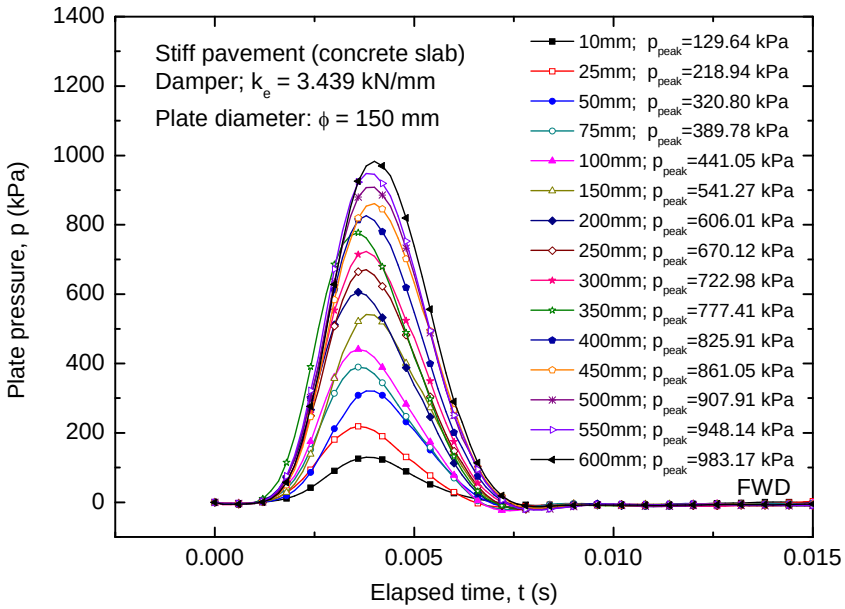

Figure 4.55 Time histories of plate pressure in FWD test for different falling heights on very stiff pavement (e.g., concrete slab).

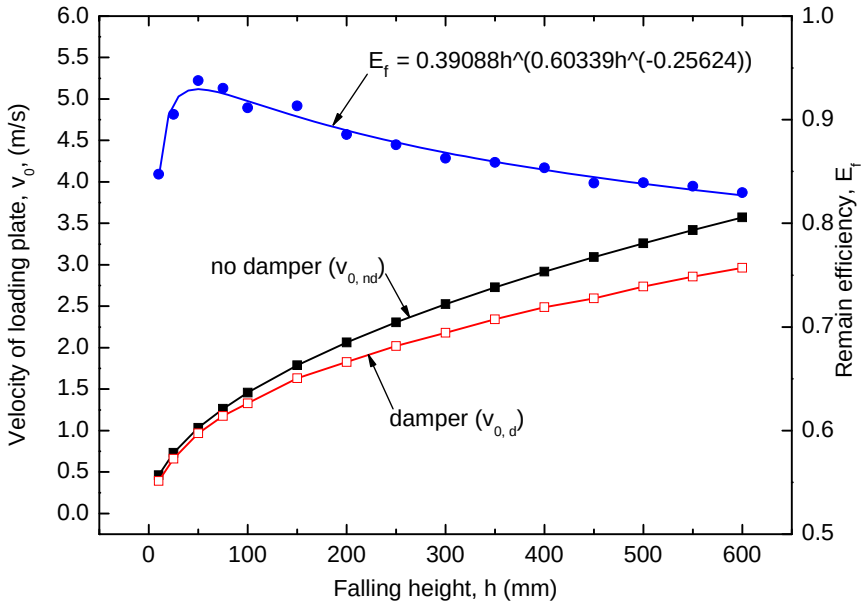

Figure 4.56 The velocities of loading plate with of damper and without damper and the remain efficiency value of FWD device at different falling heights.

4.13 Comparison of Evaluated Moduli of Subgrade Reaction between Analytical Method by Undamped Harmonic Motion on Falling Weight Deflectometer Test and Static Plate Load Test for Subgrade

The $k_{sub} - h$ relationships were obtained by undamped harmonic motion in a FWD test as shown Figure 4.57. From this figure, the average k_{sub} value before and after adjustment for the remain efficiency are: 61.82 and 79.31 kPa/mm, respectively. Then, by comparing these k_{sub} values before and after adjustment for E_f with the k_{sub} in a PLT test following AASHTO designation methods, it was found that the differences are: 37.01 % and 19.20 %, respectively.

By comparing the k_{sub} in a PLT test following Florida designation method, the differences before and after adjustment for the remain efficiency are: 28.08 and 7.74 %, respectively.

4.14 Comparison of Evaluated Moduli of Subgrade Reaction between Analytical Method by Undamped Harmonic Motion on Falling Weight Deflectometer Test and Static Plate Load Test for Unpaved Surface

The $k_{sub} - h$ relationships were obtained by undamped harmonic motion in a FWD test as shown Figure 4.58. From this figure, the average k_{sub} value before and after adjustment for the remain efficiency are: 60.28 and 77.18 kPa/mm, respectively. Then, by comparing these k_{sub} values before and after adjustment for E_f with the k_{sub} in a PLT test following AASHTO designation methods, it was found that the differences are: 23.25 % and 1.74 %, respectively.

By comparing the k_{sub} in a PLT test following Florida designation method, the differences before and after adjustment for the remain efficiency are: 17.76 and 5.29 %, respectively.

4.15 Comparison of Evaluated Moduli of Subgrade Reaction between Analytical Method by Undamped Harmonic Motion on Falling Weight Deflectometer Test and Static Plate Load Test for Paved Surface

The $k_{sub} - h$ relationships were obtained by undamped harmonic motion in a FWD test as shown Figure 4.59. From this figure, the average k_{sub} value before and after adjustment for the remain efficiency are: 143.70 and 184.14 kPa/mm, respectively. Then, by comparing these k_{sub} values before and after adjustment for E_f with the k_{sub} in a PLT

test following AASHTO designation methods, it was found that the differences are: 48.94 % and 34.57 %, respectively.

By comparing the k_{sub} in a PLT test following Florida designation method, the differences before and after adjustment for the remain efficiency are: 29.24 and 9.33 %, respectively.

From Sections 4.13, 4.14 and 4.15, the k_{sub} value evaluated by undamped harmonic motion by FWD tests on various pavement structures are close to the results from respective PLT tests. That is, the undamped harmonic motion method can be applied to evaluate the k_{sub} value of flexible pavement structure in this research. The summary of percent differences of k-value by undamped harmonic motion compared with the ones by PLT tests on various pavement surfaces are tabulated in Table 4.7.

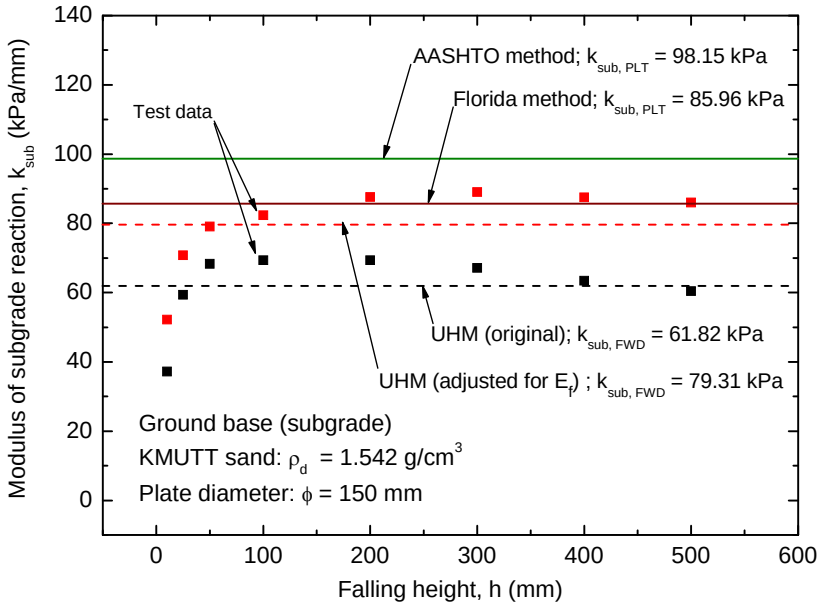

Figure 4.57 Comparison of the k_{sub} values by undamped harmonic motion method before and after adjustment for the remain efficiency, E_f, with the k_{sub} value in a PLT test on subgrade.

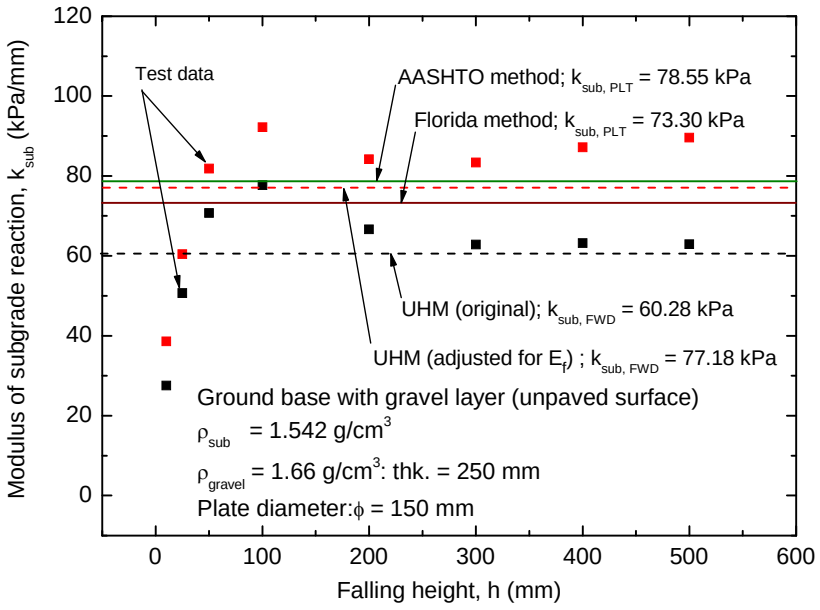

Figure 4.58 Comparison of the k_{sub} values by undamped harmonic motion method before and after adjustment for the remain efficiency, E_f, with the k_{sub} value in a PLT test on unpaved surface.

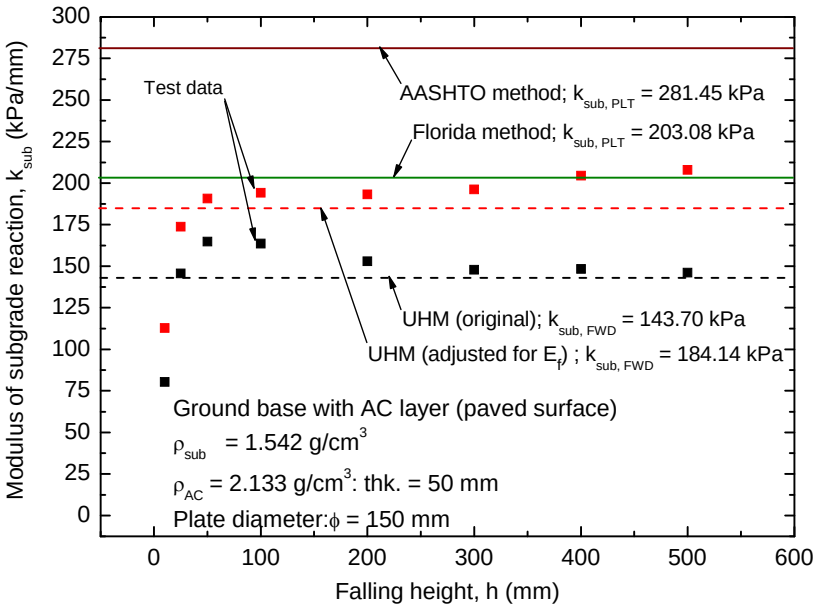

Figure 4.59 Comparison of the k_{sub} values by undamped harmonic motion method before and after adjustment for the remain efficiency, E_f, with the k_{sub} value in a PLT test on paved surface.

CHAPTER 5 CONCLUSIONS

5 CONCLUSIONS

5.1 Conclusions

In this research, the flexible pavement structures were modeled from full scale to laboratory scale. That is, the single layer (e.g., subgrade layer) and two-layer (e.g., unpaved surface and paved surface) pavement systems. All pavement surfaces were tested by FWD device and PLT method and were evaluated for the modulus of subgrade reaction (k value) and the PLT results are used as reference data. The following conclusion can be made as follows:

1. For the same test condition, the originally obtained modulus of subgrade reaction values from FWD are always greater than the ones obtained by PLT.

2. It was clearly seen that the there were significant differences in the modulus of subgrade reaction values when performed FWD and PLT tests on the very stiff pavement surface.

3. The differences of the modulus of subgrade reaction values between FWD and PLT were due to the influence of the wave propagation or time-lag (dynamic-effect) into the pavement layer.

4. The differences of the modulus of subgrade reaction values between FWD and PLT were also due to the different loading rate (rate-effect) caused by the viscosity of the tested materials.

5. After being adjusted for dynamic and loading rate effects, relationships between the plate pressure and the plate settlement obtained by FWD became close to the ones by PLT. Therefore, FWD test can be used in place of PLT to accurately obtain the modulus of subgrade reaction value, when adjustments for dynamic and loading rate effects were performed

6. Using UHM method to obtain the modulus of subgrade reaction of pavement surface from FWD provides similar results to those of PLT and this method is relevant for both single and multiple layer systems.

7. After being adjusted for remain efficiency by UHM method, the modulus of subgrade reaction of pavement surface from FWD became close to the ones by PLT. Therefore, UHM method for FWD test can be used in place of PLT to accurately obtain the modulus of subgrade reaction value.

5.2 Recommendations for Further Researchs

The research presented in this research leads to the recommendation of the surface stiffness values of the flexible pavement structures of which further research will be fruitful. The following recommendations are suggested for future researchs:

1. The research should determine the rate-sensitivity coefficients (β value) of a given multilayer pavement structure for directly adjusting for loading rate effects on the multilayer pavement structure.

2. The research should evaluate the layer stiffness values of the various pavement structures, for both flexible and rigid pavements, for evaluating the layer stiffness values during and after constructions by FWD.

3. The research should propose a simplified analytical method for calculating the stiffness values of pavement structure (e. g., computer program).

4. The research should investigate the temperature effects on the various pavement structures in a FWD test.
5. The research should apply this method in laboratory to investigate the real pavement condition in field

REFERENCES

Adam, C. and Adam, D., 2003, "Modelling of the dynamic load plate test with the light falling weight device", Asian Journal of Civil Engineering (Building and Housing), Vol. 4, No. 2, pp. 73-89.

Almassy, K., 2002, "Examination of mechanical properties in unbound road bases", Periodica Polytechnical Ser. Civ. Eng., Vol. 46, No. 1, pp. 53-69.

American Association of State Highway and Transportation Officials (AASHTO), 1972, AASHTO Interim Guide for Design of Pavement Structures, 2nd ed., American Association of State Highway and Transportation Officials, Washington, D.C.

American Association of State Highway and Transportation Officials (AASHTO), 1986, Guide for Design of Pavement Structures, Vol. I, American Association of State Highway and Transportation Officials, Washington, D.C.

American Association of State Highway and Transportation Officials (AASHTO), 1993, Guide for Design of Pavement Structures, Vol. II, American Association of State Highway and Transportation Officials, Washington, D.C.

Barkdale, R.D. and Hicks, R.G., 1972, "Material characterization and layered theory for use in fatigue analysis pavements", Proc., Highway Research Board, Special Report No. 40, Washington, D.C., pp. 20-48.

Bishop, A.W. and Henkel, D. J., 1962, The Measurement of Soil Properties in the Triaxial Test, 2nd ed., Edward Arnold, London.

Boresi P. and Schmidt R.J., 2003, Advanced Mechanics of Materials, 6th ed., John Wiley & Sons, New York.

Boussinesq, J., 1885. Application of Potential to the Study of the Equilibrium and Movements in Elastic Soils, Gauthier-Villars, Paris.

REFFERENCES

Burmister, D.M., 1943, "The theory of stresses and displacements in layered systems and application to the design of airport runways", Proc., Highway Research Board, Washington, D.C., Vol. 23, pp. 125-148.

Burmister, D.M., 1945, "The general theory of stresses and displacements in layered systems", Journal of Applied Physics, Vol. 16, No. 2. pp. 84-94.

Burmister, D.M., 1947, "General Discussion", Symposium on Load Tests of Bearing Capacity of Soils, Special Technical Publication No. 79, ASTM, Philadelphia, pp. 139-146.

Bush III, A. J., Alexander, D.R. and Hall, J.W., 1985, "Nondestructive airfield rigid pavement evaluation", Proceedings of the 3rd International Conference on Concrete Pavement Design and Rehabilitation, April, Purdue University, West Lafayette, Indiana.

Bush III, A.J. and Baladi, G.Y. (Eds), 1989, Nondestructive Testing of pavements and Backcalculation of Moduli, ASTM STP 1026, American Society for Testing and Materials, Marryland.

Das, B.M., 1992, Principles of Soil Dynamics, PWS-KENT, Boston.

Di Benedetto, H., Geoffroy, H. and Sauzeat, C., 2001, "Viscous and non viscous behaviour of sand obtained from hollow cylinder tests", Advanced Laboratory Stress-Strain Testing of Geomaterials, Tatsuoka et al. (Eds.), Balkema, pp. 217–226.

Di Benedetto, H., Tatsuoka, F. and Ishihara, M., 2002, "Time-dependent deformation characteristics of sand and their constitutive modeling", Soils and Foundations, Vol. 42, No. 2, pp. 1-22.

Di Benedetto, H., Tatsuoka, F., Lo Presti, D., Sauzéat, C. and Geoffroy H., 2004, "Time effects on the behaviour of geomaterials", Keynote Lecture, Proc. 3rd Int. Sym. on Deformation Characteristics of Geomaterials, IS Lyon 03, September 2003, Balkema, Di Benedetto et al. (eds), Vol. 2, pp. 59-123.

REFFERENCES

Di Benedetto, H., Tatsuoka, F., Lo Presti, D., Sauzéat, C., and Geoffroy, H., 2005, "Time effects on the behaviour of geomaterials", Keynote Lecture, Proc. 3rd Int. Sym. on Deformation Characteristics of Geomaterials, IS Lyon 03 (Di Benedetto et al. eds.), Balkema, September, 2003, Vol.2, pp.59-123.

Enomoto, T., Tatsuoka, F., Shishime, M., Kawabe, S. and Di Benedetto, H., 2006, "Viscous property of granular material in drained triaxial compression", Soil Stress-Strain Behavior: Measurement, Modeling and Analysis, Ling, et al. (Eds.), Springer, Dordrecht, pp. 383-397.

Faikratok, T. and Sonthong, S., 1998, Relationship between Temperature and Elastic Modulus of Asphalt Concrete Pavement Surface by Falling Weight Deflectometer (FWD), RD. 170, Bureau of Road Research and Development, Department of Highways, Bangkok.

Federal Aviation Adminiatration (FAA), 2004, Used of Nondestructive Testing Devices in the Evaluation of Airport Pavements, Advisory Circular No. 150/5370-11A, Federal Aviation Adminiatration, Washington, D.C.

Federal Highway Administration (FHWA), 1984, Synthesis Study of Nondestructive Testing Devices for Use in Overlay Thickness Design of Flexible Pavements, Report No. FHWA-JRD-83/097, Federal Highway Administration, Virginia.

Federal Highway Admirtration (FHWA), 2006, Guidelines for Review and Evaluation of Backcalculation Results, Report No. FHWA-HRT-05-152, Federal Highway Administration, Virginia.

Florida Department of Transportation (FDOT), 1998, Manual of Florida Sampling and Testing Methods, Florida Department of Transportation, Tallahassee, Florida.

Foster, C.R. and Ahlvin, R. G., 1954, "Stress and Deflections Induced by a Uniform Circular Load", Proceedings of Highway research Board, Vol. 33, pp. 467-470.

George, K.P., 2003, Falling Weight Deflectometer for Estimateing Subgrade Resilient Moduli, FHWA/MS-DOT-RD-03-153, University of Mississippi, Mississippi.

REFFERENCES

Green, J. L. and Hall. J. W., 1975, Nondestructive Vibratory Testing of Airport Pavements, Volume I: Experimental Test Result and Development of Evaluation Methodology and Procedure, Technical Report No. FAA-RD-73-205-1, Federal Aviation Adminiatration, Washington, D.C.

Grontmij & Carl Bro Co., Ltd., 2007, Phoenix Falling Weight Deflectometer [Online], Available : http://www.pavement-consultants.com/en/Menu/About+us/History/FWDhistory/TheStoryofFWDs.htm [2008, August 10].

Hall, J. L, 1975, "Dynamic stiffness modulus for NDT evaluation", Symposium of Nondestructive Testing and Evaluation of Airport Pavements, 18 -20 November 1975, Vicksburg, Mississippi. pp. 61-91.

Hayano, K., Matsumoto, M., Tatsuoka, F. and Koseki, J., 2001, "Evaluation of time-dependent deformation property of sedimentary soft rock and its constitutive modelling", Soils and Foundations, Vol.41, No.2, pp. 21-38.

Head, K.H., 1982, Manual of Soil Laboratory Testing, Vol. 1: Soil Classification and Compaction Test, Pentech Press, London.

Hirakawa, D., 2003, Study on residual deformation characteristics of geosynthetic-reinforced soil structures, Ph.D. Thesis, University of Tokyo (in Japanese).

Hirakawa, D., Masuda, N., Tatsuoka, F. and Kawasaki, H., 2008, Relationship between sand ground stiffness values from FWD and from plate loading tests, JGS Journal, May 2008, Vol. 3, No.4, 307-320 (in Japanese)

Huang, Y.H., 2003, Pavement Analysis and Design, 2nd ed., Pearson Education, Inc., New Jersy.

Kancherla, A., 2004, Resilient Modulus and Permanent Deformation Testing of Unbound Granular Materials, M.S. Thesis, Texas A&M University, Texas.

Kawabe, S., 2008, "Triaxial test results on KMUTT sand", Personal Communication.

REFFERENCES

Kiyota, T. and Tatsuoka, F., 2006, "Viscous property of loose sand in triaxial compression, extension and cyclic loading", Soils and Foundations, Vol.46, No. 5, pp. 665-684.

Kongkitkul, W., Tatsuoka, F., Duttine, A., Kawabe, S., Enomoto, T. and Di Benedetto, H., 2008, "Modelling and simulation of rate-dependent stress-strain behaviour of granular materials in shear", Soils and Foundations, Vol.48, No.2, pp.175-194.

Kongsukprasert, L., Tatsuoka, F. and Tateyama, M., 2004 "Several factors affecting the strength and deformation characteristics of cement-mixed gravel", Soils and Foundations, Vol. 45, No. 3, pp.107-124.

Lekarp, F., Ulf, I., and Dawson, A., 2000, "State of the art. I: resilient response of unbound aggregates." Journal of Transportation Engineering, ASCE, Vol. 126, No.1, pp. 66-75.

Loizos, A., Boukovalas, G. and Karlaftis, A., 2003, "Dynamic stiffness for pavement subgrade evaluation", Journal of Transportation Engineering, Vol. 129, No. 4, pp. 434-443.

Lysmer, J., 1965, Vertical Motion of Rigid Footing, Ph.D. Thesis, University of Michigan, Ann Arbor, Michigan.

Lytton, R.L., 1989, "Backcalculation of pavement layer properties", Nondestructive Testing of pavements and Backcalculation of Moduli, Bush III, A.J. and Baladi, G.Y. (Eds), ASTM STP 1026, American Society for Testing and Materials, Philadelphia, pp. 7-38.

Mairaing, W., Chotickrai, C. and Duangdeun, P., 1982, Soil Mechanics: theory and experiments, 2nd, Physics Center Press, Bangkok.

Masuda, N., 2007, Investigation of Relationship between Sand Ground Stiffness Values from FWD and Plate Loading Tests, M.Eng. Thesis, Tokyo University of Science (in Japanese).

REFFERENCES

Matsushita, M., Tatsuoka,F., Koseki,J., Cazacliu, B., Di Benedetto, H. and Yasin, S.J.M., 1999, "Time effects on the pre-peak deformation properties of sands", Proc. Second Int. Conf. on Pre-Failure Deformation Characteristics of Geomaterials, IS Torino '99, Jamiolkowski et al. (Eds.), Balkema, Vol.1, pp. 681-689.

Miura, S. and Toki, S., 1982, "A sample preparation method and its effect on static and cycle deformation-strength properties of sand", Soils and Foundations, March 1982, Vol. 22, No.1, pp. 61-77.

Mooney, M.A. and Miller, P.K., 2009, "Analysis of lightweight deflectometer test based on in situ stress and strain response", Journal of Geotechnical and Geoenvironmental Engineering, February 2009, Vol. 135, No. 2, pp. 199-207.

NAASRA, 1987, Pavement Design: A Guide to the Structural Design of Road Pavements, National Association of Australian State Road Authorities, New South Wales.

Nawir, H., Tatsuoka, F. and Kuwano, R., 2003, "Experimental evaluation of the viscous properties of sand in shear", Soils and Foundations, Vol.43, No.6, pp.13-31.

Ping, W.V., ASCE, M., Yang, Z. and Gao, Z., 2002, "Field and laboraty determination of granular subgrade moduli", Journal of Performance of Constructed Facilities, Vol. 16, No.4, pp. 149-159.

Roesset, J. M., Kausel, K., Cuellar, V., Monte, J. L., and Valerio, J., 1996, "Closure to 'impact of weight falling onto the ground'", Journal of Geotechnical and Geoenvironmental Engineering, Vol. 122, No. 5, pp. 416–417.

Royal Institute of Technology, 1980, Testing Different FWD Loading Times, Bulletin 1980:8, Department of Highway Engineering, Royal Institute of Technology, Stockholm.

Ruenkrairergsa, T. and Phromsorn. C., 2001, Engineering Properties of Asphalt Concrete Mixtures Utilized in Thailand, Bureau of Road Research and Development, Department of Highways, Ministry of Transport, Bangkok, Thailand.

REFFERENCES

Shahin, M.Y., 1994, Pavement Management for Airports, Roads, and Parking Lots, Chapman & Hall, New York.

Siddiquee, M. S. A., Tatsuoka, F. and Tanaka, T., 2006, "FEM simulation of the viscous effects on the stress-strain behaviour of sand in plane strain compression", Soils and Foundations, Vol.46, No.1, pp. 99-108.

Sousa, J.B. and Monismith, C.L., 1987, "Dynamic response of paving materials", Transportation Research Record No. 1136, Transportation Research Board, Washington, D.C., pp. 57-68.

Suklje, L., 1969, Rheological Aspects of Soil Mechanics, Wiley-Interscience, London.

Touma, B.E., Crovetti, J., and Shahin, M.Y., 1990, "The effect of various load distributions on the back calculated moduli values in flexible pavements", Transportation Research Record No. 1293, Transportation Research Board, Washington, D.C., pp. 31-41.

Thaisri, K., Youwai, S. and Kongkitkul, W., 2008, "Behavior of reinforced flexible pavement under monotonic loading condition", Proceedings of the 13th National Convention on Civil Engineering, 14-16 May 2008, Pattaya, Thailand, pp. 344-347.

Tatsuoka, F., Santucci de Magistris, F. and Momoya, M. and Maruyama, N., 1999, "Isotach behaviour of geomaterials and its modelling", Proc. Second Int. Conf. on Pre-Failure Deformation Characteristics of Geomaterials, IS Torino '99, Balkema, Jamiolkowski et al. (eds), Vol. 1, pp. 491-499.

Tatsuoka, F., Santucci de Magistris, F., Hayano, K., Momoya, Y. and Koseki, J., 2000, "Some new aspects of time effects on the stress-strain behaviour of stiff geomaterials", Keynote Lecture, The Geotechnics of Hard Soils-Soft Rocks, Proc. of Second Int. Conf. on Hard Soils and Soft Rocks, 1998, Napoli, Balkema, Evamgelista and Picarelli (eds.), Vol. 2, pp. 1285-1371.

REFFERENCES

Tatsuoka, F., Uchimura, T., Hayano, K., Di Benedetto, H., Koseki, J. and Siddiquee, M.S.A., 2001, "Time-dependent deformation characteristics of stiff geomaterials in engineering practice", the Theme Lecture, Proc. of the Second International Conference on Pre-failure Deformation Characteristics of Geomaterials, 1999, Torino, Balkema, Jamiolkowski et al. (eds.), Vol. 2, pp. 1161-1262.

Tatsuoka, F., Ishihara, M., Di Benedetto, H. and Kuwano, R., 2002, "Time-dependent deformation characteristics of geomaterials and their simulation", Soils and Foundations, Vol.42, No.2, pp. 103-129.

Tatsuoka, F., Di Benedetto, H. and Nishi, T., 2003a, "A framework for modelling of the time effects on the stress-strain behaviour of geomaterials", Proc. 3rd Int. Sym. on Deformation Characteristics of Geomaterials, IS Lyon 03, September 2003, Balkema, Di Benedetto et al. (eds.), pp. 1135-1143.

Tatsuoka, F., Acosta-Martinez, H.E. and Li, J.-Z., 2003b, "Viscosity in one-dimensional deformation of clay and its modelling and simulation", Proceedings of the 38th Japan National Conference on Geotechnical Engineering, JGS, Akita, pp. 257-258.

Tatsuoka, F., 2004, "Effects of viscous properties and ageing on the stress-strain behaviour of geomaterials", Geomechanics-Testing, Modeling and Simulation, Proceedings of the GI-JGS workshop, ASCE Geotechnical Special Publication GSP No. 143, Yamamuro & Koseki (Eds.), Boston, pp. 1-60.

Tatsuoka, F., Kiyota, T. and Enomoto, T., 2006, "Viscous properties of geomaterials in drained shear", Geomechanics-Testing, Modeling and Simulation, Proceedings of the Second GI-JGS workshop, September 2005, Osaka, ASCE Geotechnical Special Publication GSP, Lade et al. (eds.).

Tatsuoka, F., 2007, "Inelastic deformation characteristics of geomaterial", Soil Stress-Strain Behavior: Measurement, Modeling and Analysis, Ling, et al. (Eds.), Springer, Dordrecht, pp. 1-108.

REFFERENCES

Tatsuoka, F., Di Benedetto, H., Enomoto, T., Kawabe, S., and Kongkitkul, W., 2008, "Various viscosity types of geomaterials in shear and their mathematical expression", Soils and Foundations, Vol. 48, No. 1, pp. 41-60.

Thaisri, K., Youwai, S. and Kongkitkul, W., 2008, "Behavior of reinforced flexible pavement under monotonic loading condition", Proceedings of the 13th National Convention on Civil Engineering, 14-16 May 2008, Pattaya, Thailand, pp. 344-347.

The Asphalt Institute, 1968, The Asphalt Handbook: Manual Series No.4 (MS-4), 4th ed., The Asphalt Institute, Marryland.

The Asphalt Institute, 1981, Thickness Design-Asphalt Pavements for Highways and Streets: Manual Series No. 1 (MS-1), The Asphalt Institute, Marryland.

Thilakasiri, S., Mullins, G., Stinnette, P., and Gunaratne, M., 1996, "Discussion of 'impact of weight falling onto the ground' by Roesset et al.", Journal of Geotechnical and Geoenvironmental Engineering, Vol. 122, No. 5, pp. 415–417.

Thompson, M.R., 1984, Unpublished Report, University of Illinois at Urbana-Champaign, Illinois.

Touma, B.E., Crovetti, J., and Shahin, M.Y., 1990, "The effect of various load distributions on the back calculated moduli values in flexible pavements", Transportation Research Board No. 1293, Transportation Research Board, Washington, D.C., pp. 31-41.

Ullidtz, P. and Stubstad, R., 1985, "Structure evaluation of highway and airfield PCC pavements using the Falling Weight Deflectometer", Proceedings of the 3rd International Conference on Concrete Pavement Design and Rehabilitation, April, Purdue University, West Lafayette, Indiana.

Umass, n.d., Lacroix Deflectograph [Online], Available : http://nersp.nerdc.ufl.edu /~tia/5837-14.pdf [2008, Septemer 15].

REFFERENCES

Van Der Poel, C., 1954, "A general system describing the visco-elastic properties of bitumens and it relation to routine test data", Journal of Applied Chemistry, Vol. 4, No. 5, pp. 221-236.

Verbic, B. and Veletsos, A.S., 1972, Impulse Response Functions for Elastic Foundations, Report No.15, Department of Civil Engineering, Rice University, Houston.

Walker, J.S., 2004, Physics, 2nd ed., Prentice Hall, New Jersy.

Wikipedia, n.d., Viscoelasticity [Online], Available : http://en.wikipedia.org/wiki/Viscoelasticity [2008, August 22].

Wood, D.M., 1990, Soil Behaviour and Critical State Soil Mechanics, Cambridge University Press, Cambridge.

Research Report 2008

ATRANS